

**Layer-by-Layer assembled thin films for
drug delivery:
Interactions at the nano-bio interface**



Dissertation zur Erlangung des Doktorgrades der Naturwissenschaften
(Dr. rer. nat.) der Fakultät Chemie und Pharmazie
der Universität Regensburg

vorgelegt von

Eva-Christina Wurster

aus Karlsruhe

im Jahr 2015

Diese Doktorarbeit entstand in der Zeit von September 2010 bis Februar 2015 am
Lehrstuhl für Pharmazeutische Technologie der Universität Regensburg.
Die Arbeit wurde angeleitet von PD Dr. Miriam Breunig

Promotionsgesuch eingereicht am: 24. Februar 2015

Datum der mündlichen Prüfung: 17. April 2015

Prüfungsausschuss:

- PD Dr. M. Breunig (Erstgutachterin)
- Prof. Dr. A. Göpferich (Zweitgutachter)
- Prof. Dr. J. Wegener (Drittprüfer)

Meiner Familie

Table of contents

Chapter 1:

Introduction and goals of the thesis1

Chapter 2:

Synthesis and characterization of gold nanoparticles27

Chapter 3:

Layer-by-Layer assembled gold nanoparticles for the delivery of nucleic acids ...55

Chapter 4:

Oligolayer coated nanoparticles: Impact of the surface topography at the
nano-bio interface79

Chapter 5:

Foerster resonance energy transfer as a tool to study the internal structure of
polyelectrolyte multilayers and the consequences for drug delivery125

Chapter 6:

Mobility of polyelectrolytes and coated nanoparticles in a collagen I matrix
investigated by fluorescence recovery after photobleaching (FRAP)159

Chapter 7:

Summary and Outlook193

Appendix199

Chapter 1

Introduction and goals of the thesis

Introduction

Nanoparticles for drug delivery

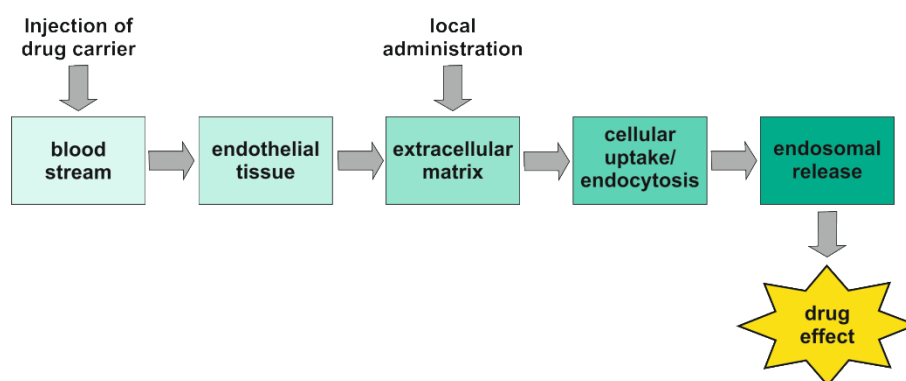
Nanoparticles for drug delivery applications gained increasing attention in the last 100 years. In 1906 Paul Ehrlich proposed his inspiring idea of a magic bullet, e.g. a drug that selectively and intrinsically finds infected cells inside an organism. This work can be regarded as the starting point of a novel strategy in drug-based medicine, and colloidal drug carriers seem to be a promising approach to reach Ehrlich's optimum of a targeted drug therapy.^{1,2} By now a myriad of different nanocarriers of inorganic or organic origin with various types of surface modifications are under scientific investigation to reach Ehrlich's goal.^{3,4} But independently of the used material some general properties are discussed for all colloidal drug carriers:

First, nanoparticle based drug delivery systems are often used to increase the applicable dose of drug compounds.^{5,6} Especially, new developed small molecule drugs often suffer from a high hydrophobicity and a poor solubility and are therefore difficult to administer therapeutically.⁷ Here, the administration in combination with a nanoparticle construct can be used to elevate the dose up to a therapeutically relevant concentration.^{5,6} In the case of a completely new class of therapeutic substances, such as proteins and nucleic acids, nanoparticles are thought to be a necessity for a therapeutic use at all. Nucleic acids and thereof especially small interfering RNA (siRNA) more recently gained increasing attention as potential therapeutic agents.⁸⁻¹⁰ Usually those materials cannot be injected directly into the

blood stream of an organism, because they strongly evoke immunogenic reactions or they are degraded by endogenous mechanisms. Additionally, their high negative charge limits the permeability through biological membranes. Here, smart packing strategies are necessary to protect the siRNA cargo and to screen the negative charges.¹¹ Those requirements can be provided by nanoparticle constructs. In this context so called non-viral vectors on the basis of polycationic compounds such as poly(ethylene imine) or cationic lipids seem to be a promising approach, although the toxicity of polycations is always a concern.¹²⁻¹⁴

Second, nanoparticles are able to improve the risk-to-benefit ratio of highly effective drugs, for example chemotherapeutics. Ideally, drug carriers transport a high drug concentration and accumulate only at the desired target sites, either by active or by passive targeting.^{1,4} Consequently, healthy tissues and cells would be preserved and unwanted side-effects are reduced.

But, in fact the real situation for a “magic bullet” is much more complex. The fate of a nanoparticle formulation inside an organism is subject to various complex processes and several physiological barriers have to be overcome until the final site of action is reached (**Scheme 1**).¹¹ For example, upon injection into the blood stream serum proteins are adsorbed to the nanoparticle surface and some of them, the so called opsonins, lead to the elimination of nanomaterials from the circulation by macrophages.¹⁵⁻¹⁷ After escaping the blood vessels through the endothelial tissue, nanoparticles are facing the extracellular matrix, which fills the space between single cells, gives each tissue its specific shape and mechanical resistance and regulates signal transduction processes.¹⁸ The extracellular matrix consists of a variety of different biomacromolecules, such as proteins, proteoglycans and glycosaminoglycans and most of them are highly charged.¹⁹ As a consequence electrostatic filter effects are known to exist, hindering the mobility of nanoparticles and at the end reducing their therapeutic efficiency.^{20,21}



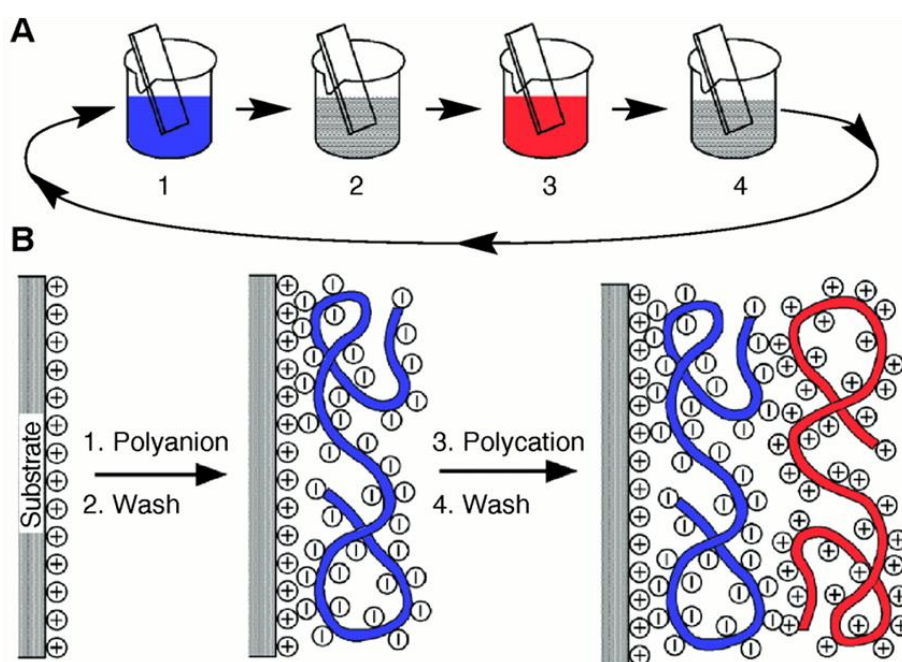
Scheme 1 Inside an organism a colloidal drug carrier has to overcome several physiological barriers. All of them are affecting the efficiency of the transported drug molecules and are mainly affected by the physicochemical properties of the carrier's materials.

After reaching the desired target, the various endocytosis mechanisms of living cells resemble another effective barrier for the efficiency of colloidal drug carriers.^{22,23} In the absence of a ligand that mediates the uptake by cells, size²⁴⁻²⁷, shape^{28,29} and charge³⁰⁻³² of the nanoparticles are the most important parameters influencing endocytosis. And finally, the release out of the endosomal system of human cells is critical for the efficiency of a drug molecule, because of chemical degradation processes occurring inside the lysosomes.³³⁻³⁵

All of the processes mentioned above are mainly influenced by the physicochemical properties of the colloidal carrier and they highly affect the final drug activity. Additionally, some effects, such as the protein adsorption, apply also for other drug delivery devices or routes of administration, for example drug loaded implants or the local administration into the desired tissue. Hence, a deep understanding of the interactions between the used materials and the biological counterparts is of highest importance for the design of potent drug delivery systems. Thin film technologies, such as the Layer-by-Layer (LbL) strategy, which easily adjust the physicochemical parameters, are ideal tools to investigate these interactions at the nano-bio interface.

Advantages and properties of LbL thin films

The LbL technology is a well-established method for thin film surface modifications based on the stepwise self-assembly polymers. Thin films are commonly defined as coatings on a flat, curved or structured substrate with a thickness below 0.1 μm . In general, the physicochemical properties of the coated substrate differ from the uncoated material for example by their electrical, optical, magnetic or biological properties.³⁶ Hence, thin film modifications are a favored tool in all areas of materials science. The ancestor of the LbL method was introduced in 1966 with a publication of Iler describing multilayers consisting of charged nanoparticles.³⁷



Scheme 2 Illustration of the basic LbL protocol. **A)** The original dipping procedure with polyelectrolyte solutions and washing steps leads to **B)** “fuzzy nanoassemblies” meaning that the polymer charges are overcompensated to form a loopy conformation (Reprinted from Decher⁴⁰. Reprinted with permission from AAAS.)

Decher and coworkers probably were inspired by these early findings and enlarged this strategy to polyelectrolytes about 30 years later, opening a whole new field of research.³⁸⁻⁴⁰

The original LbL protocol was described as an immersion procedure of a charged solid surface, e.g. a glass microscope slide, which was dipped into either the solutions of positive or negative charged polymers. Rinsing steps were performed in between to avoid aggregation of the oppositely charged polyelectrolytes.⁴⁰ After several repetitions a polymer thin film is adsorbed on the surface with a thickness of only several nanometers (**Scheme 2**).

The strength of the LbL strategy becomes evident among comparison of the technique with other available strategies for thin film modifications, e.g. the Langmuir-Blodgett technique (LB) and the self-assembled monolayers (SAM). The LB-technique transfers amphiphilic molecules from an air-water interface by immersion or emersion of a substrate, leading to multilayers which are comparable to biological membranes.⁴¹ But, LB films require specialized equipment, the so called LB-trough, and are limited to amphiphilic building blocks.⁴¹ In comparison, SAM consist of organic molecules which spontaneously take on an ordered, but monolayered, conformation on a substrate, e.g. as the binding of alkylthiols on gold surfaces.⁴² But, usually multilayers are not available with SAM modifications. Hence, the applicability of both methods is very limited, due to their specific technical and chemical requirements.

In comparison, the LbL strategy has some seminal advantages and properties. The most important strength is its flexibility concerning the applied materials. Only a minimal surface charge has to be present to apply an LbL coating and substrates of almost any size and shape.^{36,43} Additionally, a myriad of charged synthetic and biological polymers and other colloids are available as coating materials.⁴⁴ The coating process itself does not require any advanced facilities, but nevertheless automated equipment and other film deposition techniques, such as spray-coating⁴⁵ and spin-coating⁴⁶, were developed to increase the output.

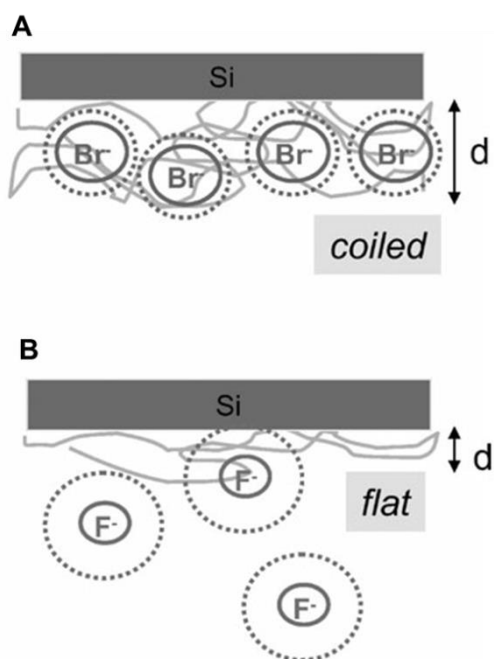
The LbL technique is not limited to electrostatic interactions only. Hydrophobic interactions⁵⁸, hydrogen bonding⁵⁹ and even covalent strategies, such as click-chemistry⁶¹, were found to be suitable for the LbL deposition. Altogether a huge set of building blocks was developed over the last 25 years which made the LbL method suitable for almost every application in almost every scale.

Table 1 Building blocks for the design of LbL multilayers.

Coating conditions	Film growth mode ⁴⁷⁻⁴⁹ Ions and pH ⁵⁰⁻⁵² Solvent polarity ^{53,54}
Deposition technique	Dipping ^{43,55,56} Spray-coating ⁴⁵ Spin-coating ⁴⁶ Microfluidics/Flow Systems ⁵⁷
Attraction forces	Electrostatic ⁵⁶ Hydrophobic ⁵⁸ Hydrogen-bonding ⁵⁹ Covalent ^{60,61}
Substrate materials	Macroscopic substrates ³⁶ Microparticles /-capsules ^{62,63} Nanoparticles ^{64,65} Free-standing films ⁶⁶
Coating materials	Synthetic polyelectrolytes ⁴⁴ Natural polyelectrolytes ⁶⁷⁻⁶⁹ Nucleic acids and proteins ^{30,70,71} Nanoparticles ^{69,72,73}

An overview, without any claim for completeness, is shown in **Table 1** to give an impression on the extent of LbL opportunities. Hence, LbL often is an ideal tool for the design of advanced materials not only for a biomedical or a drug delivery application. The by far most investigated LbL multilayer systems are electrostatic multilayers consisting of natural or synthetic polyelectrolytes. The formation forces, kinetics and the internal structure of those polyelectrolyte multilayers (PEM) have been extensively reviewed by von Klitzing⁷⁴ and just the most important facts for the understanding of electrostatic multilayer structures are mentioned here.

First, it is important to know that polyelectrolytes usually do not behave as rigid building blocks with interactions only between neighboring layers. Hence, the expression “Layer-by-Layer” is somewhat misleading. Furthermore those systems have to be regarded as entities of flexible and mobile chains, which rather can be seen as a sponge or a crosslinked network.⁷⁴ Lavallo and coworkers described an in-and-out diffusion model, where a polyelectrolyte species is able to diffuse freely inside the polyelectrolyte film.⁷⁵ The direction of its diffusion changes with the charge of the next polymer layer and this results in the so called “exponential growth” of multilayers.⁷⁵ In general, the fabrication conditions have a major impact on the final multilayer properties. Minimal changes lead to rather different thin films with specific internal conformations of the polyelectrolyte chains. For example, the type of counterion associated with the polyelectrolytes highly affects the constitution of adsorbed polymer chains (**Scheme 3**). Large anions with a comparable small hydration shell, e.g. bromide ions, lead to a coiled polymer conformation and a higher layer thickness. The exchange of bromide ions against fluoride led to a four times lower multilayer thickness, due to a flat and stratified polyelectrolyte conformation.



Scheme 3 The type of counterion has an impact on the internal conformation of the multilayer. **A)** In case of a large anion with a comparable small and weakly bound hydration shell, the polymer chains take on a coiled conformation, leading to a higher multilayer thickness. **B)** Small counterions with a larger hydration shell, lead to a flat and stratified polymer conformation and a low multilayer thickness. (Reproduced from von Klitzing⁷⁴ with permission of the Royal Society of Chemistry)

Although multilayers of polyelectrolytes are usually called “electrostatic”, the main driving force for the formation of those thin films is a gain in entropy, due to the release of counterions.⁷⁶ But, it was also shown, that next to electrostatic attraction other forces such as hydrophobic interactions between the used polymers play a major role as well.⁷⁷ Small variations of the coating conditions lead to an altered film thickness and density. Here, the most important variable is the salt concentration of the applied polyelectrolyte solutions.⁵¹ The introduced counterions screen the charges of the polymer backbone and lead to more coiled polymer structures, which results in thicker multilayers.⁵¹ Dubas and Schlenoff showed a linear correlation between ionic strength and multilayer thickness for poly(diallyl diammonium chloride)/poly(styrene sulfonate) multilayers in the range of 10^{-2} and 2 M NaCl.⁵¹ In case of weak polyelectrolytes the pH of the polymer solution has a similar effect and can also adjust the charge density of a polymer chain, leading to an increased multilayer thickness over a narrow pH range.^{78,79} Elzbieciak et al showed that depending on the applied pH of a weak polyelectrolyte not only the internal conformation of a multilayer but also the outer appearance, was altered significantly.⁵² At pH 6, the surface topography was

smooth with only minimal heights, whereas at pH 10.5 the surface roughness highly increased and sharp surface structures became visible.⁵²

The challenge for the design of future LbL based drug delivery systems is to correlate the findings on the internal structures and their deposition conditions to the desired applications in terms of drug release and interactions at the nano-bio interfaces.

Layer-by-Layer strategies for the design of drug delivery systems

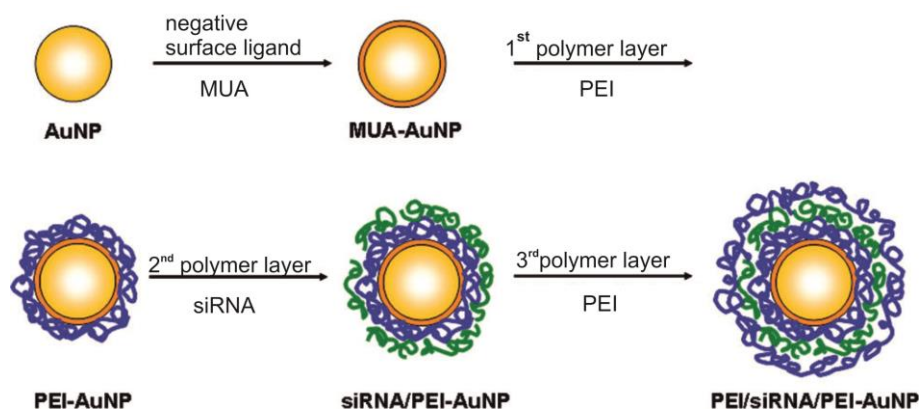
Due to its mild fabrication conditions in an aqueous medium, LbL was early discovered as a potential tool to design novel biomedical materials and drug delivery devices.⁶⁹ Here, three different applications have to be mentioned: The fabrication of LbL coated implants, of hollow microcapsules and of coated nanoparticles.

The coating of medical implants is probably the easiest way for an LbL modification in a biomedical context, due to the macroscopic size of the template. The group of Hammond strongly works on the *in vitro* and *in vivo* use of LbL coated metal implants with different kinds of small-molecule drugs incorporated into the thin film, e.g. several antibiotics, such as gentamicin or ciproflaxin, and non-steroidal anti-inflammatory drugs.⁸⁰ Due to the integration of those charged or non-charged drugs into separated polyelectrolyte layers a time-dependent control of the drug doses and a sustained release of the different therapeutic agents over up to four weeks was achieved.^{80,81} In contrast, Jewell and Lynn investigated the transfection of plasmid DNA with LbL films on glass surfaces and showed the successful of expression of enhanced green fluorescent protein after 48 h.^{82,83} Furthermore, they proposed that coating of vascular stents with this approach might lead to a gene-based treatment of cardiovascular diseases in the future.⁸⁴

In the field of particle-based drug delivery systems M \ddot{o} hwald and coworkers invented the principle of LbL coated microparticles to form hollow drug containing microcapsules.^{62,85} This approach was further improved by de Geest and Caruso, but it still suffers from the large size of the applied microparticles which cannot be endocytosed by most of the human cells.^{63,86,87} But, more recently LbL microcapsules were found to be a promising approach for the mild and adjuvant-free delivery of vaccines.^{88,89}

Smaller particle cores in the nanometer scale results in functional particles that fit to the size limits of cellular uptake mechanisms.²² Hence, the size as a prerequisite for the design of future nanomedicines for the treatment of cancer, infectious diseases and others, can be met by LbL coated nanoparticles.⁹⁰ But, in contrast to the coating of microparticles, LbL modifications on nanoparticles are technical challenging due to their high tendency towards aggregation. But especially gold nanoparticles^{65,91} were shown to be stable enough to resist the coating and washing steps of an LbL procedure and probably became the most common used core material.⁹² Nevertheless, other nanomaterials of organic or inorganic origin were also used as LbL templates.⁹³ Based on LbL coated gold nanoparticles, Elbakry et al. designed a drug delivery system for nucleic acids based on a gold nanoparticle core which is coated with the polyelectrolyte poly(ethylene imine), PEI, and siRNA (**Scheme 4**).⁶⁴ PEI was chosen because of its known transfection capability and consequently the transfection efficiency of this siRNA delivery system was reported in 2009.⁶⁴ Here, it was shown that by the use of only a single siRNA layer, close to 800 siRNA molecules could be delivered by a single 16 nm small nanoparticle; a prove for the high loading dose of LbL coated particle designs.⁶⁴ Additionally it was shown that by changing the amount of polyelectrolyte layers, the charge state of the final delivery system affected significantly the delivery efficacy. In a second publication the size of the drug delivery system was tuned by the size of the initial gold

nanoparticle core in a range of 20 to 80 nm, what also had a major impact on the particle uptake and the transfection efficiency.²⁷



Scheme 4 LbL coating of gold nanoparticles with PEI and siRNA (Reprinted (adapted) with permission from Elbakry et al.⁶⁴. Copyright (2009) American Chemical Society)

In the last years further comparable examples of LbL modified nanoparticulate delivery systems were published. The group of Hammond strongly forces the *in vivo* feasibility of LbL coated nanoparticles. They showed that the stability and clearance of LbL coated quantum dots strongly depends on the amount of coated bilayers, but they also proved the passive targeting of a tumor in a mouse model.⁹⁴ Deng et al. designed nanoparticles for the codelivery of an anticancer drug and siRNA with a single particle design, based on coated liposomes.⁹⁵ The combination of the two therapeutic agents was beneficial, as the siRNA targeted a drug-resistance protein and therefore enhanced the efficiency of doxorubicin by 4–fold.⁹⁵

Despite those promising examples several issues concerning the therapeutic application of LbL coated nanoparticles still remain. A major disadvantage is the high stability of the electrostatic multilayer shell, leading to a low drug release. To overcome these limitations the

properties of the LbL films have to be improved and understood in more detail. Hence, in the next future it would be necessary to connect these findings to the distinct requirements of drug delivery applications.

Goals of the thesis

The main goal of this thesis was to get a deeper insight into the interactions between LbL thin films and their biological counterparts in terms of a drug delivery scenario. Especially if applied in a drug delivery approach, various processes, such as the adsorption of proteins, the association with cells or the interaction with extracellular matrix are unavoidable. All together are influencing the efficacy of a delivered drug compound or are altering the LbL structure itself.

The coating of nanoparticles is challenging, due to their tendency towards aggregation. Hence, an improved protocol for the coating of gold nanoparticles had to be developed, first ([Chapter 2](#)). During the surface modification of colloids, their characterization, concerning the particle size, is always a concern. Especially in the case of gold nanoparticles some peculiarities have to be considered, when applying dynamic light scattering for the determination of the hydrodynamic diameter. Hence, the characterization of nanoparticle sizes and the calculation of the molar concentration of gold nanoparticle suspensions was addressed in [Chapter 3](#).

All these findings led to a detailed study about various LbL coated gold nanoparticles at the nano-bio interface. In [Chapter 4](#) different series of three polycations, poly(allylamine hydrochloride), poly(ethylene imine) and poly(diallyl diammonium chloride) were coated on gold nanoparticles and their LbL deposition behavior on macroscopic surfaces was investigated. Additionally, the impact of the LbL deposition mechanisms on the surface

topography was evaluated and at the end the interactions of those LbL coated nanoparticles with cell culture medium and its impact on the cell association behavior was further highlighted.

As described above, LbL systems on a macroscopic scale can also be interesting for biomedical applications. Hence, the internal constitution of different multilayer conformations and its impact on the permeability for small molecule drugs was compared using an approach based on Foerster resonance energy transfer ([Chapter 5](#)).

Concerning the different barriers colloidal drug carriers have to overcome on their journey to their cellular site of action, the extracellular matrix is known to have an important influence. Effective filter mechanisms, especially known for the basal membrane, highly reduce the activity of systemically administered drug delivery systems. But also the interstitial connective tissue, with its main component collagen I, can be assumed to limit the mobility of nanoparticles. This question is addressed in [Chapter 6](#), where the mobility of LbL coated nanoparticles and polyelectrolytes in a collagen I model matrix is described.

Altogether, this thesis gives further details on the interactions of LbL coated materials at the nano-bio interface and wants to highlight the capabilities of multilayers, with a special focus on the design of drug delivery devices.

References

- (1) Langer, R. Drug Delivery And Targeting. *Nature* **1998**, *392*, 5-10.
- (2) Duncan, R. Nanomedicine Gets Clinical. *Mater. Today* **2005**, *8*, 16-17.
- (3) Mishra, B.; Patel, B.; Pharm, B.; Tiwari, S.; Pharm, M. Colloidal Nanocarriers: A Review On Formulation Technology, Types And Applications Toward Targeted Drug Delivery. *Nanomedicine: NBM* **2010**, *6*, 9-24.
- (4) Faraji, A.; Wipf, P. Nanoparticles In Cellular Drug Delivery. *Bioorg. Med. Chem.* **2009**, *17*, 2950-2962.
- (5) Szczepanowicz, K.; Bazylińska, U.; Pietkiewicz, J.; Szyk-Warszyńska, L.; Wilk, K. A.; Warszyński, P. Biocompatible Long-Sustained Release Oil-Core Polyelectrolyte Nanocarriers: From Controlling Physical State And Stability To Biological Impact. *Adv. Colloid Interface Sci.* **2014**, *in press*.
- (6) Bonifácio, B. V.; Da Silva, P. B.; Ramos, dos, M. A. S.; Negri, K. M. S.; Bauab, T. M.; Chorilli, M. Nanotechnology-Based Drug Delivery Systems And Herbal Medicines: A Review. *Int. J. Nanomed.* **2014**, *9*, 1-15.
- (7) Lipinski, C. A. Drug-Like Properties And The Causes Of Poor Solubility And Poor Permeability. *J. Pharmacol. Toxicol. Methods* **2000**, *44*, 235-249.
- (8) Dorsett, Y.; Tuschl, T. siRNAs: Applications In Functional Genomics And Potential As Therapeutics. *Nature Rev. Drug Discovery* **2004**, *3*, 318-329.
- (9) Patil, S. D.; Rhodes, D. G.; Burgess, D. J. DNA-Based Therapeutics And DNA Delivery Systems: A Comprehensive Review. *AAPS J.* **2005**, *7*, E61-E77.
- (10) Opalinska, J.; Gewirtz, A. Nucleic-Acid Therapeutics: Basic Principles And Recent Applications. *Nat. Rev. Drug Discovery* **2002**, *1*, 503-514.

- (11) Whitehead, K. A.; Langer, R.; Anderson, D. G. Knocking Down Barriers: Advances In Sirna Delivery. *Nat. Rev. Drug Discovery* **2009**, *8*, 129-138.
- (12) Gao, X.; Kim, K.; Liu, D. Nonviral Gene Delivery: What We Know And What Is Next. *AAPS J.* **2007**, *9*, E92-104.
- (13) Breunig, M.; Lungwitz, U.; Liebl, R.; Goepferich, A. Breaking Up The Correlation Between Efficacy And Toxicity For Nonviral Gene Delivery. *Proc. Natl. Acad. Sci. USA* **2007**, *104*, 14454-14459.
- (14) Breunig, M.; Hozsa, C.; Lungwitz, U.; Watanabe, K.; Umeda, I.; Kato, H.; Goepferich, A. Mechanistic Investigation Of Poly(Ethylene Imine)-Based Sirna Delivery: Disulfide Bonds Boost Intracellular Release Of The Cargo. *J. Controlled Release* **2008**, *130*, 57-63.
- (15) Owens, D. E.; Peppas, N. A. Opsonization, Biodistribution, And Pharmacokinetics Of Polymeric Nanoparticles. *Int. J. Pharm.* **2006**, *307*, 93-102.
- (16) Hühn, D.; Kantner, K.; Geidel, C.; Brandholdt, S.; de Cock, I.; Soenen, S. J.; Rivera-Gil, P.; Martos, J. M.; Braeckmans, K.; Mullen, K.; *et al.* Polymer-Coated Nanoparticles Interacting With Proteins And Cells: Focusing On The Sign Of The Net Charge. *ACS Nano* **2013**, *7*, 3253.
- (17) Alexis, F.; Pridgen, E.; Molnar, L. K.; Farokhzad, O. C. Factors Affecting The Clearance And Biodistribution Of Polymeric Nanoparticles. *Mol. Pharmaceutics* **2008**, *5*, 505-515.
- (18) Hynes, R. O. The Extracellular Matrix: Not Just Pretty Fibrils. *Science* **2009**, *326*, 1216-1219.
- (19) Hynes, R. O.; Naba, A. Overview Of The Matrisome--An Inventory Of Extracellular Matrix Constituents And Functions. *Cold Spring Harbor Perspect. Biol.* **2012**, *4*, a004903-a004903.
- (20) Lieleg, O.; Ribbeck, K. Biological Hydrogels As Selective Diffusion Barriers. *Trends Cell Biol.* **2011**, *21*, 543-551.
- (21) Zamecnik, J.; Vargova, L.; Homola, A.; Kodet, R.; Sykova, E. Extracellular Matrix Glycoproteins And Diffusion Barriers In Human Astrocytic Tumours. *Neuropathol. Appl. Neurobiol.* **2004**, *30*, 338-350.

- (22) Connor, S. D.; Schmid, S. L. Regulated Portals Of Entry Into The Cell. *Nature* **2003**, *422*, 37-44.
- (23) Hillaireau, H.; Couvreur, P. Nanocarriers' Entry Into The Cell: Relevance To Drug Delivery. *Cell. Mol. Life Sci.* **2009**, *66*, 2873-2896.
- (24) Lu, F.; Wu, S.; Hung, Y.; Mou, C. Size Effect On Cell Uptake In Well-Suspended, Uniform Mesoporous Silica Nanoparticles. *Small* **2009**, *5*, 1408-1413.
- (25) Zhang, S.; Li, J.; Lykotrafitis, G.; Bao, G.; Suresh, S. Size-Dependent Endocytosis Of Nanoparticles. *Adv. Mater.* **2009**, *21*, 419-424.
- (26) Rejman, J.; Oberle, V.; Zuhorn, I. S.; Hoekstra, D. Size-Dependent Internalization Of Particles Via The Pathways Of Clathrin- And Caveolae-Mediated Endocytosis. *Biochem. J.* **2004**, *377*, 159.
- (27) Elbakry, A.; Wurster, E.; Zaky, A.; Liebl, R.; Schindler, E.; Bauer-Kreisel, P.; Blunk, T.; Rachel, R.; Goepferich, A.; Breunig, M. Layer-By-Layer Coated Gold Nanoparticles: Size-Dependent Delivery Of DNA Into Cells. *Small* **2012**, *8*, 3847-3856.
- (28) Champion, J.; Mitragotri, S. Shape Induced Inhibition Of Phagocytosis Of Polymer Particles. *Pharm. Res.* **2009**, *26*, 244-249.
- (29) Chithrani, B. D.; Ghazani, A. A.; Chan, W. C. Determining The Size And Shape Dependence Of Gold Nanoparticle Uptake Into Mammalian Cells. *Nano Lett.* **2006**, *6*, 662-668.
- (30) Elbakry, A.; Zaky, A.; Liebl, R.; Rachel, R.; Goepferich, A.; Breunig, M. Layer-By-Layer Assembled Gold Nanoparticles For siRNA Delivery. *Nano Lett.* **2009**, *9*, 2059-2064.
- (31) Cho, E. C.; Xie, J.; Wurm, P. A.; Xia, Y. Understanding The Role Of Surface Charges In Cellular Adsorption Versus Internalization By Selectively Removing Gold Nanoparticles On The Cell Surface With A I/KI Etchant. *Nano Lett.* **2009**, *9*, 1080-1084.
- (32) Harush-Frenkel, O.; Debotton, N.; Benita, S.; Altschuler, Y. Targeting Of Nanoparticles To The Clathrin-Mediated Endocytic Pathway. *Biochem. Biophys. Res. Commun.* **2007**, *353*, 26-32.

- (33) Sonawane, N. D.; Szoka, F. C.; Verkman, A. S. Chloride Accumulation And Swelling In Endosomes Enhances DNA Transfer By Polyamine-DNA Polyplexes. *J. Biol. Chem.* **2003**, *278*, 44826-44831.
- (34) Cho, Y.; Kim, J.; Park, K. Polycation Gene Delivery Systems: Escape From Endosomes To Cytosol. *J. Pharm. Pharmacol.* **2003**, *55*, 721-734.
- (35) Suma, T.; Miyata, K.; Anraku, Y.; Watanabe, S.; Christie, R. J.; Takemoto, H.; Shioyama, M.; Gouda, N.; Ishii, T.; Nishiyama, N.; *et al.* Smart Multilayered Assembly For Biocompatible Sirna Delivery Featuring Dissolvable Silica, Endosome-Disrupting Polycation, And Detachable PEG. *ACS Nano* **2012**, *6*, 6693-6705.
- (36) de Villiers, M. M.; Otto, D. P.; Strydom, S. J.; Lvov, Y. M. Introduction To Nanocoatings Produced By Layer-By-Layer (Lbl) Self-Assembly. *Adv. Drug Delivery Rev.* **2011**, *63*, 701-715.
- (37) Iler, R. K. Multilayers Of Colloidal Particles. *J. Colloid Interface Sci.* **1966**, *21*, 569-594.
- (38) *Multilayer Thin Films*; Decher, G.; Schlenoff, J. B., Eds.; Wiley -VCH: Weinheim, Germany, 2003.
- (39) Decher, G.; Hong, J. D. Buildup Of Ultrathin Multilayer Films By A Self-Assembly Process: II. Consecutive Adsorption Of Anionic And Cationic Bipolar Amphiphiles And Polyelectrolytes On Charged Surfaces. *Ber. Bunsen-Ges.* **1991**, *95*, 1430-1434.
- (40) Decher, G. Fuzzy Nanoassemblies: Toward Layered Polymeric Multicomposites. *Science* **1997**, *277*, 1232-1237.
- (41) Ariga, K.; Yamauchi, Y.; Mori, T.; Hill, J. P. 25Th Anniversary Article: What Can Be Done With The Langmuir-Blodgett Method? Recent Developments And Its Critical Role In Materials Science. *Adv. Mater.* **2013**, *25*, 6477-6512.
- (42) Huang, X. R.; Carney, R. P.; Stellacci, F.; Lau, B. L. Colloidal Stability Of Self-Assembled Monolayer Coated Gold Nanoparticles: The Effects Of Surface Compositional And Structural Heterogeneity. *Langmuir* **2013**, 11560-11566.
- (43) Ariga, K.; Hill, J. P.; Ji, Q. Layer-By-Layer Assembly As A Versatile Bottom-Up Nanofabrication Technique For Exploratory Research And Realistic Application. *Phys. Chem. Chem. Phys.* **2007**, *9*, 2319-2340.

- (44) Bertrand, P.; Jonas, A.; Laschewsky, A.; Legras, R. Ultrathin Polymer Coatings By Complexation Of Polyelectrolytes At Interfaces: Suitable Materials, Structure And Properties. *Macromol. Rapid Commun.* **2000**, *21*, 319-348.
- (45) Schaaf, P.; Voegel, J.; Jerry, L.; Boulmedais, F. Spray-Assisted Polyelectrolyte Multilayer Buildup: From Step-By-Step To Single-Step Polyelectrolyte Film Constructions. *Adv. Mater.* **2012**, *24*, 1001-1016.
- (46) Lefaux, C. J.; Zimmerlin, J. A.; Dobrynin, A. V.; Mather, P. T. Polyelectrolyte Spin Assembly: Influence Of Ionic Strength On The Growth Of Multilayered Thin Films. *J. Polym. Sci., Part B: Polym. Phys.* **2004**, *42*, 3654-3666.
- (47) Xu, L.; Pristinski, D.; Zhuk, A.; Stoddart, C.; Anker, J. F.; Sukhishvili, S. A. Linear Versus Exponential Growth Of Weak Polyelectrolyte Multilayers: Correlation With Polyelectrolyte Complexes. *Macromolecules* **2012**, *45*, 3892-3901.
- (48) Lavalle, P.; Picart, C.; Mutterer, J.; Gergely, C. Modeling The Buildup Of Polyelectrolyte Multilayer Films Having Exponential Growth. *J. Phys. Chem. B* **2004**, *108*, 635-648.
- (49) Picart, C.; Mutterer, J.; Richert, L.; Luo, Y.; Prestwich, G. D.; Schaaf, P.; Voegel, J. - C.; Lavalle, P. Molecular Basis For The Explanation Of The Exponential Growth Of Polyelectrolyte Multilayers. *Proc. Nat. Acad. Sci. U.S.A.* **2002**, *99*, 12531-12535.
- (50) Izumrudov, V.; Kharlampieva, E.; Sukhishvili, S. A. Salt-Induced Multilayer Growth: Correlation With Phase Separation In Solution. *Macromolecules* **2004**, *37*, 8400-8406.
- (51) Dubas, S. T.; Schlenoff, J. B. Factors Controlling The Growth Of Polyelectrolyte Multilayers. *Macromolecules* **1999**, *32*, 8153-8160.
- (52) Elzbiaciak, M.; Zapotoczny, S.; Nowak, P.; Krastev, R. Influence Of Ph On The Structure Of Multilayer Films Composed Of Strong And Weak Polyelectrolytes. *Langmuir* **2009**, *25*, 3255-3259.
- (53) Kamineni, V.; Lvov, Y.; Dobbins, T. Layer-By-Layer Nanoassembly Of Polyelectrolytes Using Formamide As The Working Medium. *Langmuir* **2007**, *23*, 7423-7427.

- (54) Hirsjärvi, S.; Peltonen, L.; Hirvonen, J. Layer-By-Layer Polyelectrolyte Coating Of Low Molecular Weight Poly (Lactic Acid) Nanoparticles. *Colloids Surf. B: Biointerfaces* **2006**, *49*, 93-99.
- (55) Clark, S. L.; Hammond, P. T. Engineering The Microfabrication Of Layer-By-Layer Thin Films. *Adv. Mater.* **1999**, *10*, 1515-1519.
- (56) Decher, G.; Hong, J. D. Buildup Of Ultrathin Multilayer Films By A Self-Assembly Process, 1 Consecutive Adsorption Of Anionic And Cationic Bipolar Amphiphiles On Charged Surfaces. *Makromol. Chem., Macromol. Symp.* **1991**, *46*, 321-327.
- (57) Madaboosi, N.; Uhlig, K.; Jäger, M. S.; Möhwald, H.; Duschl, C.; Volodkin, D. V. Microfluidics As A Tool To Understand The Build-Up Mechanism Of Exponential-Like Growing Films. *Macromol. Rapid Commun.* **2012**, *33*, 1775-1779.
- (58) Deshmukh, P. K.; Ramani, K. P.; Singh, S. S.; Tekade, A. R.; Chatap, V. K.; Patil, G. B.; Bari, S. B. Stimuli-Sensitive Layer-By-Layer (LbL) Self-Assembly Systems: Targeting And Biosensory Applications. *J. Controlled Release* **2013**, *166*, 294-306.
- (59) Such, G.; Johnston, A.; Caruso, F. Engineered Hydrogen-Bonded Polymer Multilayers: From Assembly To Biomedical Applications. *Chem. Soc. Rev.* **2011**, *40*, 19-29.
- (60) Seo, J.; Schattling, P.; Lang, T.; Jochum, F.; Nilles, K.; Theato, P.; Char, K. Covalently Bonded Layer-By-Layer Assembly Of Multifunctional Thin Films Based On Activated Esters. *Langmuir* **2010**, *26*, 1830-1836.
- (61) Such, G. K.; Tjipto, E.; Postma, A.; Johnston, A. P. R.; Caruso, F. Ultrathin, Responsive Polymer Click Capsules. *Nano Lett.* **2007**, *7*, 1706-1710.
- (62) Ibarz, G.; Dähne, L.; Donath, E.; Möhwald, H. Smart Micro- And Nanocontainers For Storage, Transport, And Release. *Adv. Mater.* **2001**, *13*, 1324-1327.
- (63) de Cock, L. J.; de Koker, S.; de Geest, B. G.; Grooten, J.; Vervaet, C.; Remon, J. P.; Sukhorukov, G. B.; Antipina, M. N. Polymeric Multilayer Capsules In Drug Delivery. *Angew. Chem., Int. Ed.* **2010**, *49*, 6954-6973.
- (64) Elbakry, A.; Zaky, A.; Liebl, R.; Rachel, R.; Goepferich, A.; Breunig, M. Layer-By-Layer Assembled Gold Nanoparticles For Sirna Delivery. *Nano Lett.* **2009**, *9*, 2059-2064.

- (65) Gittins, D. I.; Caruso, F. Tailoring The Polyelectrolyte Coating Of Metal Nanoparticles. *J. Phys. Chem. B* **2001**, *105*, 6846-6852.
- (66) Jiang, C.; Tsukruk, V. V. Freestanding Nanostructures Via Layer-By-Layer Assembly. *Adv. Mater.* **2006**, *18*, 829-840.
- (67) Almodóvar, J.; Place, L. W.; Gogolski, J.; Erickson, K.; Kipper, M. J. Layer-By-Layer Assembly Of Polysaccharide-Based Polyelectrolyte Multilayers: A Spectroscopic Study Of Hydrophilicity, Composition, And Ion Pairing. *Biomacromolecules* **2011**, *12*, 2755-2765.
- (68) Hsu, B. B.; Hagerman, S. R.; Jamieson, K.; Veselinovic, J.; O'Neill, N.; Holler, E.; Ljubimova, J. Y.; Hammond, P. T. Multilayer Films Assembled From Naturally-Derived Materials For Controlled Protein Release. *Biomacromolecules* **2014**, *15*, 2049-2057.
- (69) Costa, R.; Mano, J. Polyelectrolyte Multilayered Assemblies In Biomedical Technologies. *Chem. Soc. Rev.* **2014**, *43*, 3453-3479.
- (70) Becker, A.L.; Johnston, A.; Caruso, F. Peptide Nucleic Acid Films And Capsules: Assembly And Enzymatic Degradation. *Macromol. Biosci.* **2010**, *10*, 488-495.
- (71) Johnston, A. P. R.; Read, E. S.; Caruso, F. DNA Multilayer Films On Planar And Colloidal Supports: Sequential Assembly Of Like-Charged Polyelectrolytes. *Nano Lett.* **2005**, *5*, 953-956.
- (72) Caruso, F.; Lichtenfeld, H.; Giersig, M.; Möhwald, H. Electrostatic Self-Assembly Of Silica Nanoparticle-Polyelectrolyte Multilayers On Polystyrene Latex Particles. *J. Am. Chem. Soc.* **1998**, *120*, 8523-8524.
- (73) Polakiewicz, A.; Dodiuk, H.; Kenig, S. Super-Hydrophilic Coatings Based On Silica Nanoparticles. *J. Adhes. Sci. Technol.* **2014**, *28*, 466-478.
- (74) Klitzing, von, R. Internal Structure Of Polyelectrolyte Multilayer Assemblies. *Phys. Chem. Chem. Phys.* **2006**, *8*, 5012.
- (75) Lavalle, P.; Picart, C.; Mutterer, J.; Gergely, C.; Reiss, H.; Voegel, J.; Senger, B.; Schaaf, P. Modeling The Buildup Of Polyelectrolyte Multilayer Films Having Exponential Growth. *J. Phys. Chem. B* **2004**, *108*, 635-648.
- (76) Bucur, C. B.; Sui, Z.; Schlenoff, J. B. Ideal Mixing In Polyelectrolyte Complexes And Multilayers: Entropy Driven Assembly. *J. Am. Chem. Soc.* **2006**, *128*, 13690-13691.

(77) Schlenoff, J. B.; Rmaile, A. H.; Bucur, C. B. Hydration Contributions To Association In Polyelectrolyte Multilayers And Complexes: Visualizing Hydrophobicity. *J. Am. Chem. Soc.* **2008**, *130*, 13589-13597.

(78) Yoo, D.; Shiratori, S. S.; Rubner, M. F. Controlling Bilayer Composition And Surface Wettability Of Sequentially Adsorbed Multilayers Of Weak Polyelectrolytes. *Macromolecules* **1998**, *31*, 4309-4318.

(79) Shiratori, S. S.; Rubner, M. F. Ph-Dependent Thickness Behavior Of Sequentially Adsorbed Layers Of Weak Polyelectrolytes. *Macromolecules* **2000**, *33*, 4213-4219.

(80) Hammond, P. Building Biomedical Materials Layer-By-Layer. *Mater. Today* **2012**, *15*.

(81) Moskowitz, J. S.; Blaisse, M. R.; Samuel, R. E.; Hsu, H.; Harris, M. B.; Martin, S. D.; Lee, J. C.; Spector, M.; Hammond, P. T. The Effectiveness Of The Controlled Release Of Gentamicin From Polyelectrolyte Multilayers In The Treatment Of Staphylococcus Aureus Infection In A Rabbit Bone Model. *Biomaterials* **2010**, *31*, 6019-6030.

(82) Flessner, R. M.; Yu, Y.; Lynn, D. M. Rapid Release Of Plasmid DNA From Polyelectrolyte Multilayers: A Weak Poly(Acid) Approach. *Chem. Commun.* **2010**, *47*, 550-552.

(83) Jewell, C. M.; Lynn, D. M. Surface-Mediated Delivery Of DNA: Cationic Polymers Take Charge. *Curr. Opin. Colloid Interface Sci.* **2008**, *13*, 395-402.

(84) Jewell, C. M.; Zhang, J.; Fredin, N. J.; Wolff, M. R.; Hacker, T. A.; Lynn, D. M. Release Of Plasmid DNA From Intravascular Stents Coated With Ultrathin Multilayered Polyelectrolyte Films. *Biomacromolecules* **2006**, *7*, 2483-91.

(85) Caruso, F.; Caruso, R. A.; Möhwald, H. Nanoengineering Of Inorganic And Hybrid Hollow Spheres By Colloidal Templating. *Science* **1998**, *282*, 1111-1114.

(86) de Koker, S.; Hoogenboom, R.; de Geest, B. G. Polymeric Multilayer Capsules For Drug Delivery. *Chem. Soc. Rev.* **2012**, *41*, 2867.

(87) Schüler, C.; Caruso, F. Decomposable Hollow Biopolymer-Based Capsules. *Biomacromolecules* **2001**, *2*, 921-926.

(88) de Temmerman, M. D.; de Temmerman, M.; Rejman, J.; Vandenbroucke, R. E.; de Koker, S.; Libert, C.; E., R.; Grooten, J.; Demeester, J.; Gander, B.; *et al.* Polyelectrolyte Lbl

Microcapsules Versus PLGA Microparticles For Immunization With A Protein Antigen. *J. Controlled Release* **2012**, *158*, 233-239.

(89) de Geest, B. G.; Willart, M. A.; Hammad, H.; Lambrecht, B. N.; Pollard, C.; Bogaert, P.; de Filette, M.; Saelens, X.; Vervaet, C.; Remon, J. P.; *et al.* Polymeric Multilayer Capsule-Mediated Vaccination Induces Protective Immunity Against Cancer And Viral Infection. *ACS Nano* **2012**, *6*, 2136-2149.

(90) Hammond, P. T. Polyelectrolyte Multilayered Nanoparticles: Using Nanolayers For Controlled And Targeted Systemic Release. *Nanomedicine* **2012**, *7*, 619-622.

(91) Schneider, G.; Decher, G. Functional Core/Shell Nanoparticles Via Layer-By-Layer Assembly. Investigation Of The Experimental Parameters For Controlling Particle Aggregation And For Enhancing Dispersion Stability. *Langmuir* **2008**, *24*, 1778-1789.

(92) Pereira, S. O.; Barros-Timmons, A.; Trindade, T. Biofunctionalisation Of Colloidal Gold Nanoparticles Via Polyelectrolytes Assemblies. *Colloid Polym. Sci.* **2014**, *292*, 33-50.

(93) Labouta, H. I.; Schneider, M. Tailor-Made Biofunctionalized Nanoparticles Using Layer-By-Layer Technology. *Int. J. Pharm.* **2010**, *395*, 236-242.

(94) Poon, Z.; Lee, J. B.; Morton, S. W.; Hammond, P. T. Controlling In Vivo Stability And Biodistribution In Electrostatically Assembled Nanoparticles For Systemic Delivery. *Nano Lett.* **2011**, *11*, 2096-103.

(95) Deng, Z. J.; Morton, S. W.; Ben-Akiva, E.; Dreaden, E. C.; Shopsowitz, K. E.; Hammond, P. T. Layer-By-Layer Nanoparticles For Systemic Codelivery Of An Anticancer Drug And siRNA For Potential Triple-Negative Breast Cancer Treatment. *ACS Nano* **2013**, *7*, 9571-9584.

Chapter 2:

Synthesis and characterization of

gold nanoparticles

This chapter contains experimental results obtained from collaboration with another institute of the University of Regensburg.

Cooperation with Prof. Dr. Reinhard Rachel, Centre for Electron Microscopy at the Institute for Anatomy: Transmission electron microscopy images (Figure 3).

Abstract

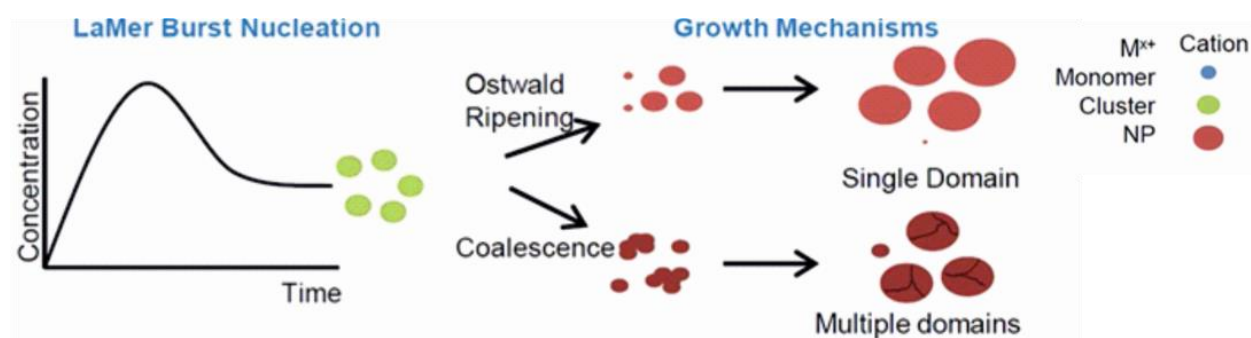
Gold nanoparticles are a fascinating colloidal material with distinct optical properties. Due to their facile and size-specific synthesis, they were often used in biomedical and drug delivery applications. But especially in the case of bio-interaction studies a profound knowledge of the particle size and the molar concentration of the nanoparticle suspension are of utmost importance. This is due to the fact that interactions between a nanomaterial and biological counterparts are highly influenced by the physico-chemical properties of the colloid.

Usually, dynamic light scattering (DLS) is applied for the determination of the hydrodynamic diameter of nanoparticles, which is presented as size distribution functions. In this chapter it is shown, that DLS at a 173° scattering angle led to a false measurement artefact in the case of citrate-reduced gold nanoparticles. Control experiments with transmission electron microscopy (TEM) proved that this artefact could be neglected. Furthermore, it is presented that the hydrodynamic diameter and the absorption of the gold nanoparticles could be used to calculate the molar extinction coefficient, which is the basis for the use of Lambert-Beer's law. Hence, combining two common analytical methods, DLS and Vis-spectroscopy, the molar concentration of a gold suspension became available, which is a requirement for any quantitative experiment at the nano-bio interface.

Introduction

Gold nanoparticles are a fascinating colloidal material and are suitable for a magnitude of applications.¹ Due to their intense red color, they are famous as stains for glass windows and were first synthesized by Faraday in 1857.^{2,3} In case of biomedical research, gold colloids are promising candidates for hyperthermic therapies⁴, as biosensors⁵ or as drug carriers^{6,7}.

There are several different synthetic routes for their fabrication available, resulting in different sizes and shapes of gold colloids.⁸ Among them, the most widespread bottom-up procedure is based on the gold salt tetrachloroauric(III) acid (HAuCl_4) and the reducing agent trisodium citrate (Na_3Cit), which also serves as the stabilizing ligand.⁹ With this protocol gold nanoparticles of a size range between 20 and 60 nm become available. Although this reaction is well known and often applied, the underlying formation mechanism is still not fully elucidated.¹⁰ Hence, depending on the reaction conditions, several variations of the classical nucleation-and-growth model^{11,12} have been reported during the last years.¹³⁻¹⁶ Most of them are variations of the classical nucleation-and-growth model as it was defined by LaMer (**Scheme 1**).¹² Here, after the nucleation step, which is the formation of particle clusters out of monomers¹², larger particles are formed either by Ostwald-ripening or by coalescence.



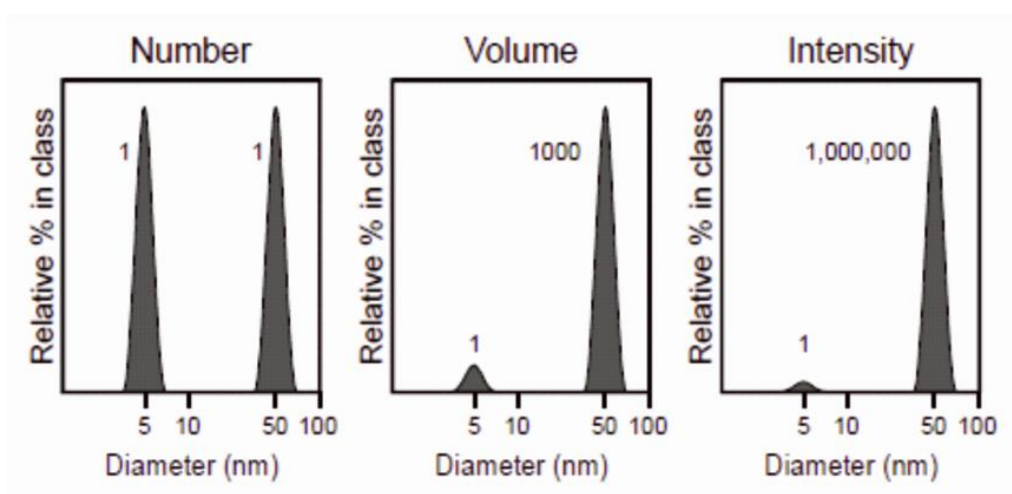
Scheme 1 Classical stages of a nucleation-and-growth mechanism. After LaMer nucleation, small clusters undergo either an Ostwald-Ripening or a coalescence step. (Reprinted (adapted) with permission from Thanh et al¹⁰. Copyright (2014) American Chemical Society)

The Ostwald-ripening is characterized by the dissolution of small nanoparticles in favor of insoluble larger particles.¹⁷ Whereas, coalescence describes the aggregation of small particles into larger species without a specific orientation.¹⁸ But independent on the reaction mechanism, the synthesis of nanoparticles always leads to a distribution of different particle sizes, which requires proper characterization.

Among several available techniques, transmission electron microscopy (TEM) and dynamic light scattering (DLS) are the two most popular methods for the characterization of gold nanoparticle size distributions. TEM is a visual technique and hence also gives a qualitative result on the shape and constitution of the colloid, despite the statistical analysis of particle sizes^{19,20}. In case of metal nanoparticles, such as gold nanoparticles, the visualization requires no special sample preparation such as contrast agents, due to the high electron density of the material.²¹ But the technique requires expensive instrumentation and is often only available as an addition to a more facile particle sizing method.

Therefore, DLS became a straight-forward method for the size-measurements at the nanoscale. Here, the scattering profile of the colloid in a liquid medium is recorded, which

requires only a few minutes of measurement time. Based on the Stokes-Einstein-equation, the mobility of the particles due to Brownian motion and hence the changes in the scattering patterns are correlated to the particle size.²² It is important to remember that for DLS, the particles are assumed to be spheres and that a correlation function is used to generate a size distribution.^{22,23}



Scheme 2 Examples for the three available particle size distributions gained from a DLS measurement. The volume and the number distribution are derived from the intensity weighted distribution. A profound evaluation of the results of all three distributions is necessary to conclude the correct particle size of the sample. (Reproduced from Zetasizer User Manual²³, Copyright (2009) Malvern Instruments)

After a DLS measurement, three different size distributions are available, which have to be evaluated carefully (**Scheme 2**). The most fundamental one is the distribution by intensity.²⁴ It is often discussed whether this distribution overweighs larger particle species, because the scattering intensity is proportional to the sixth power of the particle diameter. Hence, in a sample containing a small and large nanoparticle species, the signal for the large particles results in a high signal, while the one of the smaller particles might disappear at all.²³

An often used alternative is the number-weighted size distribution, where the particles are actually presented as their relative amount on the total sum of the particles. This distribution can easily be compared with the results obtained from microscopic methods, such as TEM, where a statistical analysis of the images is performed.²⁴ But, as the number distribution in DLS is derived from the intensity distribution this presentation might lead to incorrect results.²³ The same problem is also addressed for the volume distribution of nanoparticles.

In case of studies on nano-bio-interactions, the determination of the correct nanoparticle science is of utmost importance. For example, the association and uptake of nanoparticles by living cells are mainly determined by the physico-chemical parameters of a colloid.²⁵

In this chapter it is shown that a profound knowledge of the differences between the available size distributions is necessary to get a correct interpretation of the size of gold nanoparticles. It is further beneficial to compare the results obtained from a DLS measurement with an imaging method, such as TEM, to exclude any effects, such as multiple scattering problems or solvent effects, disturbing the accuracy of the DLS technique. This was investigated by synthesizing gold nanoparticles of different sizes, following their characterization by DLS and TEM. At the end, a solution is presented to calculate the molar extinction coefficient of gold nanoparticles based on their optical properties. This procedure is of high interest for experiments at the bio-nano-interfaces, where the molar concentration of particle suspensions has to be known.

Materials and Methods

Materials

If not otherwise stated all chemicals were purchased from Sigma-Aldrich Chemical Company (Taufkirchen, Germany). Ultrapure water was obtained using a Milli-Q-System (Merck Chemicals, Schwalbach, Germany).

Methods

Gold nanoparticles were synthesized with the citrate reduction method developed by Frens and Turkevich, whereby the ratio between the gold precursor and the reduction agent was varied.^{14,26} Hence, to a boiling solution of 0.1% (w/v) gold(III) chloride (CAS 27988-77-8, 339.8 g/mol) a variable amount of a 1% (w/v) aqueous sodium citrate trihydrate (CAS 6132-04-3, 294.1 g/mol, Merck KgGa, Darmstadt, Germany) solution were added under vigorous stirring. These conditions were kept for 10 min until the red color of the colloidal gold appeared. The reaction mixture was chilled to room temperature slowly and the gold nanoparticles were used for characterization as prepared.

The size of the gold nanoparticles was determined with transmission electron microscopy. Therefore, the gold nanoparticles were air-dried on a carbon-coated copper grid and imaged with a Philips CM 12 transmission electron microscope (Philips, Eindhoven, The

Netherlands). Here, the particle diameter was analyzed by image analysis using ImageJ 1.45s software (Rasband, W.S., ImageJ, U. S. National Institutes of Health, Bethesda, Maryland, USA, <http://imagej.nih.gov/ij/>, 1997-2014).

The hydrodynamic diameter was determined by dynamic light scattering using a Zetasizer Nano ZS (Malvern Instruments, Herrenberg, Germany). For all size measurements concerning the calculation of gold nanoparticle concentrations 173 ° backward scatter in general purpose mode was applied and the maximum peak of the intensity distribution is always stated. If indicated the scattering angle was changed to forward scatter at 12.8 °.

Vis spectrometry (UVIKON 941, Kontron, now Goebel Instrumentelle Analytik, Au/Hallertau, Germany) was used to determine the absorbance of the colloidal gold in order to calculate the extinction coefficients and the AuNP particle concentration.

The calculation of the extinction coefficients was previously reported.²⁷ Therefore, gold nanoparticles of five different sizes were synthesized and the obtained particle concentration was calculated.

Equation (1) gives the amount of gold atoms per spherical nanoparticle, N , of a distinct size with σ as the density of bulk gold in a face-centered cubic ($\sigma = 19.3 \text{ g/cm}^3$) and M as the atomic weight of gold ($M = 197 \text{ g/mol}$).

$$N = \frac{\pi}{6} \times \frac{\sigma D^3}{M} \quad (1)$$

The molar concentration, C , of synthesized nanoparticles was calculated with equation (2), where N_{total} is amount of gold atoms, which were added to the reaction mixture, V is the volume of the reaction mixture in liter and N_A is Avogadro's constant.

$$C = \frac{N_{total}}{N V N_A} \quad (2)$$

Based on this molar concentration a dilution series was performed and its absorption at 506 nm was measured. The slope of the linear regression of absorption versus concentration was the molar extinction coefficient, ϵ . The natural logarithm of ϵ was plotted against the logarithm of the particle size to give a linear fit. The obtained linear regression function could be used to calculate all further ϵ for gold nanoparticle suspensions of a known size and its concentration could be calculated with Lambert-Beer's law.

Results and Discussion

Gold nanoparticle synthesis

Gold nanoparticles are a well investigated colloidal material with fascinating properties.¹ The classical and most often used synthesis procedure is the Turkevich citrate-reduction method, where the precursor salt HAuCl_4 is reduced to elemental gold by sodium citrate (Na_3Cit) upon formation of gold nanoparticles.¹⁴

Frens reported in the early 1970`s that the size of the resulting particles can be adjusted by the ratio of the precursor salt and the reducing agent.²⁶ Doing this, gold nanoparticles between 20 and 50 nm were obtained and upon variation of $\text{HAuCl}_4:\text{Na}_3\text{Cit}$ up to a 10-fold molar excess of the Na_3Cit an interesting trend was observed (**Figure 1**). The hydrodynamic diameter of the nanoparticles first decreased with increasing amount of the reducing agent, but turned back to larger particles for ratios larger than 1:5 (**Figure 1**). Hence, the upper and lower size limits of the resulting particles were determined. Particles smaller than 20 nm were not obtained by further increasing the amount of Na_3Cit . Additionally, synthesizing particles larger than 60 nm was troublesome, because of a deficit of Na_3Cit . As Na_3Cit is not only the reducing agent but also the stabilizing ligand of the final particles, a low amount of this compound is critical for the colloidal stability and therefore the tendency against aggregation increased. Nevertheless, gold nanoparticles beyond these size boundaries are available by other synthesis routes. For example, the Brust-Shiffrin method is a two-phase synthesis leading to particles smaller than 10 nm.²⁸ Alternatively particles of lower sizes can be obtained by a stronger

reducing agent such as sodium borohydride.²⁹ On the other hand, larger gold nanoparticles are available with different seeding-growth strategies, where a particle species of a smaller size is added to the reaction mixture to further grow to larger sizes.³⁰ But as the gold nanoparticles synthesized here were intended for the use as Layer-by-Layer substrates and cellular studies, an available size window between 20 and 60 nm agreed well with the experimental necessities.

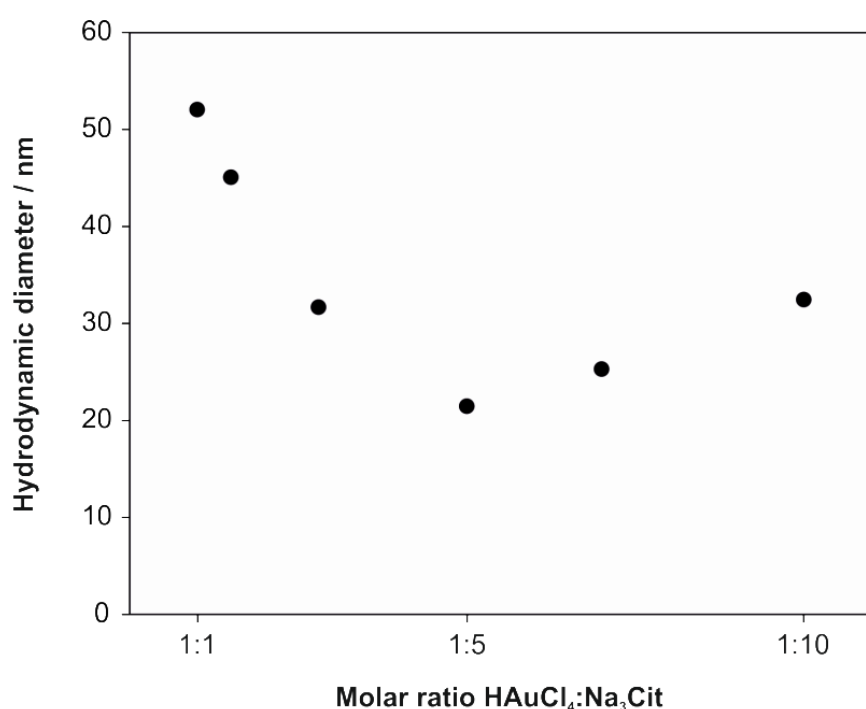


Figure 1 The resulting size of gold nanoparticles depended on the ratio of the gold precursor, HAuCl₄ and the reducing agent, Na₃Cit. A transition point of the size trend occurred at the ratio of 1:5, which is due to a changing reaction mechanism.

To explain the unusual trend of the sizes available by the citrate-reduction method, one has to consider the underlying reaction mechanism, which is still under scientific discussion. Especially the role of Na₃Cit is still unclear.¹⁰ Polte et al. proposed a four-step mechanism, where the precursor is consumed over time and particles develop in a classical nucleation-and-growth mechanism.¹⁵ But, here the particles would get smaller with increasing amount of Na₃Cit, because of the increasing formation of starting nuclei.¹⁵ Hence, a further function of citrate has to be considered and Ji and Peng showed that Na₃Cit also has an important impact

on the pH of the reaction mixture.¹⁶ At a distinct pH threshold the reaction mechanism most likely changes from nucleation-and-growth to a nucleation-aggregation-smoothing mechanism.¹⁶ This change of the reaction mechanism appeared also at a precursor to citrate ratio of approximately 1:5 and confirms the observed phenomenon.¹⁶

Characterization of gold nanoparticles

A facile and reproducible method for the size characterization of nanoparticles is dynamic light scattering, which is also called photon correlation spectroscopy. Here, the number of scattered photons is correlated with the diffusion coefficient and hence the size of the nanoparticles, which is presented as size distribution curves or histograms. Two intensity distributions of two different gold synthesis (Syn A and B) are shown in **Figure 2A**.

For a single species of spherical particles also a single peak in DLS corresponding to their hydrodynamic diameter was assumed. But instead, two maxima were found, indicating a second particle species to be present. The maxima of the main peak were 31.7 nm (Syn A) and 54.4 nm (Syn B), respectively, and the second maxima were found at 1.6 nm and 4.7 nm, respectively. But the use of the intensity distribution has some typical drawbacks, such as the tendency to overweigh larger particles. Hence, the number distribution is more commonly used instead. But in this case, it made no sense to convert the intensity distribution into the number-weighted values. The obtained number distribution showed only the lower weight maximum between 1 and 10 nm, due to an overestimation of small nanoparticles. The former main maximum, which was assumed to represent the synthesized nanoparticles, disappeared completely (**Figure 2B**).

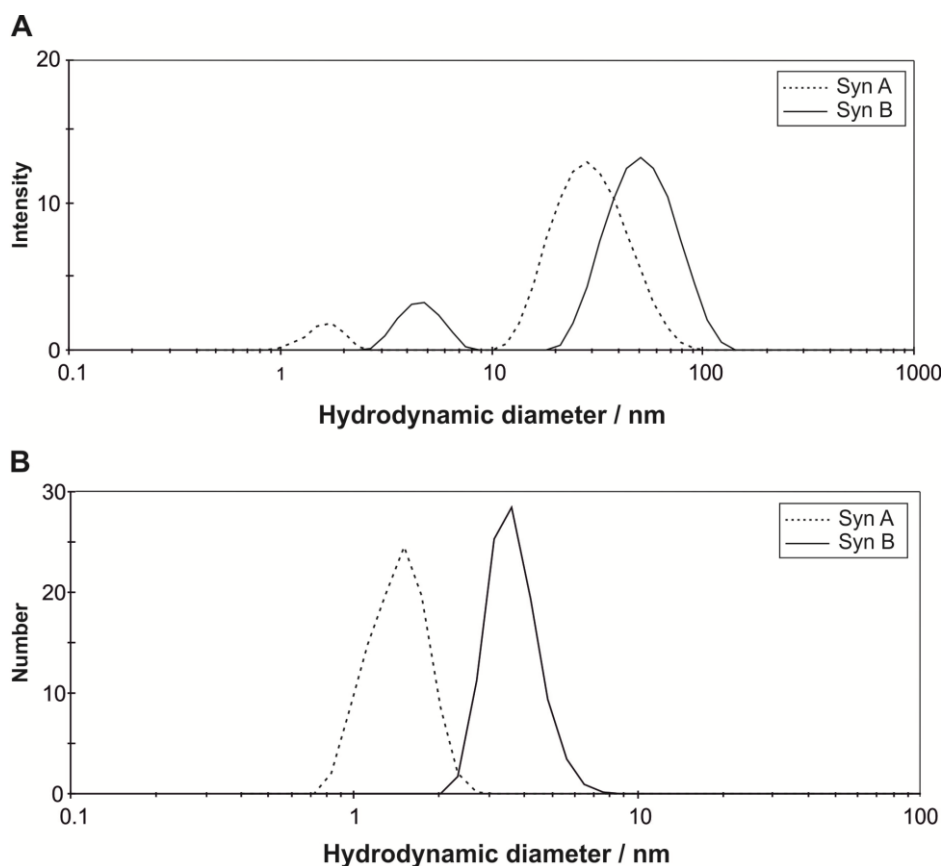


Figure 2 Dynamic light scattering is a standard method for the measurement of the hydrodynamic diameter of colloids. Usually the size distribution by intensity (**A**) or by number (**B**) is stated. But in case of gold nanoparticles an additional peak between 1 and 5 nm was visible which disturbs the calculation of the number distribution. Hence, the value of the main peak in the intensity distribution was always stated as the hydrodynamic diameter resulting in 31.7 nm (Syn A) and 54.4 nm (Syn B).

To confirm the assumption that the lower size peak corresponds to an artefact and the larger one to the actual particle size and to prove the actual size of the gold nanoparticles an imaging method was chosen. As gold nanoparticles have a high electron density, they can easily be imaged by TEM with only minimal preparatory effort. The gold nanoparticles were visible as dark black nanoparticles with a good contrast to the background (**Figure 3**). The particles of Syn A were found to be monodisperse and spherical with an average diameter of 18.0 ± 5.4 nm (**Figure 3A**). The lower size value compared to the DLS result is due to the difference

between the isolated particle size and the hydrodynamic diameter that takes adsorbed water molecules into account.

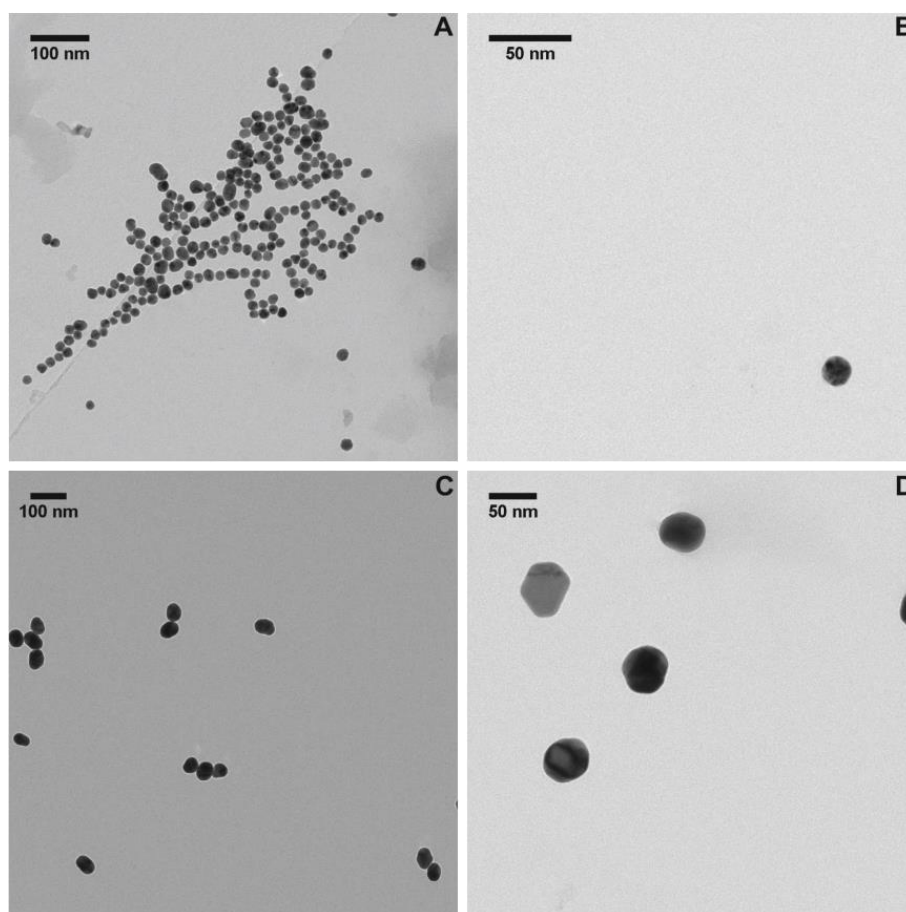


Figure 3 TEM images were taken to evaluate the size and the shape of Syn A (**A and B**) and Syn B (**C and D**). The determined sizes were 18.0 ± 5.4 nm for Syn A and 43.6 ± 4.6 nm for Syn B respectively, which are in good agreement to the maximum of the DLS intensity distribution. All particles could be regarded as monodisperse, although the larger particles showed a tendency to an elliptical shape. In the images of higher resolution (**B and D**) no small particles of the size of the low size peak of the intensity distributions of the hydrodynamic diameter could be detected.

Also a high resolution image did not show any smaller particles which would match to the low-size maximum of 1.6 nm, which was found in the intensity distribution of DLS (**Figure**

3B). The same result was also found for the larger particle species of Syn B (**Figure 3C**). Here, the lower sized particle fraction of the DLS measurement had a hydrodynamic diameter of 5.6 nm. Hence, this particle size should have been detectable with TEM, but no particles corresponding to this size were observed. Additionally, the larger particles of Syn B, clearly showed a tendency towards an elliptical shape instead of spheres, leading to a rod-like shape in three-dimensions.

Now, why does the rather reliable DLS measurement show a second particle species, which could not be detected in TEM?

First, rod-like nanoparticles, having two geometrical axes, also show two maxima in a DLS experiment, corresponding to the transversal and rotational translocation. Together with the finding of more rod-like than spherical gold nanoparticles this might be an explanation. But then, why did this phenomenon not appear in early literature, although citrate-reduced gold nanoparticles were often characterized with DLS, before? Khlebtsov attributed this phenomenon to a technical specification of the often used Zetasizer Nano ZS, a DLS instrument which became popular during the last 5 years: Compared to other convenient DLS devices or older Zetasizer models, the new Zetasizer Nano ZS does not apply a 90° rectangular scattering angle, but a 173° backward angle.^{23,31} A fact which makes the instrument on one hand very sensitive for small nanoparticle sizes and on the other hand larger particle aggregates are less detected with this set-up.²³

But, in combination with the high scattering properties of gold, this technique was assumed to be a drawback. The shorter geometrical axes and its rotational translocation of the not perfectly spherical gold nanoparticles appeared in this measurement settings.³¹ Khlebtsov further gives an approach to circumvent this effect and suggests using the also available 12.8° forward scatter instead.³¹

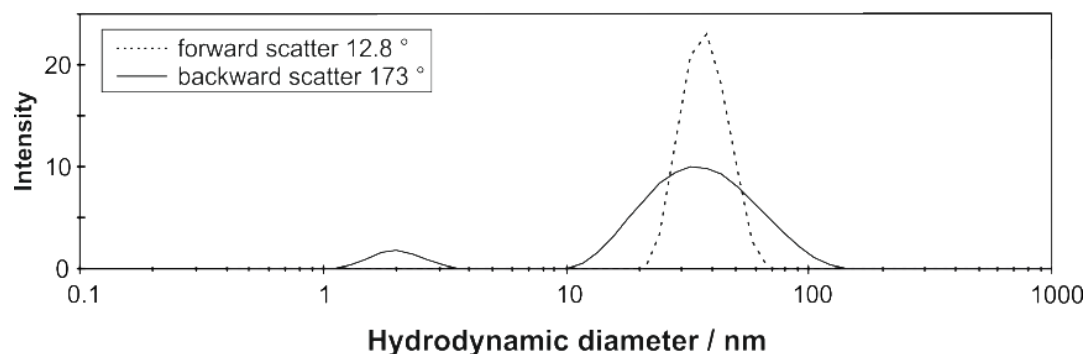


Figure 4 At the use of forward scatter at 12.8° instead of backward scatter 173° the additional peak at low diameters disappeared. The maximum of the intensity distributions were 40.4 nm in for the backward scatter and 38.0 nm in case of forward scatter. This variation seemed to be a valuable alternative for the size characterization of AuNP using the Zetasizer Nano ZS.

As shown in **Figure 4** the lower size fraction disappeared and the particle distribution became narrower, which was in agreement to the findings of Khlebtsov³¹. The obtained hydrodynamic diameters when determined at the maxima of the intensity distributions, were comparable with 38.0 nm and 40.4 nm for the forward scattering instead of the backward angle. Hence, this technical modification seemed to be a valuable improvement for the size characterization of gold nanoparticles by DLS. But, further comparison measurements on LbL coated nanoparticles relativized the applicability of the forward angle. Due to the coating protocol with its repetitive centrifugation steps, a moderate amount of aggregated particles is unavoidable and in those cases the particle diameters got overestimated by the use of the 12.8° measurement settings. Hence, it was decided to still state the maximum of the intensity distribution, determined at the 178° scattering angle to be the hydrodynamic diameter of the synthesized gold nanoparticles and to neglect the additional peak at low size values.

Calculation of the concentration of AuNP suspensions

The molar concentration of a compound is a standard unit for chemical reactions and has to be known to get quantitative results of an experiment. But in case of nanoparticles this simple parameter often is not available. An often applied approach is the determination of the chemical composition of a colloidal sample by inductively coupled plasma optical emission spectrometry (ICP-OES) or inductively coupled plasma mass spectrometry (ICP-MS). Both methods are very sensitive, especially for the quantification of heavy metals, but the techniques usually require the destruction of the sample and advanced instrumentation. Hence, an alternative without the loss of the sample was desired.

Table 2 Calculated molar extinction coefficients for AuNP of different sizes.

Hydrodynamic diameter (d) / nm	ln (d)	Molar extinction coefficient (ϵ) / $l \text{ mol}^{-1} \text{ cm}^{-1}$	ln (ϵ)
25.00	3.22	1.54E+09	21.15
36.00	3.58	4.87E+09	22.31
38.00	3.64	4.62E+09	22.25
47.00	3.85	1.16E+10	23.18
62.00	4.13	1.91E+10	23.67

In case of gold nanoparticles a special property of the material can be used to calculate the concentrations of gold nanoparticle suspensions.^{27,32} Due to its surface plasmon effect, gold nanoparticles show a brilliant red color. The absorption maximum usually lies between 520

and 550 nm and shifts to red with larger particle sizes.³³⁻³⁵ But, to calculate the concentration of an unknown gold nanoparticle suspension using the rule of Lambert-Beer, the extinction coefficient has to be known first.

Therefore, a combined calculation and experimental procedure was performed.²⁷ Several concentration series of gold nanoparticle suspensions of different sizes were prepared and their extinction coefficients calculated. These extinction coefficients were in the range of 1.5×10^9 and $1.9 \times 10^{10} \text{ l mol}^{-1} \text{ cm}^{-1}$, depending on the particle size (**Table 2**). Altogether, those molar extinction coefficients were extraordinary high, compared to convenient organic dyes. For example, Ponceau 4R (E 124) a red azo dye, and a food additive only has a molar extinction coefficient of $1.27 \times 10^4 \text{ l mol}^{-1} \text{ cm}^{-1}$.³⁶

The obtained exponential correlation between particle size and extinction coefficient was linearized by a double-logarithmic plot, resulting in an equation for the calculation of the extinction coefficient at a known particle size (**Figure 5**).

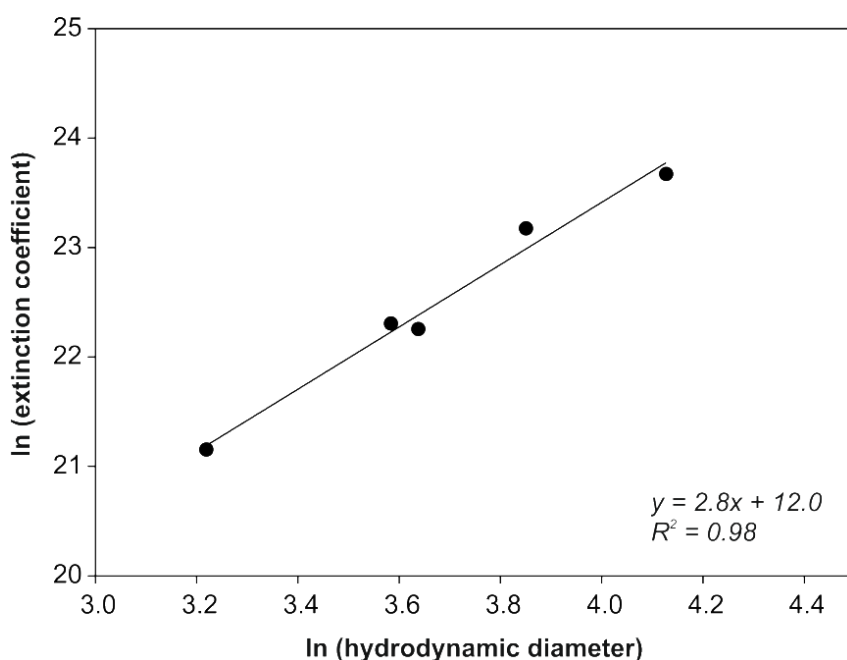


Figure 5 Linear regression of the determined extinction coefficient and the hydrodynamic diameter. The extinction coefficient obtained by this correlation could be used for the calculation of AuNP concentrations after Lambert-Beer's law.

This procedure was previously applied by Liu et al., where the actual particle size, determined from TEM imaging was used instead of the hydrodynamic diameter.²⁷ But, here it was shown that the hydrodynamic diameter, determined from the intensity distribution, also gives a good linear correlation and the deviation to the linear regression parameters determined by Liu are tolerable. Furthermore Liu et al. also reported that the same equation can also be used for gold nanoparticles carrying a different capping ligand instead of citrate.²⁷ In terms of a Layer-by-Layer coating it was followed that the once determined size-dependent equation was also suitable for polymer coated gold nanoparticles. Because of the repetitive washing steps of a Layer-by-Layer protocol, the knowledge of the final particle concentration is of high importance for the set-up of following experiments (see **Chapter 4**).

Conclusion

A profound knowledge of the physico-chemical properties of colloids is the basis for further studies on their size-dependent interaction with biological systems, such as cells or biological matrices. Therefore, the techniques to characterize the size of gold nanoparticles were evaluated carefully. The maximum of the intensity distribution obtained from dynamic light scattering agreed well with the actual particle size determined by TEM. It was found that a measurement artefact, which resulted from the elliptical shape and the high scattering capacity of gold nanoparticles in combination with the backward scattering angle, can be neglected. Upon synthesis of gold nanoparticles of different sizes an interesting trend was observed, which was attributed to a change in the reaction mechanism of the citrate-reduction method. Furthermore, a linear correlation between the hydrodynamic diameter and the extinction coefficient was confirmed. Hence, the combined use of two standard laboratory instruments, a dynamic light scattering device and a common UV-Vis photometer, allowed the fast and convenient determination of the molar concentrations of gold nanoparticle suspensions.

References

- (1) Daniel, M. C.; Astruc, D. Gold Nanoparticles: Assembly, Supramolecular Chemistry, Quantum-Size-Related Properties, And Applications Toward Biology, Catalysis, And Nanotechnology. *Chem. Rev.* **2004**, *104*, 293-346.
- (2) Ozin, G. A.; Cademartiri, L. Chapter 3 Gold. In *Concepts of Nanochemistry*; Wiley-VCH-Verlag: Weinheim, 2009; pp. 85-111.
- (3) Faraday, M. The Bakerian Lecture: Experimental Relations Of Gold (And Other Metals) To Light. *Philos. Trans. R. Soc. London* **1857**, *147*, 145-181.
- (4) Lal, S.; Verma, J.; van Noorden, C. J. F. Nanoparticles For Hyperthermic Therapy: Synthesis Strategies And Applications In Glioblastoma. *Int. J. Nanomed.* **2014**, *10*, 2863-2877.
- (5) Holzinger, M.; Le Goff, A.; Cosnier, S. Nanomaterials For Biosensing Applications: A Review. *Front. Chem.* **2014**, *2*, 63.
- (6) Han, G.; Ghosh, P.; de M.; Rotello, V. Drug And Gene Delivery Using Gold Nanoparticles. *NanoBioTechnology* **2007**, *3*, 40-45.
- (7) Cao-Milán, R.; Liz-Marzán, L. M. Gold Nanoparticle Conjugates: Recent Advances Toward Clinical Applications. *Expert Opin. Drug Delivery* **2014**, *11*, 741-752.
- (8) Nguyen, D. T.; Kim, D.; Kim, K. Controlled Synthesis And Biomolecular Probe Application Of Gold Nanoparticles. *Micron* **2011**, *42*, 207-227.
- (9) Enüstün, B. V.; Turkevich, J. Coagulation Of Colloidal Gold. *J. Am. Chem. Soc.* **1963**, *85*, 3317-3328.
- (10) Thanh, N.; Maclean, N.; Mahiddine, S. Mechanisms Of Nucleation And Growth Of Nanoparticles In Solution. *Chem. Rev.* **2014**, *114*, 7610-7630.
- (11) LaMer, V. K. Nucleation In Phase Transitions. *Ind. Eng. Chem.* **1952**, *44*, 1270-1277.

- (12) LaMer, V. K.; Dinegar, R. H. Theory, Production And Mechanism Of Formation Of Monodispersed Hydrosols. *J. Am. Chem. Soc.* **1950**, *72*, 4847-4854.
- (13) Pong, B.; Elim, H. I.; Chong, J.; Ji, W.; Trout, B. L.; Lee, J. New Insights On The Nanoparticle Growth Mechanism In The Citrate Reduction Of Gold(III) Salt: Formation Of The Au Nanowire Intermediate And Its Nonlinear Optical Properties. *J. Phys. Chem. C* **2007**, *111*, 6281-6287.
- (14) Turkevich, J.; Stevenson, P.; Hillier, J. A Study Of The Nucleation And Growth Processes In The Synthesis Of Colloidal Gold. *Discuss. Faraday Soc.* **1951**, *11*, 55-75.
- (15) Polte, J.; Ahner, T. T.; Delissen, F.; Sokolov, S.; Emmerling, F.; Thunemann, A. F.; Kraehnert, R. Mechanism Of Gold Nanoparticle Formation In The Classical Citrate Synthesis Method Derived From Coupled In Situ XANES And SAXS Evaluation. *J. Am. Chem. Soc.* **2010**, *132*, 1296-1301.
- (16) Ji, X.; Song, X.; Li, J.; Bai, Y.; Yang, W.; Peng, X. Size Control Of Gold Nanocrystals In Citrate Reduction: The Third Role Of Citrate. *J. Am. Chem. Soc.* **2007**, *129*, 13939-13948.
- (17) Ostwald, W. On The Supposed Isomerism Of Red And Yellow Mercury Oxide And The Surface Tension Of Solid Substances. *Zeitschrift für Physikalische Chemie* **1900**, *34*, 495.
- (18) Zheng, H.; Smith, R. K.; Jun, Y. -.; Kisielowski, C.; Dahmen, U.; Alivisatos, A. P. Observation Of Single Colloidal Platinum Nanocrystal Growth Trajectories. *Science* **2009**, *324*, 1309-1312.
- (19) Pyrz, W. D.; Buttrey, D. J. Particle Size Determination Using TEM: A Discussion Of Image Acquisition And Analysis For The Novice Microscopist. *Langmuir* **2008**, *24*, 11350-11360.
- (20) Sun, Y.; Xia, Y. Shape-Controlled Synthesis Of Gold And Silver Nanoparticles. *Science* **2002**, *298*, 2176-2179.
- (21) Horisberger, M.; Rosset, J. Colloidal Gold, A Useful Marker For Transmission And Scanning Electron Microscopy. *J. Histochem. Cytochem.* **1977**, *25*, 295-305.
- (22) Brar, S. K.; Verma, M. Measurement Of Nanoparticles By Light-Scattering Techniques. *TrAC, Trends Anal. Chem.* **2011**, *30*, 4-17.

- (23) Zetasizer Nano User Manual; MAN0317; 2009 ed.; Malvern Instruments, 2009; pp. 13-7 f.
- (24) Kato, H.; Suzuki, M.; Fujita, K.; Horie, M.; Endoh, S.; Yoshida, Y.; Iwahashi, H.; Takahashi, K.; Nakamura, A.; Kinugasa, S. Reliable Size Determination Of Nanoparticles Using Dynamic Light Scattering Method For In Vitro Toxicology Assessment. *Toxicol. In Vitro* **2009**, *23*, 927-934.
- (25) Chithrani, B. D.; Ghazani, A. A.; Chan, W. C. Determining The Size And Shape Dependence Of Gold Nanoparticle Uptake Into Mammalian Cells. *Nano Lett.* **2006**, *6*, 662-668.
- (26) Frens, G. Controlled Nucleation For Regulation Of Particle-Size In Monodisperse Gold Suspensions. *Nature (London), Phys. Sci.* **1973**, *241*, 20-22.
- (27) Liu, X.; Atwater, M.; Wang, J.; Huo, Q. Extinction Coefficient Of Gold Nanoparticles With Different Sizes And Different Capping Ligands. *J. Colloids Surf. B* **2007**, *58*, 3-7.
- (28) Brust, M.; Walker, M.; Bethell, D.; Schiffrin, D. J.; Whyman, R. Synthesis Of Thiol-Derivatised Gold Nanoparticles In A Two-Phase Liquid-Liquid System. *J. Chem. Soc., Chem. Commun.* **1994**, 801-802.
- (29) Green, M.; O'Brien, P.; O'Brien, P. A Simple One Phase Preparation Of Organically Capped Gold Nanocrystals. *Chem. Commun.* **2000**, 183-184.
- (30) Carrot, G.; Valmalette, J.; Plummer, C. Gold Nanoparticle Synthesis In Graft Copolymer Micelles. *Colloid Polym. Sci.* **1998**, *276*, 853-859.
- (31) Khlebtsov, B. N.; Khlebtsov, N. G. On The Measurement Of Gold Nanoparticle Sizes By The Dynamic Light Scattering Method. *Colloid J.* **2011**, *73*, 118-127.
- (32) Haiss, W.; Thanh, N. T.; Aveyard, J.; Fernig, D. G. Determination Of Size And Concentration Of Gold Nanoparticles From UV-Vis Spectra. *Anal. Chem.* **2007**, *79*, 4215-4221.
- (33) Kelly, K. L.; Coronado, E.; Zhao, L. L.; Schatz, G. C. The Optical Properties Of Metal Nanoparticles: The Influence Of Size, Shape, And Dielectric Environment. *J. Phys. Chem. B* **2003**, *107*, 668-677.

(34) Kimling, J.; Maier, M.; Okenve, B.; Kotaidis, V.; Ballot, H.; Plech, A. Turkevich Method For Gold Nanoparticle Synthesis Revisited. *J. Phys. Chem. B* **2006**, *110*, 15700-15707.

(35) Jain, P. K.; Lee, K. S.; El-Sayed, I. H.; El-Sayed, M. A. Calculated Absorption And Scattering Properties Of Gold Nanoparticles Of Different Size, Shape, And Composition: Applications In Biological Imaging And Biomedicine. *J. Phys. Chem. B* **2006**, *110*, 7238-7248.

(36) Ryvolová, M.; Táborský, P.; Vrábel, P.; Krásenský, P.; Preisler, J. Sensitive Determination Of Erythrosine And Other Red Food Colorants Using Capillary Electrophoresis With Laser-Induced Fluorescence Detection. *J. Chromatogr. A* **2007**, *1141*, 206-211.

Chapter 3:

Layer-by-Layer assembled gold nanoparticles

for the delivery of nucleic acids

in Nanotechnology For Nucleic Acid Delivery: Methods And Protocols (Eds.: M. Ogris,
D. Oupicky), Methods In Molecular Biology, 2013, pp. 171-182.

Abstract

The delivery of nucleic acids to mammalian cells requires a potent particulate carrier system. The physico-chemical properties of the used particles, such as size and surface charge, strongly influence the cellular uptake and thereby the extent of the subsequent biological effect. However the knowledge of this process is still fragmentary because heterogeneous particle collectives are applied. Therefore we present a strategy to synthesize carriers with a highly specific appearance on the basis of gold nanoparticles (AuNPs) and the Layer-by-Layer (LbL) technique. The LbL method is based on the alternate deposition of oppositely charged (bio-)polymers, in our case poly(ethylenimine) (PEI) and nucleic acids. The size and surface charge of those particles can be easily modified and accordingly systematic studies on cellular uptake are accessible.

Introduction

The introduction of nucleic acids into mammalian cells is a promising approach for the treatment of genetic diseases. Those strategies need a potent carrier system, so called vector, to transport nucleic acids (DNA or RNA). But, there are three major challenges a gene delivery system has to overcome: First, the nucleic acids have to be protected against the degradation by nucleases. Second, the cellular barriers, membranes and endosome, have to be crossed. And finally, the carrier itself should be toxicological and immunological inert.^{1,2}

A promising alternative to viral gene vectors are complexes of positively charged polymers or lipids and negatively charged nucleic acids. A big disadvantage of those particle collectives is that they are usually heterogeneous in size and surface charge, which are the main properties influencing the cellular uptake. Consequently, systematic studies to investigate the relationship between physicochemical particle properties and the endocytotic pathways into the cells as well as the intracellular fate of the gene vectors are nearly impossible. That is why we decided to engineer a novel gene carrier system with a highly specific appearance: The size and the shape of the particles are defined by a solid core of gold nanoparticles (AuNPs). The charge of the particles is affected by charged polymers which are deposited on the particles surface in a highly ordered manner.

In this methodology chapter we would like to introduce you to a novel gene delivery strategy on the basis of nanoparticles which are specific in size, shape and surface charge.

Layer-by-Layer (LbL)

The basic principle of the Layer-by-Layer idea is the self-assembly, that means the autonomous organization³ of oppositely charged polyelectrolytes and was introduced by Gero Decher and colleagues 20 years ago.⁴ Since that time Layer-by-layer (LbL) assemblies have entered various scientific fields, from materials science⁵ and physical chemistry⁶ to electrochemistry⁷ and biomedical engineering⁸. The fundamental concept is the electrostatic interaction of positively and negatively charged polymers, namely polycations and polyanions. The alternation of oppositely charged polymers results in a stable nanoscale film coating on a flat or curved template.⁹ The characteristics of those films can be tailored with nanometer precision with each layer. The popularity of LbL approaches in biomedical research is also due to the fact that biological components can be integrated into LbL systems under physiological conditions only by electrostatic interactions that means under conservation of the native structure.

In the field of drug delivery research there are two major approaches for LbL-based particles: On one hand there are hollow microcapsules, constructed of a dissolvable core with a shell of LbL-assembled polyelectrolytes. Here, the drug is encapsulated into the interior of the hollow sphere before or after destruction of the core material. Those microcapsules are in the size range of several micrometers in diameter.^{10,11} They can be characterized by light microscopy and imaging but their biological applications are limited, because only a few cell types are able to process microparticles. On the other hand, there are core/shell particles, consisting of a solid core, coated with a shell of multilayers. In this case, the active substance can be part of the shell-multilayer.¹² LbL assembled nanoparticles are much more relevant as drug carriers because they can be applied into the bloodstream and uptaken by various cell types via endocytosis.

Gold nanoparticles (AuNPs)

Gold nanoparticles (AuNPs) are widely used metal nanoparticles for biological and biomedical purposes. Due to the easy synthesis and outstanding physical properties of colloidal gold, the applications reach from molecular imaging and diagnostics, to functional bioconjugates, treatment of cancer, and up to drug delivery strategies.^{13,14} Of course, gold atoms carry a high electron density which makes them suitable for the detection in Transmission Electron Microscopy (TEM).¹⁵ Even more important is the phenomenon of the surface plasmon resonance: Electromagnetic waves are absorbed and scattered effectively, if the wavelength hits the resonance frequency of the electron clouds surrounding the gold atoms. According to the Mie Theory, the plasmon resonance frequency is influenced by the size and the shape of the particle and by the dielectric constant of the medium.¹⁶ Therefore, suspensions of spherical gold nanoparticles show absorption of light in the region from 510 to 540 nm. The absorption spectra of colloidal gold can be tuned to the red and near-infrared (NIR) spectra, the so called “water window”, where no absorption of biological materials occurs. This is the basis for most imaging and diagnosis applications using AuNPs. Plasmon resonance is also the physical background of the hyperthermia treatment of cancer, where AuNPs emit absorbed light as heat energy.¹⁷

Chemical features are also important for the wide distribution of AuNPs. Gold surfaces can easily be modified because of a high affinity to soft bases, such as thiol groups.¹⁸ Alkanethiols form a stable self-assembled monolayer around the gold core. The mechanism of this interaction is still under discussion, but probably relies on the interaction of thiolate ions and oxidized Au⁺ ions on the particle surface. In the case of alkanethiols with further reactive head groups, e.g. carboxylic acids, the particle surface can easily be functionalized. This opportunity opens the door for a large number of bioconjugation strategies.¹⁹

Layer-by-layer modified gold nanoparticles

The versatility of the LbL surface modifications is applied to AuNPs in our studies. Those strategies have been published earlier²⁰, but not in combination with nucleic acids in the shell of LbL-AuNPs.

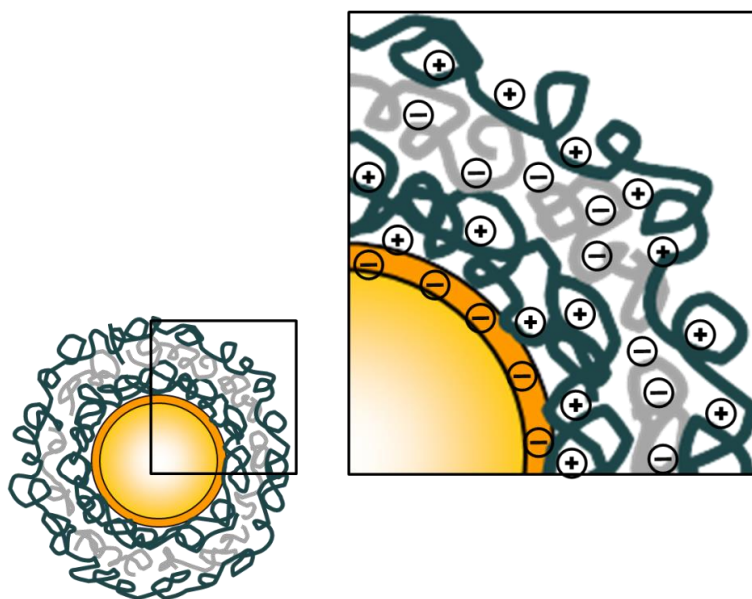


Figure 1 Core shell gold nanoparticles consist of a solid gold core and four layers. The first layer is the stabilizing agent MUA which conserves a negative charge on the particle surface. The positively charged layer of PEI is followed by the negatively charged nucleic acid. The nucleic acids are protected by a last layer of PEI.

The core-shell AuNPs for nucleic acid delivery consist of four polymer layers deposited on a gold core (**Figure 1**). Gold was chosen as the size template for several reasons: The physical properties of gold allow the detection of the deposition of polymer layers by vis-spectroscopy. The coating process can be monitored because of a red shift of the plasmon absorption band. It is therefore also possible identify particle aggregation during polymer deposition triggered

by the change of salt concentrations or purification conditions. Additionally gold nanoparticles are visible by transmission TEM with a high contrast because of their large electron density. TEM is therefore a useful tool to determine the amount and location of particles which have been endocytosed by cells.

The first layer which is deposited on the gold surface is the stabilizing agent mercaptoundecanoic acid (MUA). The thiol group binds fairly stable to the gold core and the deprotonated carboxylic group introduces a negative charge on the particle surface.²¹ This step is important to avoid aggregation of the particles and to get a stable adherence of the following polyelectrolyte layers. The basis for the nucleic acid delivery with our particles is poly(ethylenimine) (PEI) which is known to be an effective transfection agent.^{22,23} PEI consists of primary, secondary and tertiary amino groups which can be protonated and therefore carry a positive charge. This is important for the deposition of negatively charged nucleic acids and may also be responsible for the endosomal escape after cellular uptake²⁴. Accordingly PEI forms the second layer of the LbL core/shell particles, followed by the layer of negatively charged nucleic acids and a second layer of PEI as the outer shell. We could show that the last layer of PEI is essential to get a biological effect, in our case a transfection effect, with these particles and assume that it is necessary to avoid degradation of the nucleic acids.²⁵

In this methodology chapter we describe a strategy to get size and charge specific particles for the cellular delivery of nucleic acids. It is noteworthy that this strategy is not a general protocol which can easily be conferred to other polymers and nucleic acid sequences. The coating of nanoparticles is challenging because of aggregation of small particles and coating conditions have to be adjusted for each case.

Materials

Synthesis of Gold Nanoparticles (AuNPs)

1. 100 ml three neck round bottom flask and elliptic stir bar, thoroughly rinsed with aqua regia and distilled water (see Note 1).
2. Oil bath and condenser.
3. H₂AuCl₄-solution (stock solution 1% w/v).
4. Sodium citrate solution (stock solution 1% w/v).

Stabilization of AuNPs with MUA (AuNP_MUA)

1. Colloidal gold suspension.
2. MUA (stock solution: 20 mg/ml).
3. 1 mM sodium hydroxide solution, pH-Meter.
4. Snap cap vials, stir plate and stir bars.
5. 2ml Eppendorf tubes and centrifuge for purification.
6. Distilled water for resuspension of the nanoparticles.

Coating with PEI (AuNP_MUA_PEI)

1. Stabilized gold nanoparticles.
2. PEI (molecular weight: 25 kDa, stock solution: 10 mg/ml).

3. Snap cap vials, stir plate and stir bars.
4. 2ml Eppendorf tubes and centrifuge for purification.
5. 1mM sodium chloride solution.

Coating with Nucleic Acids (AuNP_MUA_PEI_DNA/RNA)

1. Gold nanoparticles coated with PEI.
2. DNA or RNA stock solution (100 μ M).
3. Snap cap vials, stir plate and stir bars.
4. Eppendorf tubes and centrifuge for purification.
5. 1 mM sodium chloride solution.

Characterization by Dynamic Light Scattering, electrophoretic mobility and UV-Vis spectrometry

1. Characterization of the particles by dynamic light scattering and electrophoretic mobility (Zeta-Potential) was performed on a Zetasizer Nano ZS (Malvern Instruments).
2. UV-Vis- Spectra were measured with a Uvikon 900 double beam photometer (Kontron Instruments).

Characterization by TEM

1. Transmission electron micrographs were taken on a Philips CM 12 microscope (FEI, Eindhoven, Netherlands).
2. Carbon-coated copper grids, pretreated in a plasma beam.

3. Image J-software for statistical analysis of TEM micrographs.

Methods

Preparation of AuNPs

1. AuNPs are prepared according to the method published by Frens²⁶. The size of the particles can be adjusted by variation of the HAuCl₄ to sodium citrate ratio. The preparation described here, resulted in particles of about 50 nm in diameter. 25 ml of a 0.01% HAuCl₄ solution is prepared in a three neck round bottom flask with a condenser. The solution is heated to 100 °C in an oil bath and stirred vigorously. 180µl of the sodium citrate solution (stock solution 1% w/v) is added to the reaction mixture and heating is continued until the color changed from pale yellow to dark red. This indicates the formation of AuNPs. The AuNPs obtained from this synthesis are stabilized by a shell of citrate ions preventing aggregation of the particles. The suspension can be stored over months if they are not purified by dialysis or centrifugation.

Stabilization with MUA (AuNP_MUA)

1. The AuNPs are further stabilized by MUA. Gold surfaces show a stable affinity to sulfur groups, such as thiols and disulfides. MUA consists of a thiol group and a deprotonated carboxylic acid group. This conserves a stable negative charge on the particle surface, which cannot be displaced like the citrate ligands (**Figure 2**).

This negative charge is important for the stability of the particle suspension and avoids aggregation and is the basis for the deposition of positively charged polymer layers on the surface.

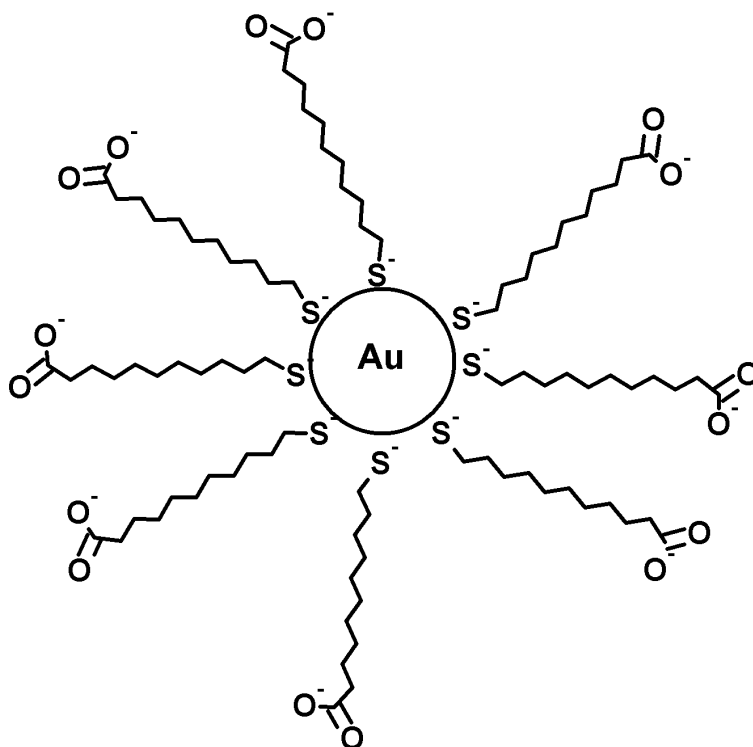


Figure 2 Schematic figure of gold nanoparticle cores stabilized by MUA. The specific interaction of thiol groups displaces the stabilizing cap of citrate ions. The negative charge of the deprotonated carboxylic acid group conserves a negative charge on the particle surface which is the basis for the further deposition of positive charged polymers and prevents aggregation by electrostatic repulsion.

2. The pH of the nanoparticle suspension is adjusted to pH 11 with 1 mM NaOH.

MUA is added under stirring to give a final concentration of 0.1 mg/ml. Stirring is continued over three days to give a stable surface modification. The particles are purified by centrifugation to remove the excess of MUA, which interferes with the charged polymers in the next layer deposition steps.

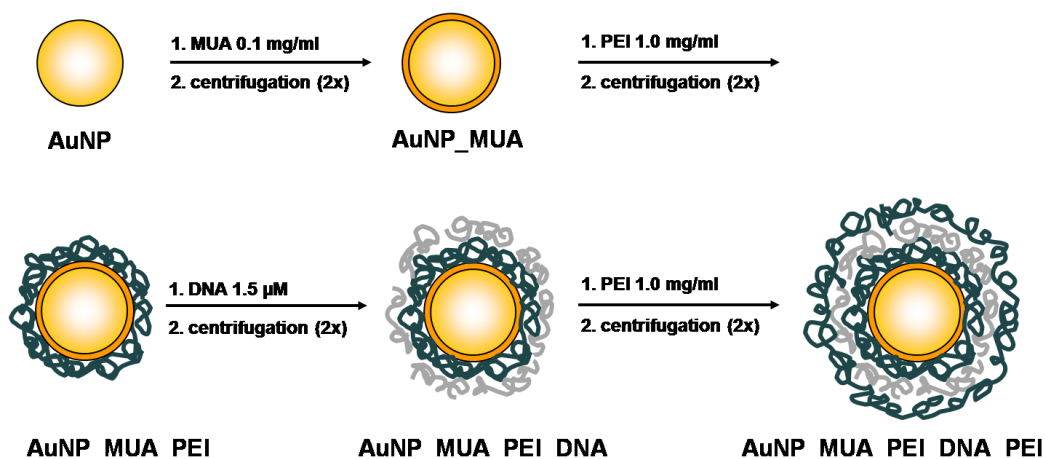


Figure 3 Schematic illustration of the LbL-process. The stabilized gold nanoparticles are alternatively covered with PEI and DNA to give the Lbl-assembled core-shell particles. (Reprinted (adapted) with permission from Elbakry et al.²⁵ Copyright 2009 American Chemical Society).

Purification of AuNPs

1. The gold suspensions are purified after each modification to remove excess reagents. The most convenient method is the purification by centrifugation. The centrifugation conditions depend strongly on the particle size (see Note 2). An Eppendorf centrifuge and 2 ml Eppendorf tubes are used (see Note 3).
2. For 50 nm particles the suspensions are centrifuged at 5000 g for 10 min at 4 °C. The supernatant is removed and the pellet is washed with water, twice (see Note 4). For the following layer-by-layer deposition the last resuspension is carried out in 1 mM sodium chloride.

Coating with PEI: Deposition of the first and third layer (AuNP_MUA_PEI and AuNP_MUA_PEI_DNA/RNA_PEI)

1. The stabilized particles are purified by centrifugation as described above and the last resuspension is performed in 1 mM NaCl.
2. The PEI stock solution (10 mg/ml in 1 mM NaCl) is placed in a small snap cap vial and stirred. The final concentration of PEI is 1mg/ml. The AuNP solution is added dropwise and stirring is continued for 30 min at room temperature (**Figure 3**). The suspension is purified afterwards as described above.

Coating with nucleic acids: Deposition of the second layer (AuNP_MUA_PEI_DNA/RNA)

1. The coating of the nanoparticles with nucleic acids is performed according to the coating with PEI. The nanoparticles are resuspended in 1 mM NaCl after purification. Double stranded DNA or RNA is placed into a snap cap vial at a final concentration of 1.5 μ M for DNA or 2.0 μ M for RNA respectively. The nanoparticle suspension is added dropwise under stirring. After 30 min the particles are purified and resuspended in 1mM NaCl for the deposition of the last layer of PEI (see Notes 5-7).

Characterization of core-shell AuNPs by Vis-spectroscopy, dynamic light scattering and zeta potential

1. The deposition of each polymer should be followed by measuring three important parameters: particle size, zeta potential and Vis-absorbance (see Note 8).
2. The particle size should increase with each polymer layer but the extent should not be more than 10 nm per layer and the size distribution should be as narrow as possible.
3. The zeta potential is a parameter for the surface charge of the particles. The polymers have opposite charges, that means that the surface charge of the particles should turn from negative (AuNP_MUA) to positive (AuNP_MUA_PEI) and so on.
4. A special characteristic of AuNP is the surface plasmon resonance, leading to a red color of the particle suspensions. The absorbance peak of the plasmon resonance depends on the particle size and the electrostatic environment of the particles, among other parameters. The size increase during the LbL process and particle aggregation can be followed by measuring the absorbance maximum of the particles. The absorbance peak should show a slight red shift of about 2 nm per polymer layer. A shift of more than 10 nm or a broadening of the absorbance spectra is a sign for particle aggregation.

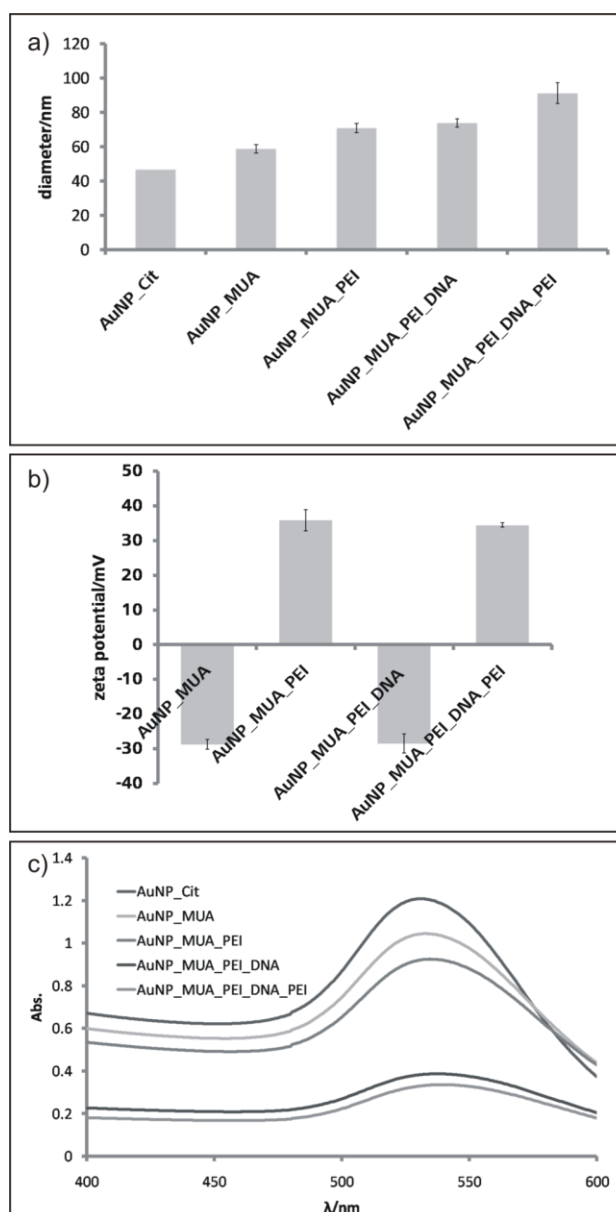


Figure 4 a) The particle size increases with the deposition of the polymer layers. The size of the particles was determined by dynamic light scattering of three independent coating batches. The extent of size growth is less than 10 nm per layer. b) The zeta potential of the core-shell assembled particles inverts its sign with the deposition of the oppositely charged polymers. c) The plasmon resonance wavelength of the gold particles depends on the particle size. That means that the absorbance maximum shows a shift of two nanometers per particle layer.

Characterization by TEM

1. Samples for TEM images are prepared by depositing the gold suspension onto carbon-coated copper grids. The grids are treated in a plasma beam before use to get a more hydrophilic surface. The grids are air dried before use.
2. The size distribution of gold suspension is analyzed by TEM images in addition to the light scattering measurements to ensure a homogenous particle size distribution.
3. TEM images can be analyzed using the free of charge available software Image J. A detailed introduction into this software can be found in the internet.

Notes

1. The glassware and stir bars for all preparation steps should be thoroughly cleaned. Especially the flask and stir bar for the AuNPs synthesis should be rinsed with aqua regia and afterwards with Millipore water. This avoids contaminations during the reduction step and enhances the quality of the nanoparticles.
2. Centrifugation conditions have to be adjusted to the particle size to avoid aggregation. Larger particles need slower and shorter centrifugation steps, smaller particles need a higher speed and longer centrifugation times. The pellet of the AuNPs should have a red color and move loosely in the vessel. A dark, small spot on the wall of the cup, which cannot be resuspended easily, means that the centrifugation conditions have been too hard and the particles aggregated.
3. Centrifugation is performed in an Eppendorf centrifuge with 2 ml Eppendorf cups filled only with 1 ml of the particle suspension. The use of larger centrifugation vessels might lead to particle aggregation.
4. The supernatant should be centrifuged as well to achieve a better recovery rate.
5. Coating conditions, especially the salt concentrations and incubation times, have to be adjusted carefully to the used polymers and nucleic acid sequences and particle sizes. The protocol described here is not a general protocol which may not work for all kinds of nucleic acids and particle sizes. Before starting an experiment a concentration series with different salt concentrations (for example between 1 mM and 10 mM NaCl) and different polymer concentrations (for example between

- 0.5 mg/ml and 5 mg/ml polymer) should be performed to establish the ideal coating conditions.
6. The nanoparticles need special storing conditions. In general purified particles should not be stored. The AuNPs_MUA are stable over weeks at room temperature (The excess of MUA may precipitate at lower temperatures). The particles covered with PEI are stable for weeks as well, as long as the excess of the polymer is still present. Storing the particles with the nucleic acids as the outer layer should be avoided, because nucleic acids are sensitive to nucleases. So either Therefore particles should be stored with the first or the last layer of PEI on the particle surface.
 7. The coating steps per polymer layers needed at least 30 min, but the time can be extended largely.
 8. It is recommended to follow each deposition step by measuring the size, zeta potential and Vis absorbance of the particles. The increase of the particle size should be less than 10 nm per polymer layer and the shift of the absorbance maximum should be one or two nanometers per layer. If the particle suspension turns to a purple or violet color the particles are aggregated.

References

- (1) Gao, X.; Kim, K.; Liu, D. Nonviral Gene Delivery: What We Know And What Is Next. *AAPS J.* **2007**, *9*, E92-104.
- (2) Mintzer, M. A.; Simanek, E. E. Nonviral Vectors For Gene Delivery. *Chem. Rev.* **2009**, *109*, 259-302.
- (3) Whitesides, G. M.; Grzybowski, B. Self-Assembly At All Scales. *Science* **2002**, *295*, 2418-2421.
- (4) Decher, G. Fuzzy Nanoassemblies: Toward Layered Polymeric Multicomposites. *Science* **1997**, *277*, 1232-1237.
- (5) Hammond, P. T. Form And Function In Multilayer Assembly: New Applications At The Nanoscale. *Adv. Mater.* **2004**, *16*, 1271-1293.
- (6) Ariga, K.; Hill, J. P.; Ji, Q. Layer-By-Layer Assembly As A Versatile Bottom-Up Nanofabrication Technique For Exploratory Research And Realistic Application. *Phys. Chem. Chem. Phys.* **2007**, *9*, 2319-2340.
- (7) Lutkenhaus, J. L.; Hammond, P. T. Electrochemically Enabled Polyelectrolyte Multilayer Devices: From Fuel Cells To Sensors. *Soft Matter* **2007**, *3*, 804-816.
- (8) Boudou, T.; Crouzier, T.; Ren, K.; Blin, G.; Picart, C. Multiple Functionalities Of Polyelectrolyte Multilayer Films: New Biomedical Applications. *Adv. Mater.* **2010**, *22*, 441-467.
- (9) *Multilayer Thin Films*; Decher, G.; Schlenoff, J. B., Eds.; Wiley -VCH: Weinheim, Germany, 2003.

- (10) De Cock, L. J.; De Koker, S.; De Geest, B. G.; Grooten, J.; Vervaet, C.; Remon, J. P.; Sukhorukov, G. B.; Antipina, M. N. Polymeric Multilayer Capsules In Drug Delivery. *Angew. Chem., Int. Ed.* **2010**, *49*, 6954-6973.
- (11) Becker, A. L.; Johnston, A. P. R.; Caruso, F. Layer-By-Layer-Assembled Capsules And Films For Therapeutic Delivery. *Small* **2010**, *6*, 1836-1852.
- (12) Ai, H.; Jones, S.; Lvov, Y. Biomedical Applications Of Electrostatic Layer-By-Layer Nano-Assembly Of Polymers, Enzymes, And Nanoparticles. *Cell Biochem. Biophys.* **2003**, *39*, 23-43.
- (13) Daniel, M. C.; Astruc, D. Gold Nanoparticles: Assembly, Supramolecular Chemistry, Quantum-Size-Related Properties, And Applications Toward Biology, Catalysis, And Nanotechnology. *Chem. Rev.* **2004**, *104*, 293-346.
- (14) Boisselier, E.; Astruc, D. Gold Nanoparticles In Nanomedicine: Preparations, Imaging, Diagnostics, Therapies And Toxicity. *Chem. Soc. Rev.* **2009**, *38*, 1759-1782.
- (15) Mayhew, T. M.; Mühlfeld, C.; Vanhecke, D.; Ochs, M. A Review Of Recent Methods For Efficiently Quantifying Immunogold And Other Nanoparticles Using TEM Sections Through Cells, Tissues And Organs. *Ann. Anat.* **2009**, *191*, 153-170.
- (16) Kelly, K. L.; Coronado, E.; Zhao, L. L.; Schatz, G. C. The Optical Properties Of Metal Nanoparticles: The Influence Of Size, Shape, And Dielectric Environment. *J. Phys. Chem. B* **2003**, *107*, 668-677.
- (17) *Concepts Of Nanochemistry*; Cademartiri, L.; Ozin, G. A., Eds. Wiley-VCH: Weinheim, Germany, 2009.
- (18) Bain, C. D.; Troughton, E. B.; Tao, Y. T.; Evall, J.; Whitesides, G. M.; Nuzzo, R. G. Formation Of Monolayer Films By The Spontaneous Assembly Of Organic Thiols From Solution Onto Gold. *J. Am. Chem. Soc.* **1989**, *111*, 321-335.
- (19) Massich, M.; Giljohann; Schmucker; Patel, P. Cellular Response Of Polyvalent Oligonucleotide– Gold Nanoparticle Conjugates. *ACS Nano* **2010**, *4*, 5641-5646.
- (20) Schneider, G.; Decher, G. Functional Core/Shell Nanoparticles Via Layer-By-Layer Assembly. Investigation Of The Experimental Parameters For Controlling Particle Aggregation And For Enhancing Dispersion Stability. *Langmuir* **2008**, *24*, 1778-1789.

- (21) Gittins, D. I.; Caruso, F. Tailoring The Polyelectrolyte Coating Of Metal Nanoparticles. *J. Phys. Chem. B* **2001**, *105*, 6846-6852.
- (22) Breunig, M.; Lungwitz, U.; Liebl, R.; Goepferich, A. Breaking Up The Correlation Between Efficacy And Toxicity For Nonviral Gene Delivery. *Proc. Natl. Acad. Sci. U S A* **2007**, *104*, 14454-14459.
- (23) Boussif, O.; Lezoualc'h, F.; Zanta, M. A.; Mergny, M. D.; Scherman, D.; Demeneix, B.; Behr, J. P. A Versatile Vector For Gene And Oligonucleotide Transfer Into Cells In Culture And In Vivo: Polyethylenimine. *Proc. Natl. Acad. Sci. U S A* **1995**, *92*, 7297-7301.
- (24) Sonawane, N. D.; Szoka, F. C.; Verkman, A. S. Chloride Accumulation And Swelling In Endosomes Enhances DNA Transfer By Polyamine-DNA Polyplexes. *J. Biol. Chem.* **2003**, *278*, 44826-44831.
- (25) Elbakry, A.; Zaky, A.; Liebl, R.; Rachel, R.; Goepferich, A.; Breunig, M. Layer-By-Layer Assembled Gold Nanoparticles For siRNA Delivery. *Nano Lett.* **2009**, *9*, 2059-2064.
- (26) Frens, G. Controlled Nucleation For Regulation Of Particle-Size In Monodisperse Gold Suspensions. *Nature (London) Phys. Sci.* **1973**, *241*, 20-22.

Chapter 4:

Oligolayer coated nanoparticles: Impact of the surface topography at the nano-bio interface

Wurster, EC.; Liebl, R.; Michaelis, S.; Robelek, R.; Wastl, D. S.; Giessibl, F. J.; Goepferich, A.; Breunig, M. Oligolayer Coated Nanoparticles: Impact Of The Surface Topography At The Nano-Bio Interface. *ACS Applied Materials & Interfaces* **2015**, 7, 7891-7900.

This chapter contains experimental results obtained from collaborations with other institutes of the University of Regensburg.

Cooperation with Dr. Rudolf Robelek and Dr. Stefanie Michaelis, Institute of Analytical Chemistry and Biosensors, University of Regensburg:

SPR-measurements (Figure 1 and S1).

Cooperation with Daniel Wastl and Prof. Dr. Franz. J. Giessibl, Institute of Experimental and Applied Physics, University of Regensburg:

AFM images (Figure 2 and S2-S4) and root mean square roughness values (Table 2).

Abstract

The layer-by-layer coating of nanoparticles with a layer number in the single-digit range gained increasing attention in nanomedicinal research. But the impact of using various polyelectrolytes on the oligolayer formation and what is even more important, the influence on the interaction with the biological system has often not been considered in the past. Hence, we investigated the polyelectrolyte deposition profiles and the resulting surface topographies of up to three polyelectrolyte layers on a flat gold sensor surface using three different polycations, namely poly(ethylene imine) (PEI), poly(allylamine hydrochloride) (PAH) and poly(diallylammonium chloride) (PD) each in combination with poly(styrene sulfonate) (PSS). Surface plasmon resonance spectroscopy and atomic force microscopy revealed that particularly the PEI/PSS pair showed a so-called overshoot phenomenon, which is associated with partial polyelectrolyte desorption from the surface. This is also reflected by a significant increase of the surface roughness. Then, after having transferred the oligolayer assembly on nanoparticles of about 32 nm, we realized that quite similar surface topographies must have been emerged on a curved gold surface. A major finding was that the extent of surface roughness significantly contributes to the fashion by which the oligolayer-coated nanoparticles interact with serum proteins and associate with cells. For example for the PEI/PSS system, both the surface roughness and the protein adsorption increased by a factor of about 12 from the second to the third coating layer and at the same time the cell association massively decreased to only one third. Our study shows that the surface roughness is besides

other particle properties such as size, shape, zeta potential and hydrophobicity another decisive factor for nanoparticles in a biological context, which has been indeed discussed in the past but not been investigated for oligolayers so far.

Introduction

The layer-by-layer (LbL) assembly is a powerful tool for the functional modification of surfaces and gained great interest for various biomedical applications.¹⁻³ It is based on the alternating deposition of oppositely charged polyelectrolytes or other multivalent species on solid surfaces. Initially, the LbL technique solely focused on the formation of films on macroscopic flat surfaces and involved an extensive series of deposition cycles leading to polyelectrolyte multilayers with up to 30 bi-layers or even more.^{4,5} Because the polyelectrolyte deposition on flat surfaces is highly efficient and rapid, the formation of very complex and rather thick multilayers with completely new structural and dynamic features was easily possible.^{4,5}

In contrast, on curved surfaces of the sub-100-nm range, the generation of multilayer films was recognized as a tremendous challenge due to several time-consuming washing steps and the probability of producing particle aggregates.^{6,7} Therefore, it is not astonishing that a reduction of the layer number to the lower single-digit range was performed as soon as LbL-coated nanoparticles were identified as a favorable tool for the delivery of macromolecular drugs such as nucleic acids.⁸⁻¹² As an example we were the first to report a delivery system for nucleic acids with only two or three polyelectrolyte layers assembled on gold nanoparticles.^{8,13} Similarly, Tan et al. developed hydroxyapatite nanoparticles coated with poly(l-arginine), dextran and small interfering RNA.¹² In addition to facilitating particle up-

scaling, which would be a requirement for a possible clinical application,¹⁴ the limitation to the fabrication of so-called oligolayers has also another important reason: Endocytosis by living cells requires a narrow particle size window with a size optimum of less than about 80 nm.^{13,15} Because each bi-layer adds a substantial size increment to the hydrodynamic diameter of the nanoparticles, especially if nucleic acid with a large persistence length are applied,⁸ a coating process with as few as possible layers is envisioned.

Despite the growing amount of publications in the field of oligolayer-coated nanoparticles for drug delivery, the influence of different polyelectrolytes on the formation of the oligolayers and what is even more important, the impact on the interaction with the biological system has not been evaluated in a comparative study so far. Therefore, we investigated the oligolayer deposition profiles of three different polycation-coating series in detail. For this purpose, we compared the oligolayer formation on a flat surface because it is more accessible to generally applied LbL characterization methods such as surface plasmon resonance (SPR) spectroscopy or atomic force microscopy (AFM). Then, we transferred the oligolayer assembly on nanoparticles of about 32 nm. Here, we focused on the resulting surface topography with respect to protein adsorption and cell association. The surface roughness is a decisive factor for nanoparticles in a biological context that has been indeed discussed,^{16,17} but not investigated for oligolayers in detail so far. Obtaining a more detailed insight on the formation and interaction of such oligolayers with the biological system will help to evaluate the potential of future LbL-based therapeutic nanomedicinal delivery applications.

Experimental Section

Materials

If not otherwise stated all chemicals were purchased from Sigma-Aldrich Chemical Company (Taufkirchen, Germany). The polyelectrolytes had the following molecular weights: Poly(allylamine hydrochloride) 17,000 g/mol, branched poly(ethylenimine) 25,000 g/mol, poly(diallyldimethylammonium chloride) less than 100,000 g/mol, poly(styrene sulfonate sodium salt) 15,000 g/mol (Polymer Standard Service, Mainz, Germany). Ultrapure water was obtained using a Milli-Q-System (Merck Chemicals, Schwalbach, Germany).

Surface Plasmon Resonance (SPR) Spectroscopy

High refractive index glass slides covered with a 5 nm chromium bottom and a 45 nm thick top gold layer were used as substrates for the surface plasmon excitation. Sensor slides were rinsed with 70% ethanol, air dried, and plasma treated for 2 min inside an Ar plasma generator (Harrick Plasma; NY; USA). The cleaned and activated sensor slides were then immersed in 1 mg/ml 11-mercatoundecanoic acid (MUA) for three days and then dried in a nitrogen stream. The SPR measurements were performed with a Biosuplar 400T SPR system (MiviTec GmbH, Sinzing, Germany) at 37°C. To this end, the SPR substrates were mounted

to the prism coupler of the system by using an immersion oil ($n = 1.61$; Cargille Labs, Cedar Grove NJ, USA). A homemade flow cell consisting of a 1 mm PDMS spacer and an appropriate flow cell cover with inset in- and outlets coupled to a syringe pump (TSE Systems, Bad Homburg, Germany) was used. A constant flow rate of $100 \mu\text{L}/\text{min}$ was applied. The completed sensor architecture was equilibrated with ultrapure water. After obtaining stable base line signals the MUA layer on the sensor surface was activated by 0.01 M NaOH followed by a rinsing step. $400 \mu\text{L}$ of each polyelectrolyte were successively added to the system, always followed by a water rinsing step until a stable SPR signal was achieved. The polymer concentrations were $1 \text{ mg}/\text{ml}$.

The SPR system was run in the angle or kinetic measurement mode. For the angle measurement mode a full angular scan ($\theta = 58^\circ - 68^\circ$) was performed after each polyelectrolyte incubation step. In kinetic measurement mode changes in reflectivity (Δ reflectivity) were recorded over time at a constant SPR observation angle. The used observation angle was extracted from the first complete angle scan curve recorded of the SPR sensor after its activation. In both measurement modes data was recorded using the manufacturer's software and exported to the software Origin6 (OriginLab, Northampton MA, USA) for further analysis. Data evaluation of the SPR angle scan curves for the calculation of the layer thicknesses was performed by a Maxwell equation mechanism using the free software tool "WinSpall". Further theoretical details and the used optical parameters can be found in the Supplemental Information.

Quartz Cantilever Atomic Force Microscopy (AFM)

The AFM experiments were performed on a homebuilt qPlus ambient FM-AFM system operated by a Nanonis Control System with an OC4 PLL (SPECS GmbH, Berlin, Germany)¹⁸⁻²⁰ Custom designed qPlus sensors were used that were manufactured similarly to quartz tuning-forks.^{21,22} The sensors had a characteristic resonance frequency of $f_0 = 32768$ Hz and a stiffness $k = 1280$ N/m. The qPlus Sensors were equipped with silicon tips made by splintering bulk crystals. Sensor parameters were as follows: $f_0 = 29734$ Hz, $Q_{\text{air}} = 2364$, bulk silicon tip. This tip is extremely thin and lasts only for a limited number of measurements. Because every change of the tip affects the comparability, all images were measured with the same tip instead of measuring more than one sample per preparation condition. However, to be sure that we would not measure any outlier, the layer built-up of the AFM samples was performed in the SPR measuring cell. Hence, the SPR graphs were an optimal quality criterion for the layer assembly. The surface roughness was quantified by extracting the roughness root-mean-square (Rq) with WSxM v4.0 Beta 7.0 software (Nanotec Electronica S.L., Tres Cantos, Spain).²³

Particle synthesis, LbL modification and characterization

The particle synthesis and coating protocol was already published in detail.²⁴ In brief, 30 nm gold nanoparticles (AuNP) were synthesized by citrate-reduction as follows: 2 ml of 1% (w/v) aqueous sodium citrate trihydrate (Merck KGa, Darmstadt, Germany) solution were added to a boiling solution of 0.1% (w/v) gold(III) chloride under vigorous stirring. The conditions were kept for 10 min until the red color of the colloidal gold appeared. The citrate ligands were subsequently exchanged with MUA by adjusting the pH to 11 with 1 M NaOH and

adding 0.1 mg/ml MUA in ethanol. The particle suspension was stirred at ambient temperature for three days to achieve a stable thiol bond to the gold surface. For the LbL modification particles were purified by several centrifugation steps. The purification protocol was adjusted from Balasubramanian.²⁵ The suspensions were centrifuged at 6000 g, 10 min, 4 °C and the pellets were resuspended in water. The centrifugation speed was reduced by 500 g with each polymer layer. The LbL coating procedure was as follows: The purified AuNP were added dropwise to a stirring solution of the polyelectrolyte to give a final concentration of 1 mg/ml of the polyelectrolyte and stirred for an additional 30 min. Afterwards the particles were purified again by centrifugation as described above and immediately coated with the next polyelectrolyte. The nanoparticles were characterized by their hydrodynamic diameter and zeta potentials using a Zetasizer Nano ZS (Malvern Instruments, Herrenberg, Germany). For size measurements 173° backward scattering in general purpose mode was applied and the maximum peak of the intensity distribution is always stated. The zeta potential measurements were processed in the monomodal mode. For light scattering and zeta potential measurements the pH was neutral and the ionic strength were comparably low because no ions were added to the samples. Vis spectrometry (UVIKON 941, Kontron, now Goebel Instrumentelle Analytik, Au/Hallertau, Germany) was used to determine the surface plasmon peak of the colloidal gold in order to calculate the AuNP particle concentration.²⁶

Gel electrophoresis

Equal amounts of purified LbL coated gold nanoparticles were incubated with Leibovitz Medium containing 10% FCS at 37 °C for 1 h. The particles and unadsorbed serum proteins were separated by centrifugation (5 °C, 15000 g, 60 min). Thereafter, the pellet was washed

three times in ice-cold millipore water (5°C, 9500 g, 30 min). The purified samples were analyzed by sodium dodecyl sulfate polyacrylamide gel electrophoresis (SDS-PAGE) on a 15% poly(acrylamide gel). SDS in the sample buffer removed the protein corona from the particles.²⁷ The electrophoresis was run at 120 Volt for 45 min using a Pharmacia EPS 600 gel electrophoresis device (Bio-Rad Laboratories, Munich, Germany) and subsequently stained with Coomassie Blue. The protein molecular weight standard was an unstained protein marker with a molecular weight range from 14.4 kDa to 116.0 kDa (#26610, Thermo Fisher Scientific, Schwerte, Germany). The gels were imaged using a BioRad Imaging System (ChemiDoc XRS+, BioRad, München, Germany) and evaluated with Lab Image Software (BioRad, München, Germany). The band intensities were calculated by using the BSA band (66.2 kDa) and the molecular weight marker as references. Protein bands were detected by the default band detection tool with high resolution settings.

Cell culture and cellular association

HeLa cells (ATCC No. CCL-2) were cultivated in 75 cm² culture flasks at 37 °C in a 5% CO₂ humidified environment in Eagle Minimum Essential Medium with 10% serum pyruvate (110 mg/l) (EMEM+). Cellular association of nanoparticles was measured by a photometric assay based on the absorption of gold nanoparticles in Leibovitz medium (Invitrogen, Life Technologies, Darmstadt, Germany, with 10% serum, without phenol red). The method was first published by Cho et al. and calculates the amount of cell-associated particles by the reduced absorption of gold nanoparticles after incubation with cells^{28,29} as follows:

In brief, the absorption (Abs) of the cell culture medium containing AuNP before (0) and after (t) the incubation time for a cell containing sample and a control without cells, respectively, was measured at 506 nm. Thereafter, we calculated the loss of nanoparticles due to unspecific

adsorption ($Loss_{control}$) and due to the cell association ($Loss_{w/cells}$), respectively, by using equation (1).

$$Loss\% = 100 - \left(\frac{Abs_t}{Abs_0} * 100 \right) \quad (1)$$

The difference of the two samples gave the percentage of cell-associated particles (2).

$$Cell\ association\% = Loss\%_{w/cells} - Loss\%_{control} \quad (2)$$

Using this percentage together with the added molar concentration of gold nanoparticles (c_0) and the Avogadro constant (N_A), the absolute number of associated particles (N_{assoc}) per liter was calculated (3).

$$N_{assoc} = (c_0 * Cell\ association\%) * N_A \quad (3)$$

Subsequently, the number of associated particles in the incubation volume was calculated. In addition, the cell number was determined by counting in a Neubauer Chamber. Finally, the number of associated particles in the incubation volume was divided by the number of cells, which resulted in the number of associated particles per cell (AuNP/cell).

In our case, an internal standard of 20 pM coated AuNP was added to all photometric samples to increase the absorption values over the detection limit. This internal standard was incubated with cell culture medium containing 10% serum 1 h prior to the absorption measurement to ensure the formation of a protein corona around the particles and comparable absorption spectra. As a control for unspecific adsorption of gold nanoparticles to the cell culture material the incubation was performed without cells and subtracted from the cell containing samples. For practical reasons cell association studies of concentrations of 2.5 pM and higher could only be performed in duplicates. The photometric samples were analyzed using a double-beam photometer at 506 nm (UVIKON 941, Kontron, now Goebel Instrumentelle Analytik, Au/Hallertau, Germany).

Statistics

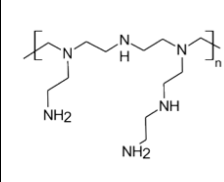
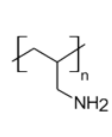
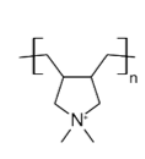
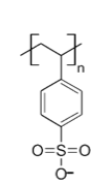
All experiments were performed in replicates of two to four and results are given with standard deviation. In case of SPR, AFM and SDS-PAGE a representative example is shown. One-way ANOVA followed by a Student-Newman-Keuls (SNK) test was performed using SigmaPlot 12.0 (Systat Software Inc. San José, USA) to test statistical significance.

Results and Discussion

In this study, the deposition of three different polycations in combination with poly(styrene sulfonate) (PSS) as polyanion on a gold surface (either flat or curved) was investigated. In a first step, the gold surface was functionalized using 11-mercaptopundecanoic acid (MUA) to yield a permanent negative surface charge for further deposition of the oppositely charged polyelectrolytes. Then, the formation of the oligolayer started with a polycation, followed by the polyanion PSS and a terminal polycation layer. Poly(ethylene imine) (PEI), poly(allylamine hydrochloride) (PAH) and poly(diallylammonium chloride) (PD) were chosen as polycations to finally give three different coating series. These polycations primarily differ in their architecture, the functional amino groups, pKa values and the molecular weight (MW) (**Table 1**).

PEI is a highly charged branched polymer, carrying primary, secondary and tertiary amines and is known to be a suitable transfection agent for nucleic acids.^{14,33} PAH is a linear polyelectrolyte with primary amino groups only. In contrast, PD consists of quaternary amines and is, therefore, completely charged, independent of the pH of the surrounding medium. The polyanion PSS with a molecular weight of 15 kDa was chosen as a surrogate for any negatively charged macromolecule and can be easily replaced by therapeutic nucleic acids to design a drug delivery system.^{8,13,15}

Table 1. Overview of the polyelectrolytes for the formation of the oligolayers on a gold surface

	PEI	PAH	PD	PSS
structure				
architecture	branched	linear	linear	linear
amines	1°, 2°, 3°	1°	4°	-
pKa	8.5 ³⁰	9.7 ³¹	-	1 ³²
MW (kDa)	25	15	<100	15

The oligolayer formation on a flat gold surface was monitored by SPR spectroscopy. To this end, the kinetic profiles were recorded by measuring the change in reflectivity (Δ reflectivity) over time (**Figure 1A-C**). In the case of the PAH- and PD-series, each polymer deposition yielded a plateau in the Δ reflectivity curves (**Figure 1B, C**). Finally, after the oligolayer was completed, a “stair-like” deposition profile was observed. The corresponding layer thicknesses, which were calculated by a Maxwell equation fit, increased with each polymer layer and the final thickness after three polymer layers was about 4.7 nm for the PAH-series and about 3.6 nm for the PD-series, respectively (**Figure 1E, F**). Altogether these SPR profiles fit to regular polyelectrolyte multilayer assemblies, where an increase in the thickness of each layer is characteristic.³⁴⁻³⁷ In addition, the calculated layer thickness of the PAH-series is in very good agreement with literature^{38,39} and hence corroborates the applicability of SPR measurements. In contrast, the PEI-series did only follow this regular deposition until the second layer. Upon the deposition of the third layer, a sharp peak appeared which was

followed by a rapid decrease in Δ reflectivity (**Figure 1A**). This was also reflected by the thickness, which was about 10 nm after two layers, but collapsed to about 1.6 nm for the tri-layered PEI/PSS/PEI system (**Figure 1D**). For data fitting to obtain the layer thickness it was assumed that the layers do not merge. It should be noted that the value of the tri-layered PEI/PSS/PEI-system is consequently afflicted with some uncertainty. Such a characteristic deposition curve, which deviates from the stair-like shape, was already published by the group of Cohen Stuart for a salt-dependent LbL system of poly(acrylic acid) and poly(dimethylaminoethyl methacrylate)⁴⁰ and was even earlier theoretically investigated by the group of Filippova⁴¹. In more detail, Cohen Stuart described a stepwise process, which involved the deposition of the polycation, followed by its mixing with the layer beneath, then a formation of polyelectrolyte complexes and finally a polyelectrolyte erosion from the surface.⁴⁰

These so called overshoots are still under scientific discussion,^{42,43} and it has not been clarified if only a layer collapse or also a layer detachment is involved. To the best of our knowledge the effect was only discussed for the polyelectrolyte pair mentioned above. Here, we show that the presented PEI/PSS pair might be another example for this phenomenon, especially because it was not possible to avoid the decrease of Δ reflectivity by variation of the used PEI concentration (data not shown). The type of the polyanion strongly seemed to play an important role because an exchange of the strong polyelectrolyte PSS (pKa 1)³² by the weak polyelectrolyte poly(acrylic acid) (PAA) (pKa 4.5)⁴⁴ did not result in such an overshoot phenomenon (Supporting Information, **Figure S1**).

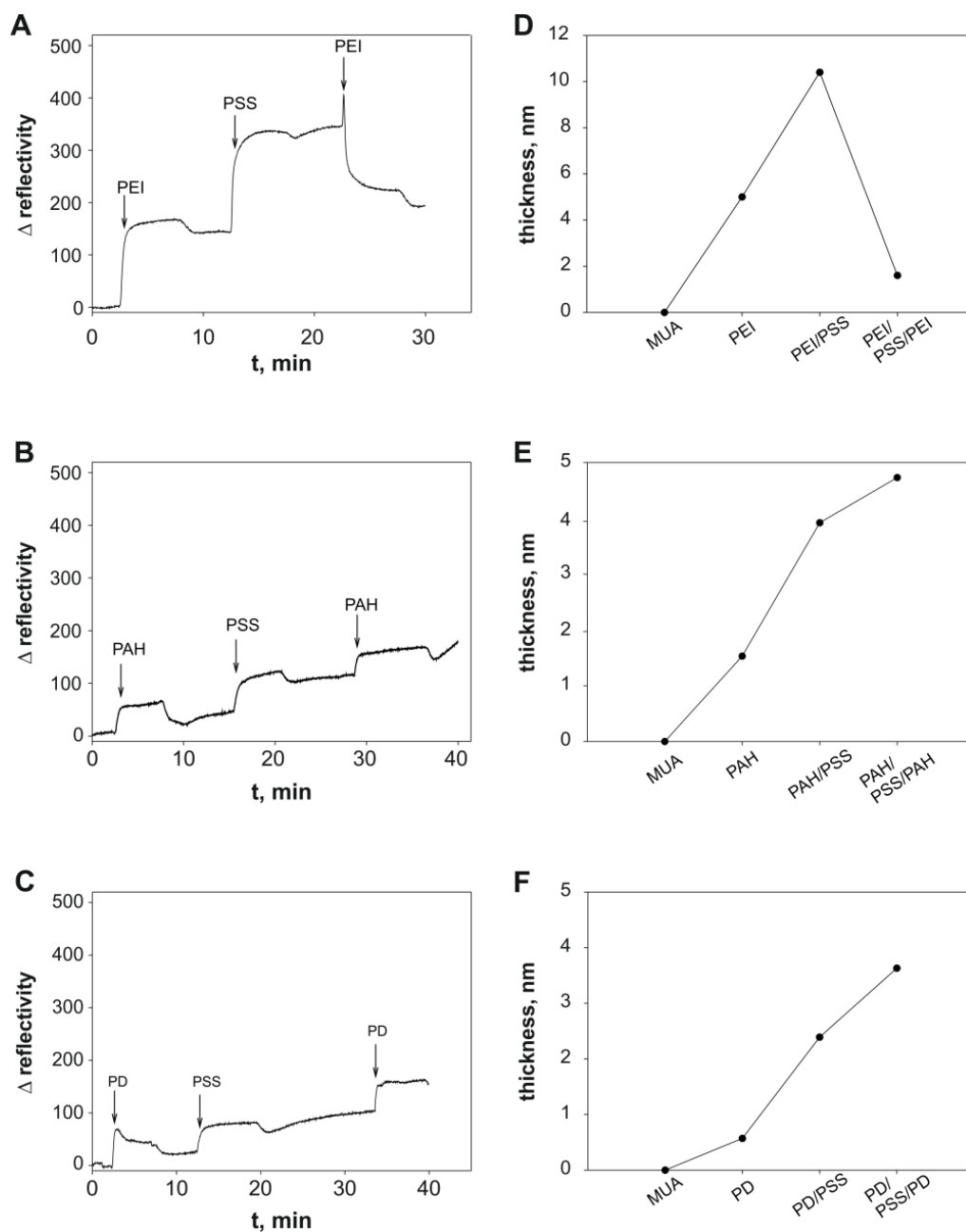


Figure 1 Deposition profiles of the different polyelectrolyte pairs measured by SPR spectroscopy on a gold sensor surface. An arrow indicates the addition of each polymer to the flow cell. The moderate decrease of Δ reflectivity after each polymer deposition is due to a water rinsing step. **A)** In the case of the PEI-series, the first and second layer adsorbed stepwise, but the third layer was not successfully adsorbed. A decrease in Δ reflectivity and a collapse of the oligolayer occurred. **B)** and **C)** PAH- and PD-series showed a characteristic stair-like increase of Δ reflectivity as well as an increase in layer thickness with each polymer layer. **D-F)** The corresponding calculated layer thicknesses for the three coating series. Note the different scaling of the y-axis.

We speculated that the overshoot of the PEI-series would most likely result in a very heterogeneous surface structure. To this end, cantilever AFM¹⁹ was used to visualize the surface of the previously coated SPR substrates and to evaluate the effect of the irregular polyelectrolyte deposition in case of the PEI-series. The MUA functionalized gold substrate was observed as control (**Figure 2A**). This surface showed diagonal rills and irregular heights and consequently proved to be a valuable indication of a successful surface coverage for the subsequent polyelectrolyte deposition. Similarly to the SPR measurements, the AFM images revealed differences between the PEI-series on the one hand and the PAH- and the PD-series on the other hand, but additionally, differences in the polymer characteristics were also retrieved. The PAH- and the PD-series indicated a regular layer build-up with an increasing polymer adsorption with increasing number of layers. Because the characteristic diagonal rills of the gold substrate were still visible through the polymer coating of the bi-layered PAH/PSS, it was concluded that these two polymer layers were not sufficient to completely cover the gold substrate (**Figure 2C**). Moreover, at this coating stage the sample was sprinkled with structures, which were attributed to polymer aggregates. But, those structures were leveled out upon the addition of the third polymer layer; the rills were no longer visible, and the PAH/PSS/PAH surface was quite smooth (**Figure 2F**). Hence, in the case of the PAH-series, at least three polymer layers were necessary for a complete coverage of the gold substrate. In the case of the PD-series, the diagonal rills of the gold substrate were completely covered at each coating step. The images are characterized by the occurrence of regular protrusions. Because the AFM technique has the potential to resolve down to the atomic scale, we attributed these protrusions to loops and coils of the PD polymer chain (for high resolution images of the regular protrusions please refer to Supporting Information, **Figure S2 and S3**). These characteristic nanostructures were already reported for higher layer numbers on silica substrates.⁴⁵ The high molecular weight and the fact that PD is completely charged leads to a strong electrostatic repulsion of the polymer segments and to a coiled surface conformation

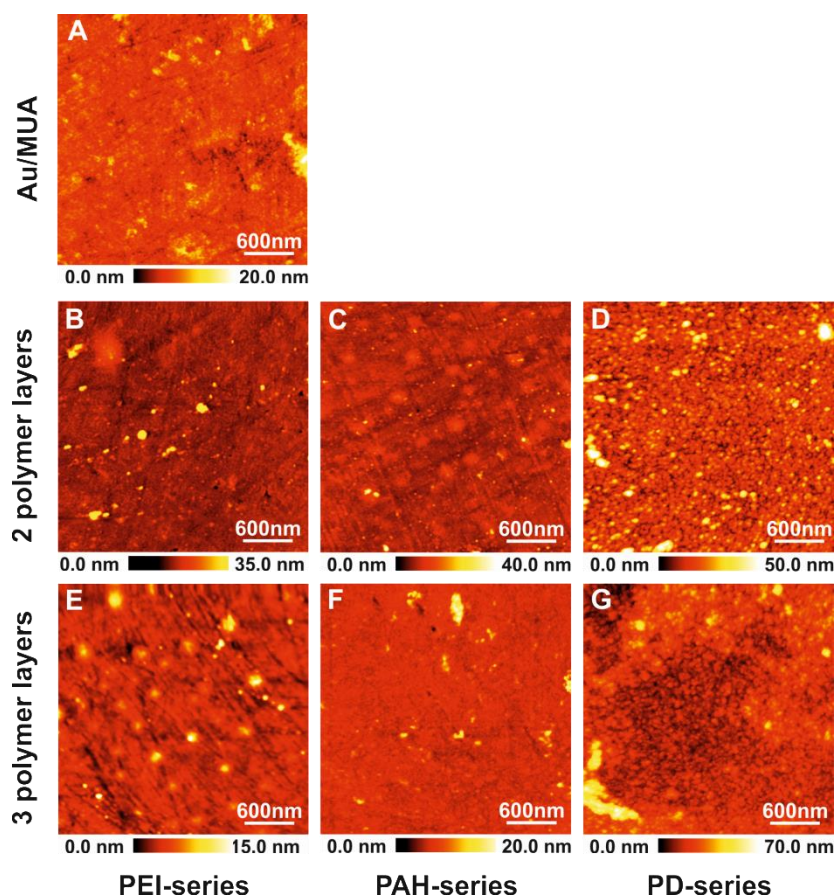


Figure 2 AFM images of coated gold surfaces. **A)** Control gold surface modified with MUA. **B)** PEI/PSS **C)** PAH/PSS **D)** PD/PSS **E)** PEI/PSS/PEI **F)** PAH/PSS/PAH **G)** PD/PSS/PSS. PD-surfaces (**D/G**) completely covered the gold substrate, whereas the bi-layered PAH/PSS (**C**) and the tri-layered PEI/PSS/PEI (**E**) surface only partially covered the template. Additional high-resolution AFM images can be found in the Supporting Information Figure S 2 and S 3. In addition, to demonstrate reproducibility more images of the PEI-series can be found in the Supporting Information (**Figure S 4**). Scan parameters: frequency shift $\Delta f = +10 - +12$ Hz, oscillation amplitude $A = 300$ pm.

(**Figure 2D, G**).^{46,47} As the bi-layered sample already showed this characteristic nanostructure, it can be assumed that even a single layer of PD is most likely sufficient to completely cover the surface features of the gold substrate. The most interesting behavior was found for the samples of the PEI-series. The bi-layered PEI/PSS surface was quite smooth,

besides a few aggregates, and in addition, the structures of the gold substrate were covered to a large part. But, the tri-layered PEI/PSS/PEI surface again showed the characteristic rill structure of the substrate in the presence of sharp surface features of around 15 nm in height (**Figure 2E**). Comparing the PEI/PSS/PEI sample with the bi-layered PEI/PSS surface (**Figure 2B**), it is obvious that these characteristic structures must have appeared upon the addition of the third layer by partial desorption of previously adsorbed polymer. It should be noted that both SPR measurements and AFM images cannot be compared by the same scale of height because SPR averages data over an area of $1 \mu\text{m}^2$, in contrast AFM measures space-resolved thereby identifying single interesting surface structures. Nevertheless, the AFM images agreed well with the SPR measurements, and supported the hypothesis of a possible overshoot phenomenon with the formation of polyelectrolyte complexes and partial desorption of the polyelectrolytes.

To substantiate these distinct differences in the surface topology within one coating series and also between the polycations, the root-mean-square roughness (Rq) of each sample was determined (**Table 2**). The surface roughness of the PD-series did only slightly increase during the coating procedure. Because the surface topography was regular on each layer, the Rq did not show any huge differences. The bi-layered PAH/PSS surface exhibited some yellow spots on its surface indicating specific surface heights, while the tri-layered PAH/PSS/PAH surface showed a homogenous red coloring, which was supported by a marginal decrease of Rq from about 17 nm to 15 nm. In contrast, this trend was reversed in the PEI-series, here Rq increased from about 8 nm in case of the bi-layered to about 95 nm for the tri-layered, roughest surface. To our knowledge this is the first report of these structural surface features for three polycations in comparison at such a low layer number.

Table 2. The root-mean-square roughness (R_q) (nm) extracted from the AFM images.

	PEI-series	PAH-series	PD-series
2 nd layer	8.08	17.31	21.58
3 rd layer	94.84	14.76	29.12

Because the R_q values were averaged over a region of $1 \times 1 \mu\text{m}$ of one representative sample, no error estimation is available.

To evaluate if these interesting surface topographies had an impact on the functionality in the biological context, we substituted the macroscopic planar gold surface by gold nanoparticles of high surface curvature. This step was necessary to achieve a size order suitable for cell association. To this end, gold nanoparticles of about 32 nm were chosen as substrate because this size is close to the optimum for cellular uptake of nanoparticles.^{13,15} To monitor the successful coating of the nanoparticles with oppositely charged polyelectrolytes we made use of two standard techniques for nanoparticle characterization, which are the hydrodynamic diameter and the zeta potential (**Figure 3**). During the coating process with MUA and the polyelectrolytes, the sign of the zeta potential converted with every polymer layer, indicating a successful deposition of oppositely charged polyelectrolytes (**Figure 3A**). The hydrodynamic diameter increased stepwise with each layer for the PAH- and PD- series comparable to SPR measurements (**Figure 3B**). This size increase of 11 nm and less per layer was due to polymer adsorption and not to particle aggregation. Aggregation would have led to larger particle multiplicates and, therefore, to a much greater shift in the particle size distribution.^{6,7} A peculiarity was found for particles of the PEI-series: A size decrease of about 5 nm instead of further particle growth upon addition of the third polymer layer was observed. Of course, the layer thicknesses that were calculated from the SPR measurements

on a flat surface can only be qualitatively compared to the hydrodynamic diameter of a colloid. But we postulate that both the size decrease of PEI-coated gold nanoparticles and the decrease of Δ reflectivity in SPR were induced by an overshoot phenomenon.

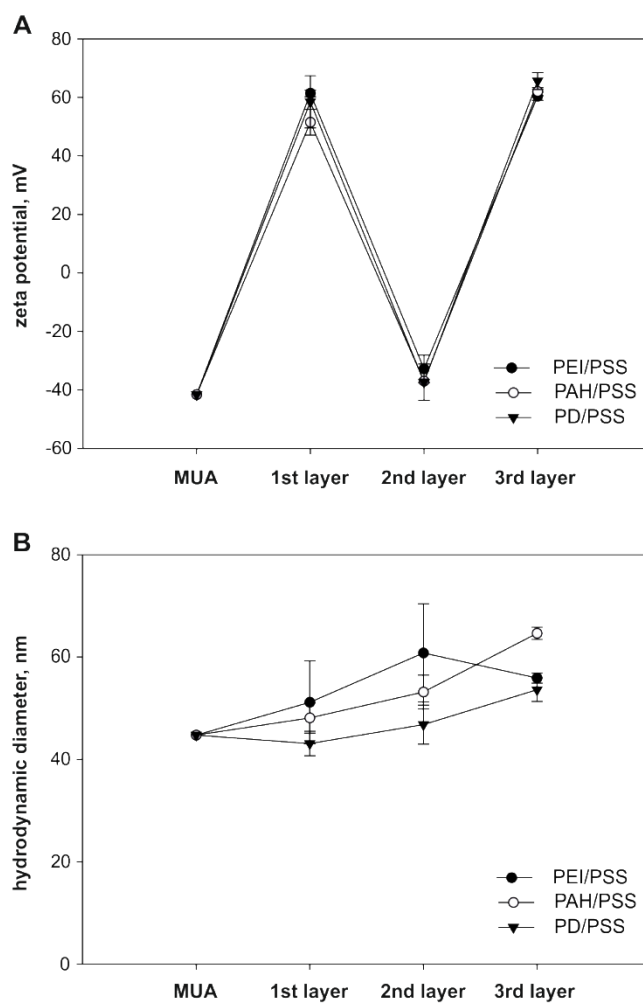


Figure 3. During the oligolayer formation the gold nanoparticles were characterized by their (A) zeta potential and (B) hydrodynamic diameter. The coating was performed from a single batch of synthesized and MUA-modified gold nanoparticles and was performed at least in triplicates.

Despite these differences during the assembly process, the nanoparticles were of similar size and zeta potential. Consequently, they were a favorable and well-defined tool to elucidate the

influence of the surface appearance and texture on the interaction with the biological system.⁴⁸ When nanoparticles enter the biological environment they will be decorated with serum proteins on the surface. Because it is known that the resulting protein corona is more decisive for the nanoparticle fate in the biological context than the physicochemical properties itself,⁴⁸ the protein corona after incubation with serum containing cell culture medium was analyzed by SDS-PAGE in a first step. Although this technique only detects the most-abundant proteins, huge differences concerning the total amount of proteins on the nanoparticles' surface were resolved (**Figure 4A**). The corresponding relative intensities of the SDS-PAGE protein lanes are illustrated in **Figure 4B**. They demonstrate that the total protein adsorption served as a good prove that oligolayer-coated nanoparticles of comparable colloidal properties interact differently with serum proteins. Thus, the coating-series followed different trends from one to the next coating level: Within the PEI-series, the protein amount increased by a factor of about 5 from the first to the second coating level, in order show an additional considerable 12-fold increase to the last layer. The protein amount on the PAH-series first increased to the second coating level and then decreased on the third layer to be only half the amount compared to layer two. In the PD-series the protein adsorption first slightly increased and then remained nearly constant to the next coating level. Surprisingly, although one could assume an identical surface coverage with negatively charged PSS at the second coating level, the intensities as well as the pattern of adsorbed proteins were different.

Because most serum proteins carry a net negative charge at physiological pH,⁴⁸ one would intuitively expect a higher amount of protein adsorption on the positively charged particles, i.e. particles with either one or three polymer layers. But as an example, in the PAH-series, the bi-layered negatively charged particles (PAH/PSS) showed the highest protein adsorption values. Consequently, differences among nanoparticles cannot be explained by electrostatics alone, and other factors seem to be important in shaping the protein corona.

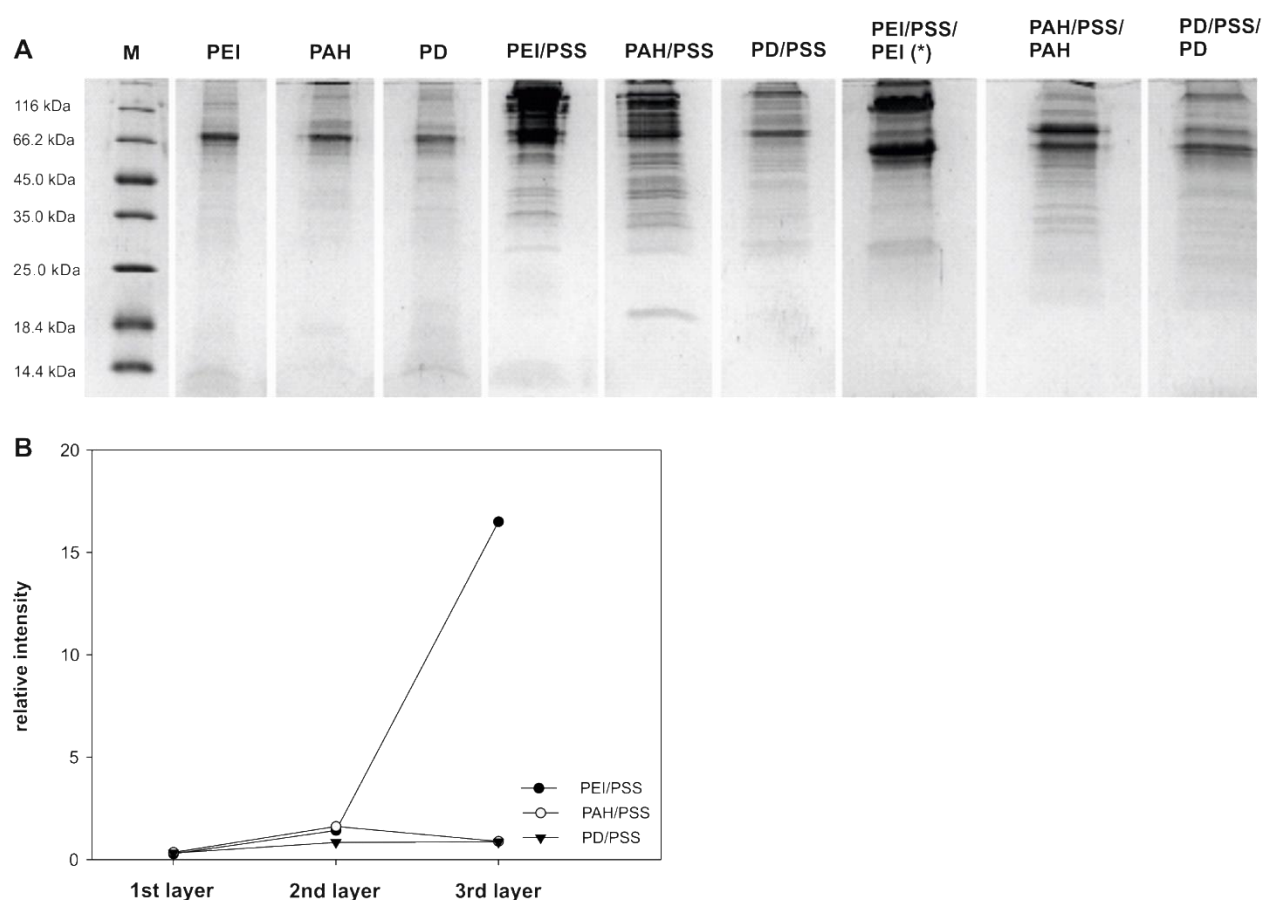


Figure 4. *A)* Analysis of the protein corona of LbL-coated gold nanoparticles using SDS-PAGE. The protein molecular weight marker is indicated with *M*. The highest protein adsorption was found for the tri-layered particles of the PEI-series (*). This sample had to be diluted by a factor of 12.5 compared to the other samples to get a clear protein separation pattern. *B)* Comparison of the relative intensities determined from SDS-PAGE analysis. Standard deviations are missing because values were extracted from one (out of two) representative gel run.

We searched for another critical particle property, and various possibilities are conceivable. The chemical identity (i.e. architecture, functional amino groups and molecular weight) of polyelectrolytes might definitively play a role, but it cannot be solely responsible because on the first coating level of each polycation, the total protein adsorption as well as the pattern of the protein bands were similar. The hydrophobicity of the surface is another aspect that is

associated with protein adsorption^{49,50} And indeed, the hydrophobicity is highest for the tri-layered PEI surface and decreases in the order PEI > PAH > PD (contact angle of about 81°, 74° and 59°, respectively, see Supporting Information **Figure S5**). But similarly, the hydrophobicity cannot be the only reason because the PAH/PSS/PAH and PD/PSS/PD surfaces show despite significant differences of the contact angle nearly a similar degree of protein adsorption. Thus, we speculated that the different layer deposition mechanisms and resulting surface topographies that were observed for their two-dimensional counterparts also had a tremendous impact on the deposition of serum proteins. Although comparing the results of a two-dimensional macroscopic substrate with a three-dimensional colloidal system is critical, a similar trend of the protein adsorption and the root-mean-square surface roughness (Rq) was found (**Table 3**). For example the tri-layered sample of the PEI-series showed a very high surface roughness (Rq = 94.84 nm) and a topography with sharp surface features. Exactly these nanoparticles also led to a massive protein adsorption. Both the roughness and protein adsorption increased by a factor of about 12 from the second to the third layer (**Table 3**). Here, one could even assume a synergistic effect of the electrostatic affinity of the polymer, its more hydrophobic surface and the presence of more binding sites due to the higher surface roughness. In the case of the PD-series, both the bi-layered and tri-layered surfaces, showed a comparable smooth topography in the AFM images and comparable Rq values as well. At the same time, the protein adsorption was always in the same low range (**Table 3**). The low surface contact area, due to the absence of high surface features, most likely hindered the adsorption of serum proteins. In case of samples belonging to the PAH-series, the surface roughness decreased from the second to the third layer. This decrease was also accompanied by a reduction in the amount of adsorbed proteins. Although there is no consensus about the precise effect of the surface roughness on protein adsorption,¹⁶ a number of reports confirmed the higher number of binding sites available on rough surfaces to induce protein adsorption.^{16,51,52}

Table 3 Correlating the relative protein adsorption data with root mean-square-surface roughness (R_q) (nm) of the bi- and tri-layered samples

	PEI-series		PAH-series		PD-series	
	protein	R_q	protein	R_q	protein	R_q
2 nd layer	1.42	8.08	1.62	17.31	0.84	21.58
3 rd layer	16.50	94.84	0.89	14.76	0.86	29.12
Relative in-/decrease	11.62	11.74	0.55	0.85	1.02	1.35

In a drug delivery scenario, the adsorbed protein corona mediates the cellular association and later the uptake into cells.⁴⁸ Because we demonstrated that the protein adsorption is a very sensitive marker for the surface properties of a colloid, the next step was to investigate if these differences were also reflected in the cell association. In general, the association of LbL-coated gold nanoparticles to cells HeLa cells, which are a commonly used model for nanoparticle cell interactions, increased at the applied concentrations without reaching a saturation level (**Figure 5A-C**).

Interestingly, even at the stage of a single polymer layer the cell association was different for each polyelectrolyte. Due to a similar amount of protein adsorption, this difference can be most likely referred to polymer specific effects. The quaternary amines of PD seem to be in general less effective compared to the other amino groups as present in PEI and PAH. Therefore it is also not surprising that polycations, especially if they contain lower order amino groups, are known to be effective transfection agents.⁵³

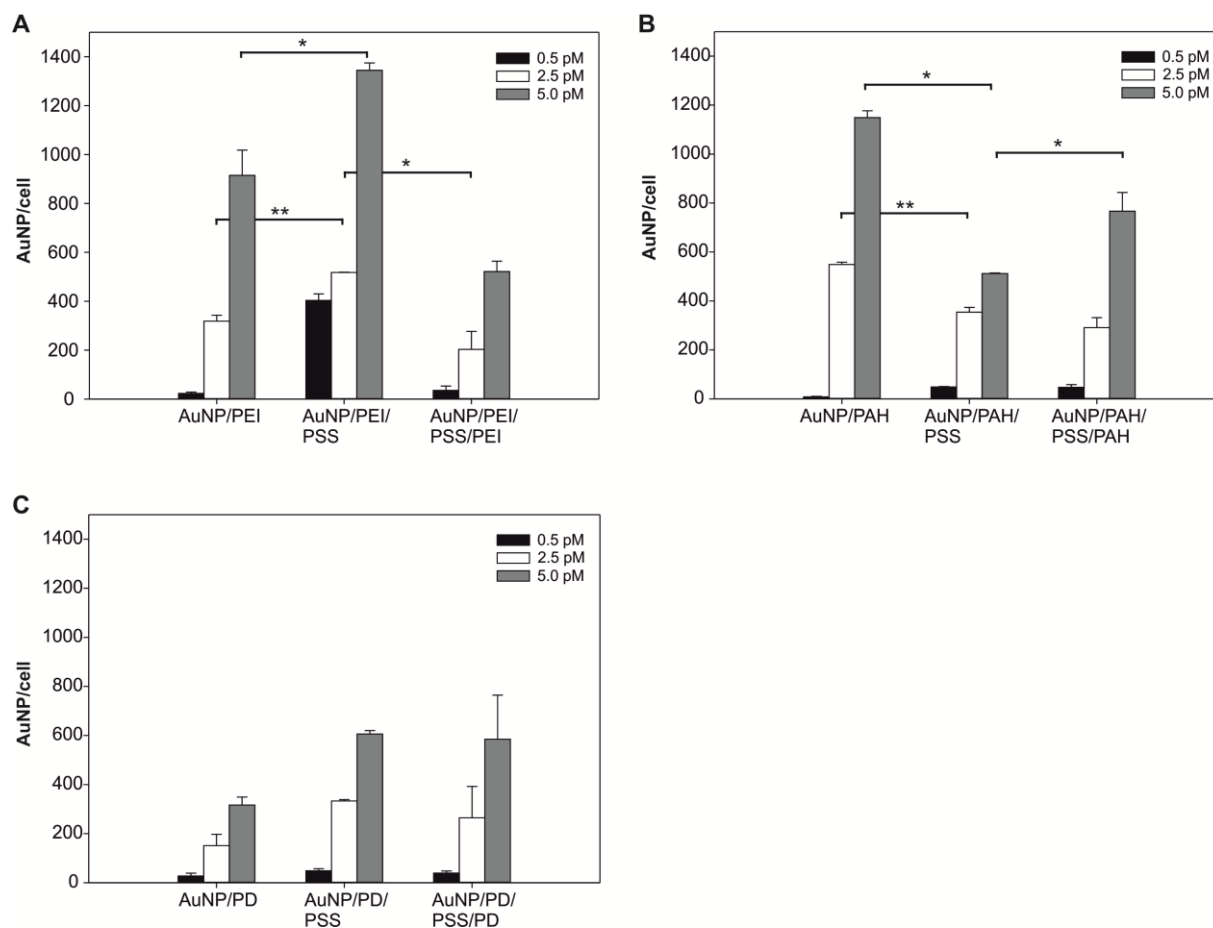


Figure 5. Cellular association of LbL-coated gold nanoparticles of the (A) PEI-series, (B) PAH-series and (C) PD-series. In general, cell association increased with an increasing particle concentration. In the PAH-series, the number of associated particles decreased from the first to the second layer, which is most likely due to the surface charge and an enhanced protein adsorption. In contrast, in the PEI-series, the cell association increased from the first to the second layer and then decreased again to the third layer. This can again be explained by the correlation between the protein adsorption and the surface topography. The cell association efficiency was similar for the bi- and tri-layered particles of the PD-series. Statistically significant differences are indicated by * $p < 0.01$, ** $p < 0.05$.

When comparing the cell association within one series from the second to the third coating step, further significant differences were observed, which also correlated well to the surface roughness of the materials. At the stages of the rougher surfaces within the PAH- and PEI-series, which were the PAH/PSS and PEI/PSS/PEI surfaces, respectively, the cell association

was reduced. On the other hand it was enhanced for the smoother PAH/PSS/PAH and PEI/PSS surfaces of both series (**Figure 5 A, B** and **Table 4**). A similar trend concerning the cellular association and uptake was already reported for PAH/PSS coated gold nanorods, and was explained by the negatively charged cell membrane of HeLa cells repelling equally charged particles.⁵⁴ But, as the PAH/PSS and PEI/PSS surfaces carried a similar charge; again electrostatics alone could not be the only responsible parameter. On the other hand, the bi- and tri-layered samples of the PD-series showed similar cell association values, which is also reflected by a similar protein adsorption extent (**Figure 5C** and **Table 4**). The corresponding toxicity data can be found in the Supporting Information (**Figure S6** and **S7**).

Table 4. *Correlating the relative protein adsorption with the cellular association of bi- and tri-layered samples*

	PEI-series		PAH-series		PD-series	
	protein	cell assoc.	protein	cell assoc.	protein	cell assoc.
2 nd layer	1.42	1450	1.62	500	0.84	600
3 rd layer	16.50	500	0.89	750	0.86	600
Relative in-/decrease	11.62	0.34	0.55	1.50	1.02	1.00

From our results we conclude that for our particles the extent of the protein corona is responsible for the cell association efficiency and that a massive protein adsorption will have an inhibitory effect on the cell association. Although total amount of proteins does not encode molecular details of nanoparticle surface that are important for cellular interaction, this correlation is possible for formulations with similar functional surface groups as in our case.⁴⁸

Hence, we assumed that an optimum of adsorbed protein is necessary on the particle surface

to enhance the cell association. But, to evaluate the effects of the protein corona on the association to cells in a more detailed fashion, especially concerning its composition, further proteomic studies would be necessary.

Conclusion

We demonstrated that the oligolayer deposition of various polycations in combination with a polyanion leads to significant differences of the surface topography. When translating the characteristic surface features from a macroscopic substrate to colloidal gold nanoparticles of comparable physicochemical properties, tremendous differences of the interactions at the bio-nano interface were observed. We conclude that the surface topography of the LbL-coated nanoparticles is decisive for the adsorption of serum proteins and later the association with cells. Thus, a pronounced surface roughness leads due to a larger surface contact area to a massive protein adsorption and consequently to a reduced cell association. Based on our findings we strongly recommend that in the case of LbL-coated nanoparticles for drug delivery applications, the oligolayer deposition mechanisms and the resulting surface topographies should be considered as important nanoparticle characteristics. This way, another parameter besides particle size, charge and hydrophobicity will help to estimate the efficacy of oligolayer-coated nanoparticles for drug delivery.

References

- (1) Boudou, T.; Crouzier, T.; Ren, K.; Blin, G.; Picart, C. Multiple Functionalities of Polyelectrolyte Multilayer Films: New Biomedical Applications. *Adv. Mater.* **2010**, *22*, 441–467.
- (2) Yan, Y.; Björnmalm, M.; Caruso, F. Assembly of Layer-by-Layer Particles and Their Interactions with Biological Systems. *Chem. Mater.* **2014**, 452-460.
- (3) Hammond, P. T. Polyelectrolyte Multilayered Nanoparticles: Using Nanolayers for Controlled and Targeted Systemic Release. *Nanomedicine* **2012**, *7*, 619–622.
- (4) *Multilayer Thin Films*; Decher, G.; Schlenoff, J. B., Eds.; Wiley -VCH: Weinheim, Germany, 2003.
- (5) *Multilayer Thin Films*; Decher, G.; Schlenoff, J. B., Eds.; Wiley -VCH: Weinheim, Germany, 2012.
- (6) Schneider, G.; Decher, G. Functional Core/Shell Nanoparticles via Layer-by-Layer Assembly. Investigation of the Experimental Parameters for Controlling Particle Aggregation and for Enhancing Dispersion Stability. *Langmuir* **2008**, *24*, 1778–1789.
- (7) Schneider, G.; Decher, G. From Functional Core/Shell Nanoparticles Prepared via Layer-by-Layer Deposition to Empty Nanospheres. *Nano Lett.* **2004**, *4*, 1833–1839.
- (8) Elbakry, A.; Zaky, A.; Liebl, R.; Rachel, R.; Goepferich, A.; Breunig, M. Layer-by-Layer Assembled Gold Nanoparticles for siRNA Delivery. *Nano Lett.* **2009**, *9*, 2059–2064.
- (9) Deng, Z. J.; Morton, S. W.; Ben-Akiva, E.; Dreaden, E. C.; Shopsowitz, K. E.; Hammond, P. T. Layer-by-Layer Nanoparticles for Systemic Codelivery of an Anticancer

Drug and siRNA for Potential Triple-Negative Breast Cancer Treatment. *ACS Nano* **2013**, *7*, 9571–9584.

(10) Dreaden, E. C.; Morton, S. W.; Shopsowitz, K. E.; Choi, J.-H.; Deng, Z. J.; Cho, N.-J.; Hammond, P. T. Bimodal Tumor-Targeting From Microenvironment Responsive Hyaluronan Layer-by-Layer (LbL) Nanoparticles. *ACS Nano* **2014**, *8*, 8374–8382.

(11) Han, L.; Zhao, J.; Zhang, X.; Cao, W.; Hu, X.; Zou, G.; Duan, X.; Liang, X.-J. Enhanced siRNA Delivery and Silencing Gold–Chitosan Nanosystem with Surface Charge-Reversal Polymer Assembly and Good Biocompatibility. *ACS Nano* **2012**, *6*, 7340–7351.

(12) Tan, Y. F.; Mundargi, R. C.; Chen, M. H. A.; Lessig, J.; Neu, B.; Venkatraman, S.; Wong, T. T. Layer-by-Layer Nanoparticles as an Efficient *siRNA* Delivery Vehicle for SPARC Silencing. *Small* **2014**, *10*, 1790–1798.

(13) Elbakry, A.; Wurster, E.-C.; Zaky, A.; Liebl, R.; Schindler, E.; Bauer-Kreisel, P.; Blunk, T.; Goepferich, A.; Breunig, M. Layer-by-Layer Coated Gold Nanoparticles: Size-Dependent Delivery of DNA Into Cells. *Small* **2012**, *8*, 3847–3856.

(14) Morton, S. W.; Herlihy, K. P.; Shopsowitz, K. E.; Deng, Z. J.; Chu, K. S.; Bowerman, C. J.; DeSimone, J. M.; Hammond, P. T. Scalable Manufacture of Built-to-Order Nanomedicine: Spray-Assisted Layer-by-Layer Functionalization of PRINT Nanoparticles. *Adv. Mater.* **2013**, *25*, 4707–4713.

(15) Chithrani, B. D.; Ghazani, A. A.; Chan, W. C. W. Determining the Size and Shape Dependence of Gold Nanoparticle Uptake Into Mammalian Cells. *Nano Lett.* **2006**, *6*, 662–668.

(16) Scopelliti, P. E.; Borgonovo, A.; Indrieri, M.; Giorgetti, L.; Bongiorno, G.; Carbone, R.; Podestà, A.; Milani, P. The Effect of Surface Nanometre-Scale Morphology on Protein Adsorption. *PLoS ONE* **2010**, *5*, e11862.

(17) Wong, S. Y.; Han, L.; Timachova, K.; Veselinovic, J.; Hyder, M. N.; Ortiz, C.; Klibanov, A. M.; Hammond, P. T. Drastically Lowered Protein Adsorption on Microbicidal Hydrophobic/Hydrophilic Polyelectrolyte Multilayers. *Biomacromolecules* **2012**, *13*, 719–726.

- (18) Wastl, D. S.; Speck, F.; Wutscher, E.; Ostler, M.; Seyller, T.; Giessibl, F. J. Observation of 4 Nm Pitch Stripe Domains Formed by Exposing Graphene to Ambient Air. *ACS Nano* **2013**, *7*, 10032–10037.
- (19) Wastl, D. S.; Weymouth, A. J.; Giessibl, F. J. Atomically Resolved Graphitic Surfaces in Air by Atomic Force Microscopy. *ACS Nano* **2014**, *8*, 5233–5239.
- (20) Wastl, D. S.; Weymouth, A. J.; Giessibl, F. J. Optimizing Atomic Resolution of Force Microscopy in Ambient Conditions. *Phys. Rev. B* **2013**, *87*, 245415.
- (21) Schneiderbauer, M.; Wastl, D.; Giessibl, F. J. qPlus Magnetic Force Microscopy in Frequency-Modulation Mode with Millihertz Resolution. *Beilstein J. Nanotechnol.* **2012**, *3*, 174–178.
- (22) Giessibl, F. J. Atomic Resolution on Si(111)-(7×7) by Noncontact Atomic Force Microscopy with a Force Sensor Based on a Quartz Tuning Fork. *Appl. Phys. Lett.* **2000**, *76*, 1470.
- (23) Horcas, I.; Fernández, R.; Gómez-Rodríguez, J. M.; Colchero, J.; Gómez-Herrero, J.; Baro, A. M. WSXM: a Software for Scanning Probe Microscopy and a Tool for Nanotechnology. *Rev. Sci. Instrum.* **2007**, *78*, 013705.
- (24) Wurster, E.-C.; Elbakry, A.; Goepferich, A.; Breunig, M. Layer-by-Layer Assembled Gold Nanoparticles for the Delivery of Nucleic Acids. In *Nanotechnology for Nucleic Acid Delivery: Methods and Protocols*; Ogris, M.; Oupicky, D.; Eds.; Methods in Molecular Biology; Humana Press: Totowa, NJ, 2012; Chapter 12, pp 171–182.
- (25) Balasubramanian, S. K.; Yang, L.; Yung, L.-Y. L.; Ong, C.-N.; Ong, W.-Y.; Yu, L. E. Characterization, Purification, and Stability of Gold Nanoparticles. *Biomaterials* **2010**, *31*, 9023–9030.
- (26) Liu, X.; Atwater, M.; Wang, J.; Huo, Q. Extinction Coefficient of Gold Nanoparticles with Different Sizes and Different Capping Ligands. *Colloids Surf. B Biointerfaces* **2007**, *58*, 3–7.
- (27) Lundquist, M.; Stigler, J.; Elia, G.; Lynch, I.; Cedervall, T.; Dawson, K. A. Nanoparticle Size and Surface Properties Determine the Protein Corona with Possible Implications for Biological Impacts. *Proc. Natl. Acad. Sci. U.S.A.* **2008**, *105*, 14265–14270.

- (28) Cho, E. C.; Liu, Y.; Xia, Y. A Simple Spectroscopic Method for Differentiating Cellular Uptakes of Gold Nanospheres and Nanorods From Their Mixtures. *Angew. Chem. Int. Ed.* **2010**, *49*, 1976–1980.
- (29) Cho, E. C.; Zhang, Q.; Xia, Y. The Effect of Sedimentation and Diffusion on Cellular Uptake of Gold Nanoparticles. *Nat. Nanotechnol.* **2011**, *6*, 385–391.
- (30) Neu, M.; Fischer, D.; Kissel, T. Recent Advances in Rational Gene Transfer Vector Design Based on Poly(Ethylene Imine) and Its Derivatives. *J. Gene Med.* **2005**, *7*, 992–1009.
- (31) Silva, C. P.; Carapuça, H. M. Glassy Carbon Electrodes Coated with Poly(Allylamine Hydrochloride), PAH: Characterization Studies and Application to Ion-Exchange Voltammetry of Trace Lead(II) at Combined PAH/Mercury Film Electrodes. *Electrochim. Acta* **2006**, *52*, 1182–1190.
- (32) Monterroso, S.; Carapuça, K.; Duarte, A. Mixed Polyelectrolyte Coatings on Glassy Carbon Electrodes: Ion-Exchange, Permselectivity Properties and Analytical Application of Poly-L-Lysine–Poly(Sodium 4-Styrenesulfonate)-Coated Mercury Film Electrodes for the Detection of Trace Metals. *Talanta* **2006**, *68*, 1655–1662.
- (33) Jungwitz, U.; Breunig, M.; Blunk, T.; Göpferich, A. Polyethylenimine-Based Non-Viral Gene Delivery Systems. *Eur. J. Pharm. Biopharm.* **2005**, *60*, 247–266.
- (34) Klitzing, von, R. Internal Structure of Polyelectrolyte Multilayer Assemblies. *Phys. Chem. Chem. Phys.* **2006**, *8*, 5012.
- (35) Plunkett, M. A.; Wang, Z.; Rutland, M. W.; Johannsmann, D. Adsorption of pNIPAM Layers on Hydrophobic Gold Surfaces, Measured in Situ by QCM and SPR. *Langmuir* **2003**, *19*, 6837–6844.
- (36) Yoo, D.; Shiratori, S. S.; Rubner, M. F. Controlling Bilayer Composition and Surface Wettability of Sequentially Adsorbed Multilayers of Weak Polyelectrolytes. *Macromolecules* **1998**, *31*, 4309–4318.
- (37) Shiratori, S. S.; Rubner, M. F. pH-Dependent Thickness Behavior of Sequentially Adsorbed Layers of Weak Polyelectrolytes. *Macromolecules* **2000**, *33*, 4213–4219.
- (38) Gong, H.; Garcia-Turiel, J.; Vasilev, K.; Vinogradova, O. I. Interaction and Adhesion Properties of Polyelectrolyte Multilayers. *Langmuir* **2005**, *21*, 7545–7550.

- (39) Caruso, F.; Niikura, K.; Furlong, D. N.; Okahata, Y. 1. Ultrathin Multilayer Polyelectrolyte Films on Gold: Construction and Thickness Determination. *Langmuir* **1997**, *13*, 3422–3426.
- (40) Kovacevic, D.; van der Burgh, S.; de Keizer, A.; Cohen Stuart, M. A. Kinetics of Formation and Dissolution of Weak Polyelectrolyte Multilayers: Role of Salt and Free Polyions. *Langmuir* **2002**, *18*, 5607–5612.
- (41) Filippov, L. K.; Filippova, N. L. Overshoots of Adsorption Kinetics. *J. Colloid Interface Sci.* **1996**, *178*, 571–580.
- (42) Buron, C. C.; Filiâtre, C. Overshoots of Adsorption Kinetics During Layer-by-Layer Polyelectrolyte Film Growth: Role of Counterions. *J. Colloid Interface Sci.* **2014**, *413*, 147–153.
- (43) Buron, C. C.; Filiâtre, C.; Membrey, F.; Bainier, C.; Charrat, D.; Foissy, A. Early Steps in Layer-by-Layer Construction of Polyelectrolyte Films: the Transition From Surface/Polymer to Polymer/Polymer Determining Interactions. *J. Colloid Interface Sci.* **2007**, *314*, 358–366.
- (44) Wiśniewska, M.; Urban, T.; Grządka, E.; Zarko, V. I.; Gun'ko, V. M. Comparison of Adsorption Affinity of Polyacrylic Acid for Surfaces of Mixed Silica–Alumina. *Colloid Polym. Sci.* **2014**, *292*, 699–705.
- (45) McAloney, R. A.; Sinyor, M.; Dudnik, V.; Goh, M. C. Atomic Force Microscopy Studies of Salt Effects on Polyelectrolyte Multilayer Film Morphology. *Langmuir* **2001**, *17*, 6655–6663.
- (46) Netz, R. R.; Joanny, J.-F. Adsorption of Semiflexible Polyelectrolytes on Charged Planar Surfaces: Charge Compensation, Charge Reversal, and Multilayer Formation. *Macromolecules* **1999**, *32*, 9013–9025.
- (47) Nestler, P.; Paßvogel, M.; Helm, C. A. Influence of Polymer Molecular Weight on the Parabolic and Linear Growth Regime of PDADMAC/PSS Multilayers. *Macromolecules* **2013**, *46*, 5622–5629.
- (48) Walkey, C. D.; Olsen, J. B.; Song, F.; Liu, R.; Guo, H.; Olsen, D. W. H.; Cohen, Y.; Emili, A.; Chan, W. C. W. Protein Corona Fingerprinting Predicts the Cellular Interaction of Gold and Silver Nanoparticles. *ACS Nano* **2014**, *8*, 2439–2455.

- (49) Walkey, C. D.; Chan, W. C. W. Understanding and Controlling the Interaction of Nanomaterials with Proteins in a Physiological Environment. *Chem. Soc. Rev.* **2012**, *41*, 2780.
- (50) Gunawan, C.; Lim, M.; Marquis, C. P.; Amal, R. Nanoparticle–Protein Corona Complexes Govern the Biological Fates and Functions of Nanoparticles. *J. Mater. Chem. B* **2014**, *2*, 2060.
- (51) Rechendorff, K.; Hovgaard, M. B.; Foss, M.; Zhdanov, V. P.; Besenbacher, F. Enhancement of Protein Adsorption Induced by Surface Roughness. *Langmuir* **2006**, *22*, 10885–10888.
- (52) Ercan, B.; Khang, D.; Carpenter, J.; Webster, T. Using Mathematical Models to Understand the Effect of Nanoscale Roughness on Protein Adsorption for Improving Medical Devices. *Int. J. Nanomed.* **2013**, *8*, 75–81.
- (53) Nguyen, J.; Szoka, F. C. Nucleic Acid Delivery: the Missing Pieces of the Puzzle? *Acc. Chem. Res.* **2012**, *45*, 1153–1162.
- (54) Szabo, I.; Brutsche, S.; Tombola, F.; Moschioni, M.; Satin, B.; Telford, J. L.; Rappuoli, R.; Montecucco, C.; Papini, E. Formation of Anion-Selective Channels in the Cell Plasma Membrane by the Toxin VacA of *Helicobacter Pylori* Is Required for Its Biological Activity. *EMBO J.* **1999**, *18*, 5517–5527.

Supporting Information

Data evaluation for SPR angle scan curves

The principle of the surface plasmon resonance technique is based on the light triggered excitation of the free electrons' fluctuations on the surface of a metal layer. The energy of the excitation light is thereby projected into an evanescent measurement field that extends into the adjacent dielectric medium in contact with the metal. The surface plasmon excitation takes place only when certain conditions regarding the optical properties of the sensor architecture are fulfilled and the excitation light hits the metal surface under a defined incident angle. As the optical properties of the glass and metal layer of the sensor do not change during a measurement, the main determinant of the resonance condition is the permittivity of the dielectric that is in contact with the sensor surface. Every change of this permittivity (e.g. adhesion of an additional layer) will change the resonance incident angle. A theoretical description of the relation between incident angle and optical parameters can be derived from the Maxwell equations:¹

$$\sqrt{\varepsilon_0} \sin \theta = \varepsilon_0 \sin \theta \sqrt{\frac{\varepsilon_1 \varepsilon_2}{\varepsilon_1 + \varepsilon_2}} \quad (1)$$

where ω is the angular light frequency, c is the speed of light, θ is the incident angle under which the excitation light hits the metal surface and ε_0 , ε_1 and ε_2 are the permittivity of the prism, the metal layer and the sensor adjacent dielectric medium. The permittivity of the different materials can furthermore be expressed by the sum of the squares of real (n) and imaginary part (k) of their refractive index:

$$\varepsilon = n^2 + k^2 \quad (2)$$

A general solution for the Maxwell equations for multilayer systems attached to a SPR sensor surface can be obtained by using the transfer matrix formalism of 2x2 matrices.²

Table S 1. Optical parameters used for SPR data fits

Material	n	k
Glass (prism)	1.61	0
Chromium (adhesion mediator)	3.396	3.504
Gold (SPR sensor layer)	0.1285	3.758
Mercaptoundecanoic acid (MUA)	1.484	0
Polyethylenimine (PEI)	1.352	0
Polyallylamine-hydrochloride (PAH)	1.354	0
Polydiallyldimethylammoniumchloride (PD)	1.352	0
Polystyrenesulfonate (PSS)	1.372	0

In the presented study the free software tool “WinSpall”³ was used to fit the measured SPR scan data according to the Maxwell formalism and so obtain thickness values of the respective layers attaching to the SPR sensor. The optical parameters of the combined Cr/Au layer used for the fit process were obtained by an initial “WinSpall” fit of a freshly prepared Cr/Au coated SPR glass slide immersed in ultrapure water. The refractive indices of the different LbL layer materials were determined by Abbe refractrometry (Carl Zeiss, Germany). The optical parameters are summarized in **Table S 1**.

LbL deposition with poly(acrylic acid) as polyanion

To evaluate if the type of the polyanion has an influence on the overshoot phenomenon, we performed SPR experiments using poly(acrylic acid), PAA, as the polyanion in combination with PEI (**Figure S 1**).

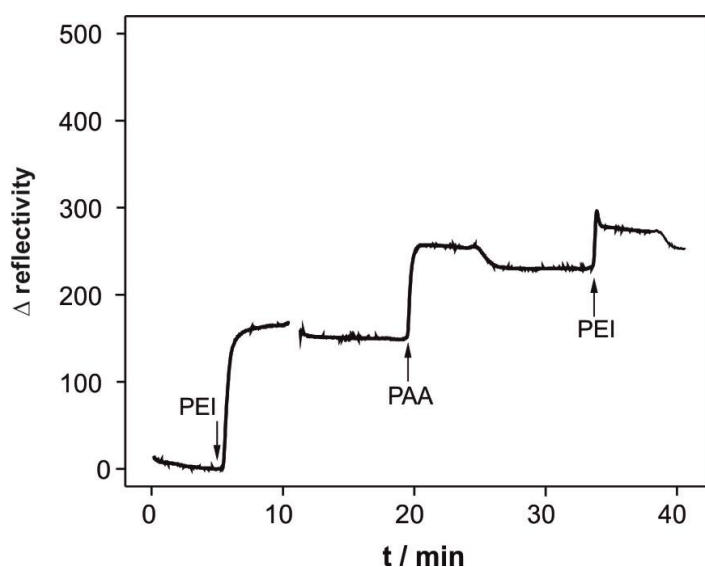


Figure S 1. Upon addition of the third layer a small injection peak was observed, but thereafter only a minimal decrease of the signal was detected. Finally, the plateau of the last layer was still higher than the plateau of the previous layer. In conclusion, the LbL deposition of PEI/PAA did not show an overshoot effect.

Atomic Force Microscopy

Figure S2 shows AFM images of the bi-layered gold surfaces. Detailed images of the tri-layered gold-surfaces are shown in **Figure S3**. AFM images of a repetition of the PEI/PSS series can be found in **Figure S4**.

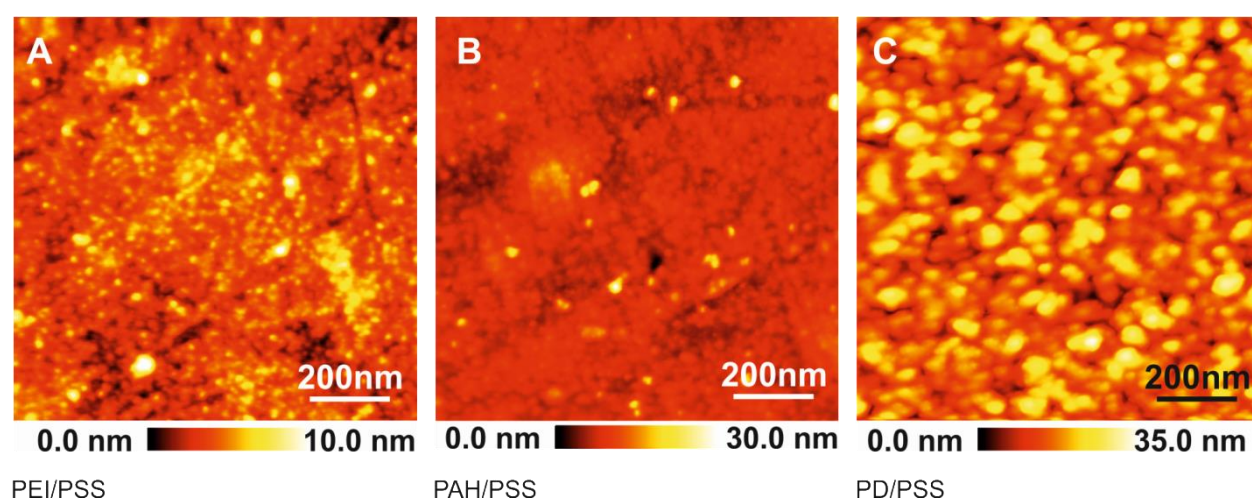


Figure S 2A) The PEI/PSS surface covered the gold substrate and only few polymer aggregates were visible. **B)** PAH/PSS: The polymer coating is not sufficient for a complete coverage of the gold substrate. In addition, polymer aggregates were visible as lighter spots on the image. **C)** The PD/PSS surface was smooth and with a polymeric nanostructure. Scan parameters: frequency shift $\Delta f = +10 - +12$ Hz, oscillation amplitude $A = 300$ pm.

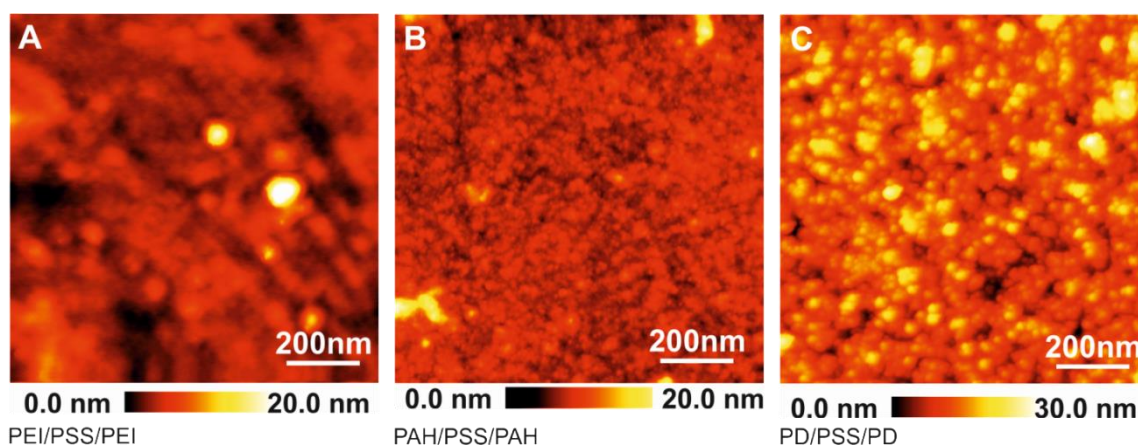


Figure S3. Detailed images of the tri-layered surfaces show the nanostructures of the samples. **A)** In the PEI/PSS/PEI surface the diagonal rills of the gold substrate were visible. **B)** PAH/PSS/PAH covered the gold substrate sufficiently. **C)** PD/PSS/PD showed a characteristic loopy nanostructure. Scan parameters: frequency shift $\Delta f = +10 - +12$ Hz, oscillation amplitude $A = 300$ pm.

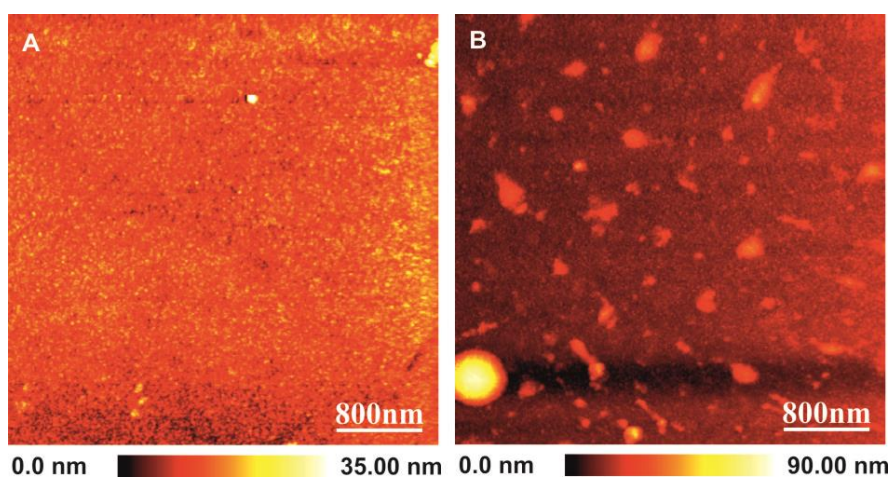


Figure S4. Additional images of the PEI-series demonstrate the increase of the surface roughness during the coating from the second to the third layer with PSS and PEI, respectively. **A)** The bi-layered PEI/PSS coated surface showed a very smooth structure without any sharp surface features. **B)** The tri-layered PEI/PSS/PEI layer had sharp surface heights, visible as light spots on the AFM image. Scan parameters: frequency shift $\Delta f = +10 - +12$ Hz, oscillation amplitude $A = 300$ pm.

Water contact angles

The water contact angles were determined by the sessile drop principle for coated glass microscope slides. The slides were coated with the polyelectrolyte layers as indicated, and the results are shown in **Figure S5**.

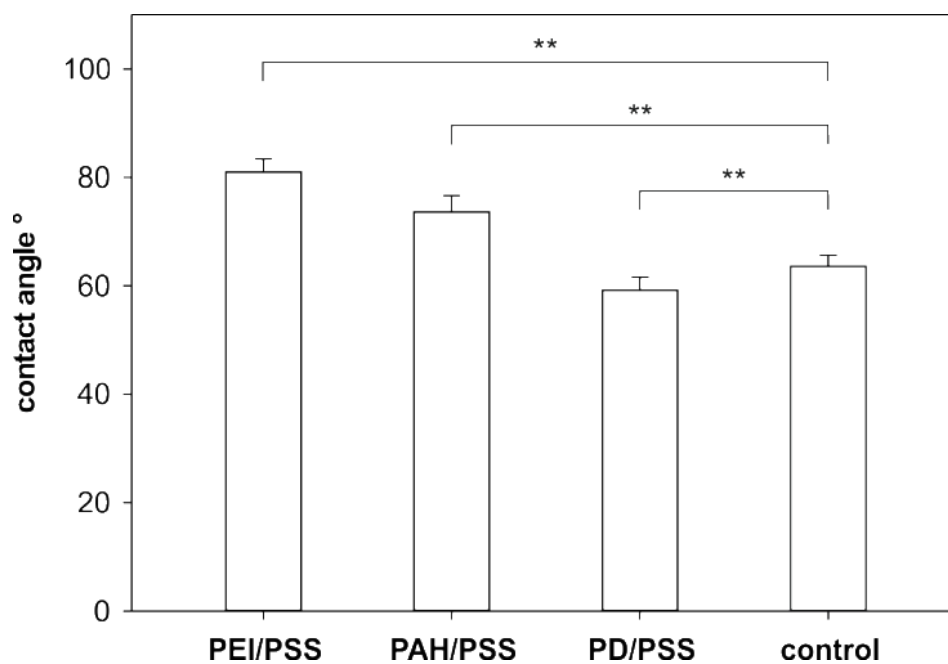


Figure S5 Contact angle measurements showed differences in the hydrophobicity of the oligolayer-coated surfaces. The PEI/PSS system was the most hydrophobic surface with a surface contact angle of about 80°, whereas the PD/PSS system was comparable hydrophilic with a contact angle lower than the control surface. (Statistical difference is indicated by ** $p < 0.05$)

Toxicity of LbL-coated gold nanoparticles

The toxicity of LbL-coated gold nanoparticles was evaluated by transmitted light microscopy (**Figure S6**). In combination with a MTT assay (**Figure S7**) it can be concluded that the nanoparticles had only minimal toxic effects at the applied concentrations.

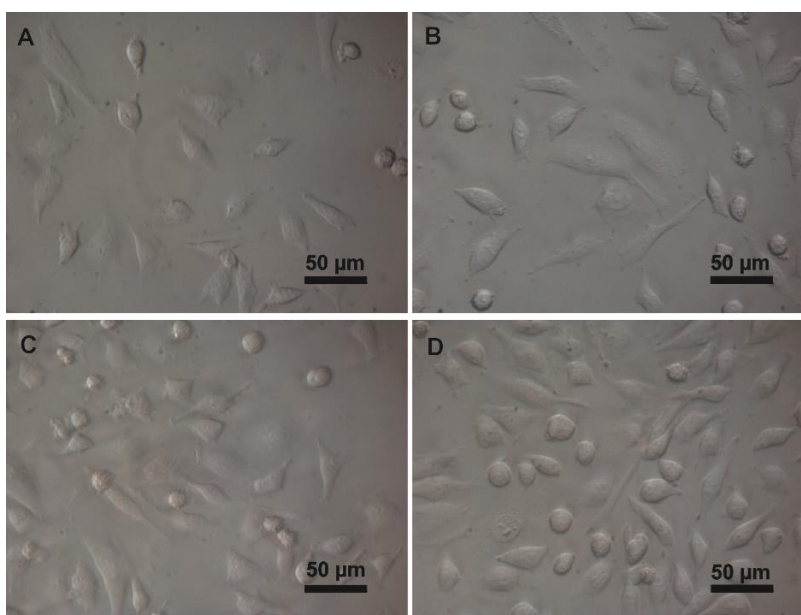


Figure S6 Transmitted light images of HeLa cells incubated with gold nanoparticles at a concentration of 5 pM. The gold nanoparticles were coated with **A)** PEI/PSS/PEI, **B)** PAH/PSS/PAH, **C)** PD/PSS/PD. The control cells (**D)** were treated as the samples but without the addition of any particles. HeLa cells that received gold nanoparticles look comparable to the control cells. The bar is 50 μm .

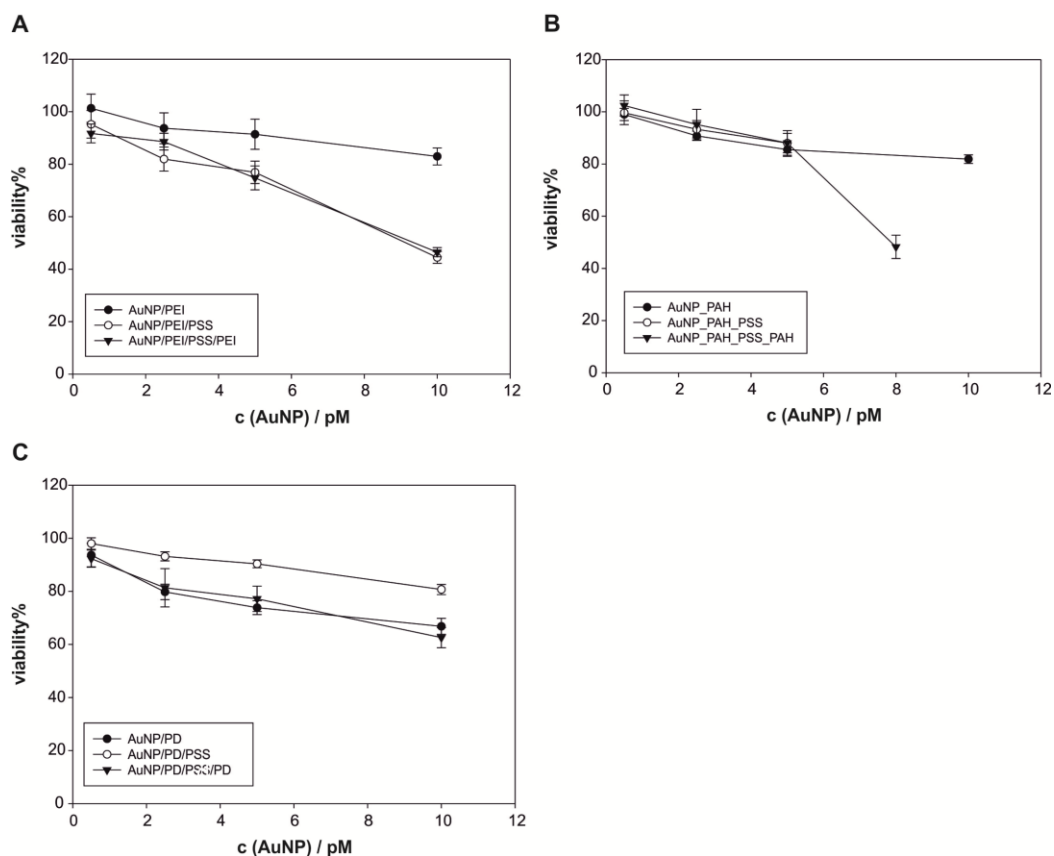


Figure S7. Evaluation of the toxicity of gold nanoparticles that were coated with **A)** PEI/PSS/PEI, **B)** PAH/PSS/PAH, **C)** PD/PSS/PD evaluated by a MTT assay. In the concentration range of the cell association studies (up to 5 pM), the cell viability was higher than 74%, which is assumed to be non-toxic. Only at higher concentrations, which were not used for cell association experiments, a reduced viability was measured.

References

- (1) Kooyman, R. P. H. Physics Of Surface Plasmon Resonance. In *Handbook of Surface Plasmon Resonance*, 1st ed.; Schaasfort, R. B. M.; Tudos, A. J., Eds.; Royal Society of Chemistry: Cambridge, Great Britain; 2008, pp 15-34.
- (2) Sadowski, J. W.; Korhonen, I. K.; Peltonen, J. P. Characterization Of Thin Films And Their Structures In Surface Plasmon Resonance Measurements. *Opt. Eng.* **1995**, *34*, 2581-2586.
- (3) Worm, J. Winspall 3.02, 2009, <http://www.mpip-mainz.mpg.de/groups/knoll/software>.

Chapter 5:

Foerster resonance energy transfer as a tool to
study the internal structure of polyelectrolyte
multilayers and the consequences for drug
delivery

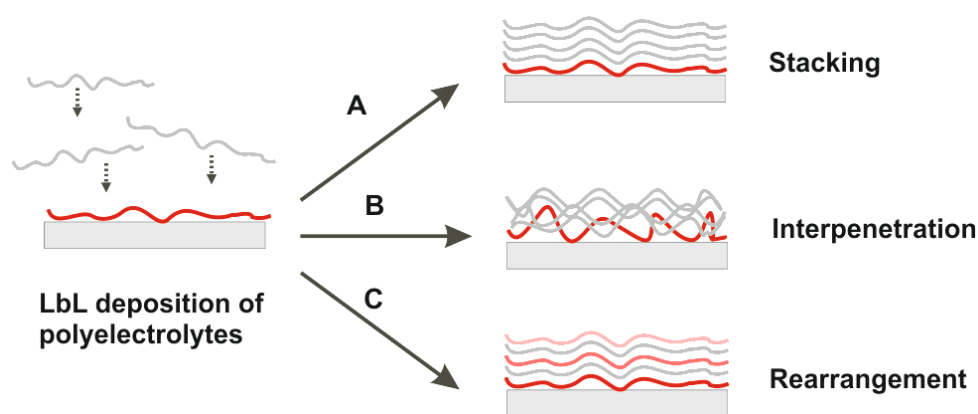
Abstract

Multilayer thin films are of great interest for the controlled delivery of both small molecule drugs and macromolecules. Control over the internal film structure is of paramount importance due to its expected impact on the mode of drug release. To this end, we developed a straightforward Foerster Resonance Energy Transfer (FRET)-based approach to determine the internal structure of multilayer films that were fabricated using the polycations poly(allylamine hydrochloride) (PAH), poly(ethylene imine) (PEI) and poly(diallyldimethyl ammonium chloride) (PD), each in combination with the polyanion poly(styrene sulfonate) (PSS). Layer interpenetration, which is associated with polymer chain indenting, dominated the PAH/PSS film, while the PEI/PSS pair showed a greater tendency toward rearrangement due to polymer diffusion. In the PD/PSS multilayer, the polyelectrolytes preferentially adopted a stratified conformation. Permeability of the multilayer to rhodamine revealed that a PAH/PSS film might be a favorable system for the delivery of small molecule drugs. Interestingly, the mode of release – from immediate to sustained – can be fine-tuned by increasing the degree of ionization of PAH. In contrast, the PAH film showed little promise for the delivery of charged macromolecules; chain indenting most likely inhibited swelling of the multilayer, thereby impeding release of these larger drugs. In this context, the PEI/PSS system is a very promising candidate. Swelling was particularly pronounced if the film assembly involved PEI with a high degree of ionization. The exquisite dependence of release on Angstrom/nanometer-scale film structure makes this FRET-based approach a valuable tool for screening polyelectrolyte pairs for use in drug delivery.

Introduction

Layer-by-layer (LbL) assembly is a simple and straightforward method for generating multilayer films on surfaces, achieved by sequential adsorption of oppositely charged polyelectrolytes.¹ In the field of drug delivery, LbL is a highly attractive technique due to the extraordinary high drug loading capacity of multilayer films,²⁻⁴ use of mild aqueous conditions for assembly,⁴ and last but not least, the potential for controlled release of multiple drugs.^{5,6} Examples range from fabrication of biodegradable films on implants, allowing for controlled release of small hydrophobic drugs over multiple months,⁷ to the incorporation of macromolecules such as nucleic acids or peptides and proteins into films that are subsequently wrapped around micro- or nano-particulate delivery vehicles.⁸

Low molecular weight drugs are typically released by diffusion,^{4,7} which in turn depends strongly on the film porosity.⁹ Alternatively, the active compound can be deposited as its own charged layer.^{2,3} Here, the drug release occurs via film erosion, which can be triggered by simple swelling or by a chemical reaction.^{4,10} Although a correlation most likely exists between the internal film structure and the mode of release,⁴ achieving precise control over release rate and duration represents tedious work, and often requires extensive trial and error. This is necessary for two reasons. First, slight modifications in film assembly conditions (e.g. pH) may have tremendous effects on the internal film structure.^{11,12} Second, the polyelectrolyte layers are dynamic and not primarily ordered as stratified layers (**Scheme 1**).^{4,13,14} For example, polymer chains interpenetrate into neighboring layers^{14,15,16} and are even able to diffuse from layer to layer within the film.^{17,18}



Scheme 1 A simplified overview of three characteristic internal structures of LbL multilayer films; smooth transitions exist between them. **A)** If the polyelectrolytes behave exclusively as rigid building blocks, the layers are flatly stacked upon one another. **B)** If interpenetration of the polymer chains occurs, the electrostatic attraction forces span several layers. This may be thought of as comparable to crosslinking between layers. **C)** Rearrangement leads to interlayer diffusion of polyelectrolyte chains during the deposition of further layers. This results in a homogenous distribution of polyelectrolyte throughout the film, independent of the sequence of deposition.

Unfortunately, detailed characterization of a multilayer's internal structure requires a significant analytical effort using methods that are not widely accessible, such as X-ray and neutron reflectivity, X-ray photoelectron spectroscopy, ellipsometry or microgravimetry.¹ In response, we developed a straightforward, accessible tool based on Foerster resonance energy transfer (FRET) to elucidate the internal structure of polyelectrolyte multilayers. We investigated multilayers of three different polycations – poly(allylamine hydrochloride) (PAH), poly(ethylene imine) (PEI) and poly(diallyldimethyl ammonium chloride)) (PD) – in combination with the polyanion poly(styrene sulfonate) (PSS). These polycations were chosen due to their widespread use as LbL building blocks^{13,19,20} or as transfection agents for nucleic acids.²¹ By systematically varying the theoretical inter-chain separation distance of a polymer-bound FRET pair within the multilayer, the internal structure was determined. In addition,

permeability and swelling of the multilayers were investigated to correlate internal structure with functionality in the context of a drug delivery application.

Materials and Methods

Materials

Unless otherwise stated, all chemicals were purchased from Sigma-Aldrich Chemical Company (Taufkirchen, Germany). Polyelectrolytes had the following molecular weights: poly(allylamine hydrochloride) (PAH) 17 kDa, branched poly(ethylene imine) (PEI) 25 kDa, poly(diallyldimethylammonium chloride) (PD) less than 100 kDa, poly(styrene sulfonate sodium salt) (PSS) 15 kDa (Polymer Standard Service, Mainz, Germany). Fluorescein isothiocyanate (FITC)- and tetramethylrhodamine isothiocyanate (TRITC)-PD with a degree of labeling of 220 were purchased from Surflay GmbH (Berlin, Germany). Ultrapure water was obtained using a Milli-Q-System (Merck Chemicals, Schwalbach, Germany).

Fluorescent Labeling of PEI and PAH

PEI and PAH were fluorescently labeled using FITC and TRITC according to a previously published protocol.²² Briefly, 0.42 ml of a 10 mg/ml solution of dye in DMSO was added to 10 ml of a 10 mg/ml aqueous solution of the polymer at pH 9. The reaction mixture was stirred overnight in the dark. The labeled polymer was subsequently purified by dialysis – using Slide-a-Lyzer Dialysis Cassettes with a molecular weight cut off of 3,500 (Thermo Scientific, Waltham, MA, USA) – against water for one week. The absence of unbound fluorescent dye was confirmed by agarose gel electrophoresis. It is important that the donor

and acceptor of the FRET pair were conjugated to different polyelectrolyte chains, meaning that each chain had only one type of conjugated molecule.

Multilayer fabrication

Multilayers for FRET analysis were prepared in 8-well chambered coverglasses (Nunc Lab Tek, NalgeNunc, Penfield, NY, USA). The chambers were prepared by rinsing with 10 mM SDS and 0.1 M HCl, followed by water, as previously described.¹⁷ The multilayers were assembled by adding 200 μ l of 1 mg/ml PEI, PAH or PD, respectively, to the chamber. The pH of the polymer solutions was adjusted to pH 7 or pH 9 by NaOH or HCl, respectively. Polymer solutions were incubated within the chamber for 30 min and then rinsed with water twice, followed by the addition of PSS as 2nd layer. Up to five polymer layers were applied by this technique and then used for FRET experiments. Fluorescently labeled polyelectrolytes were incorporated into various positions inside the LbL multilayer at various positions, as indicated in **Scheme 3**. For each FRET sample, which consisted of a FITC- and TRITC-labeled polymer pair, a control containing only the FITC-labeled donor polymer was fabricated as well.

Fluorescence spectroscopy

Fluorescence emission spectra of polymer solutions were recorded using a Perkin Elmer LS55 fluorescence spectrometer (Perkin Elmer, Waltham, MA, USA). The excitation wavelengths were 480 nm and 550 nm for FITC and TRITC, respectively, and the detector voltage was set to 650 V.

FRET measurements with Confocal Laser Scanning microscope

The fluorescence intensity of FITC emission was measured by a Zeiss confocal laser scanning microscope (Zeiss Axiovert 200 coupled to a LSM 510 META, Zeiss, Oberkochen, Germany) in the Lambda mode from 500 to 605 nm in 10.7 nm increments. The objective was a Plan-Neofluar 10x with a numerical aperture of 0.3 (Carl Zeiss, Germany). At least three images were taken per sample, and three regions of interest were used for each image. The FITC emission intensity at 526 nm was used for FRET efficiency calculations.

Calculation of FRET efficiency and dye distance

For the calculation of FRET efficiency, the FITC fluorescence intensity in a sample containing the FRET donor and acceptor ($I(\text{FITC})_{\text{DA}}$) was compared to the intensity of a sample containing only the FRET donor ($I(\text{FITC})_{\text{D}}$) (1).

$$E = 1 - \frac{I(\text{FITC})_{\text{DA}}}{I(\text{FITC})_{\text{D}}} \quad (1)$$

The Foerster equation (2) can be used for calculation of the distance between donor and acceptor fluorophores.^{23,24} The Foerster radius R_0 is defined as the distance between donor and acceptor leading to an energy transfer efficiency of 50%. For the FITC/TRITC donor/acceptor pair, R_0 is 5.4 nm.²⁵

$$E = \frac{1}{1 + (R/R_0)^X} \quad (2)$$

The exponential X in the equation stands for the spatial distribution of the donor and acceptor molecules and can take different values. For three-dimensionally distributed fluorophores, X is equal to 6.^{26,27} For resonance energy transfer of two planes of fluorophores, X is equal to 4.²⁸ For LbL-assembled FRET systems, both values can be found in the literature.^{23,24,29} As we assumed highly interpenetrating polymer layers instead of flat planes, all distances in this study were calculated with X equal to 6.

Water contact angle measurements

Water contact angle measurements were carried out on standard glass microscope slides. The slides were prepared by the same procedure as the chambered cover slides, using 10 mM SDS and 0.1 M HCl. The microscope slides were coated by a dipping protocol using 1 mg/ml polymer solutions and water rinsing steps in between addition of the polymer layers. The last layer was also rinsed with water and then air dried prior to the measurement. The water contact angle was determined with a dataphysics contact angle OCA system (dataphysics, Filderstadt, Germany) by the sessile drop principle. At least 20 measurements were taken per microscope slide and a non-coated slide served as control.

Permeability of multilayers to rhodamine

The permeability of the multilayers was investigated by allowing 5(6)-Carboxytetramethylrhodamine (rhodamine) to diffuse into a five-layered multilayer. The first layer consisted of a FITC-labeled polymer and the following four layers were non-fluorescent. After rinsing the last layer with water, the chamber slides were refilled with a 10 μ M solution of rhodamine and the FRET efficiency was measured over time as described above. The solution was exchanged with water during the fluorescence measurements to avoid signal disturbances. After each measurement, rhodamine was added again.

Swelling behavior of FRET multilayers

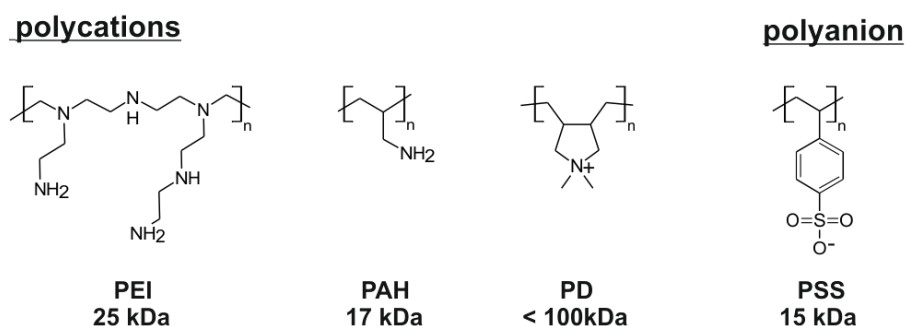
For the swelling experiments, five-layered multilayers with the FRET pair in the 1st and 3rd layer were prepared. Afterwards, the chamber slides were filled with cell culture medium with or without 10% fetal calf serum. Data points were selected to reflect typical incubation times in cell culture experiments, from 0 up to 20- 22 h.

Statistics

Results are shown as the mean \pm standard deviation (SD) of a representative sample. The SD was calculated from three regions of interest from a representative sample. All experiments were performed with two or three repetitions. Statistical significance was tested either by t-test or ANOVA/Student-Newman-Keuls analysis with SigmaPlot 12.0 (Systat Software Inc. San José, USA).

Results and Discussion

Three different polycations - PEI, PAH, PD - in combination with the polyanion PSS were alternately deposited on a substrate to assemble three film series, each with five total polyelectrolyte layers (**Scheme 2**).



Scheme 2 Chemical structures of the polyelectrolytes used to form multilayer films.

The FRET donor and acceptor molecules FITC and TRITC, respectively, were covalently linked to the primary amino groups of PEI and PAH to obtain the following polymer-bound FRET pairs: FITC-PEI / TRITC-PEI and FITC-PAH / TRITC-PAH. The labeling reaction was performed using a sub-stoichiometric amount of the dyes to avoid self-quenching and perturbation of the layer growth.³⁰ Because no primary amines are available in PD for the coupling reaction, commercially available FITC-PD and TRITC-PD copolymers were used as

a FRET pair. **Figure 1** shows the spectral overlap of FITC and TRITC, sufficient for measuring FRET efficiency after coupling to PEI (data for other FRET pairs not shown).

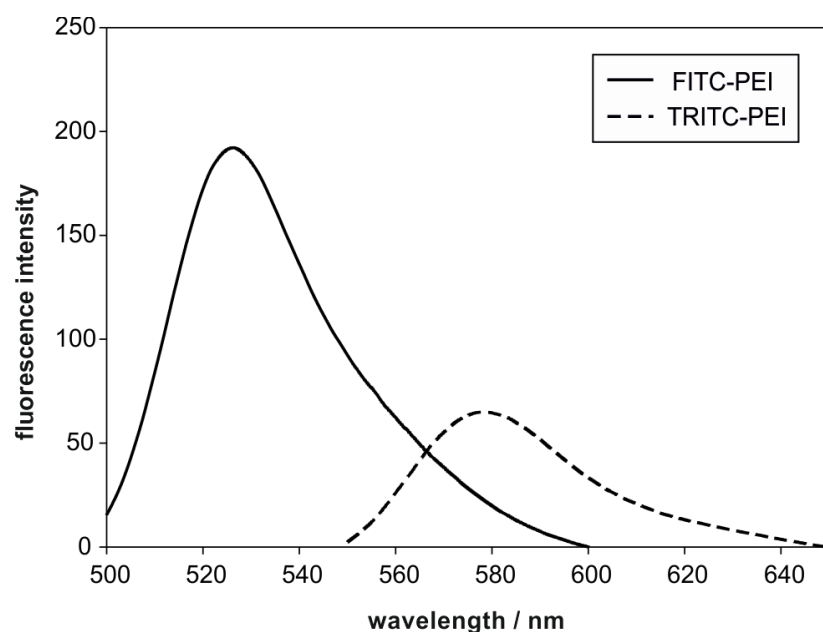


Figure 1 Fluorescence emission spectra of FITC-PEI and TRITC-PEI in solution. The excitation wavelength was 480 nm for FITC and 520 nm for TRITC.

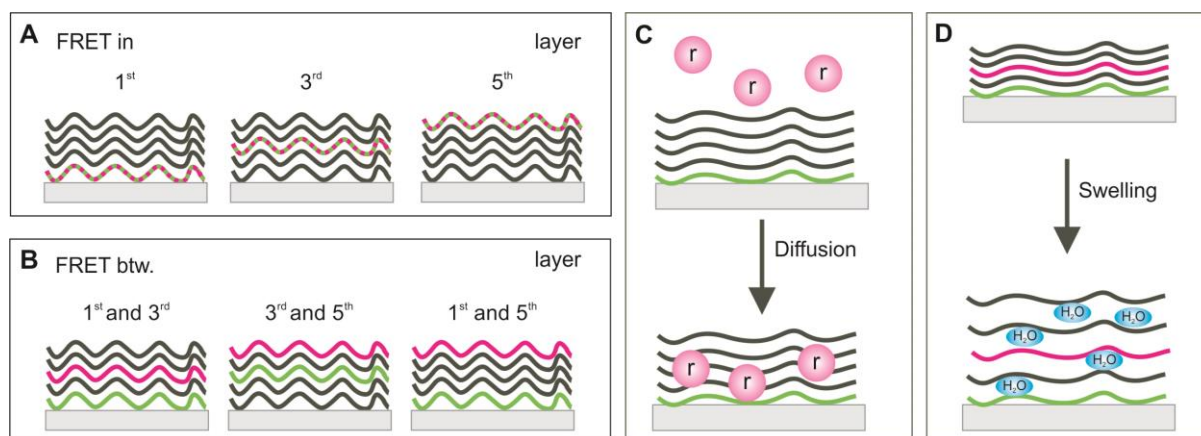
In all subsequent experiments, a calculated FRET efficiency of 1 indicates close spatial proximity of the two dyes. Correspondingly, decreasing FRET efficiency denotes increasing average distance between the two dyes.

Multilayer internal structure

To evaluate the multilayer's internal conformation, the polymer-bound FRET pair was deposited at different theoretical positions, as in **Scheme 3A** and **3B**.

As a first step, FRET-donor and FRET-acceptor polyelectrolyte conjugates were incorporated at a 1:1 ratio into either the 1st, 3rd or 5th layer (**Scheme 3A**). Using this experimental setup, it

was possible to estimate the degree of rearrangement of the polyelectrolytes within the multilayers (**Figure 2**).



Scheme 3 Multilayer coating schemes using the polymer-bound FRET donor (green) and acceptor (red), respectively. Five total layers were used in each experiment. **A)** The FRET donor and acceptor were deposited within the same layer (either the 1st, 3rd or 5th) at a 1:1 ratio. Because the donor and acceptor of the FRET pair were conjugated to different polyelectrolyte chains, each chain had only one type of conjugated molecule. **B)** The FRET pair was separated by non-fluorescent spacer layers resulting in two short-distant FRET pairs (donor in 1st layer and acceptor in 3rd layer or donor in 3rd layer and acceptor in 5th layer) and a long-distant FRET pair (donor in 1st layer and acceptor in 5th layer). **C)** To evaluate multilayer permeability, the FRET donor was deposited in the 1st layer. Free rhodamine (r) was the acceptor in this set-up, and was assumed to diffuse through the multilayer. **D)** Swelling of the multilayer leads to the incorporation of water molecules and a vertical expansion of the layers.

If the polyelectrolytes had a high tendency towards rearrangement, the FRET pair would randomly distribute within the film, consequently leading to a FRET efficacy smaller than 1. For PEI/PSS films, the FRET efficiency was about 0.5 when the dyes were incorporated into the 1st or 3rd layer. This is in good agreement with literature because PEI is not fully charged

at the selected assembly conditions (pH 10), and is thus capable of diffusing within the film.³¹ When the FRET pair was incorporated into the 5th layer, the FRET efficacy was significantly higher. Here, only a minimal degree of rearrangement occurred because no further diffusion toward the surface of the film was possible.

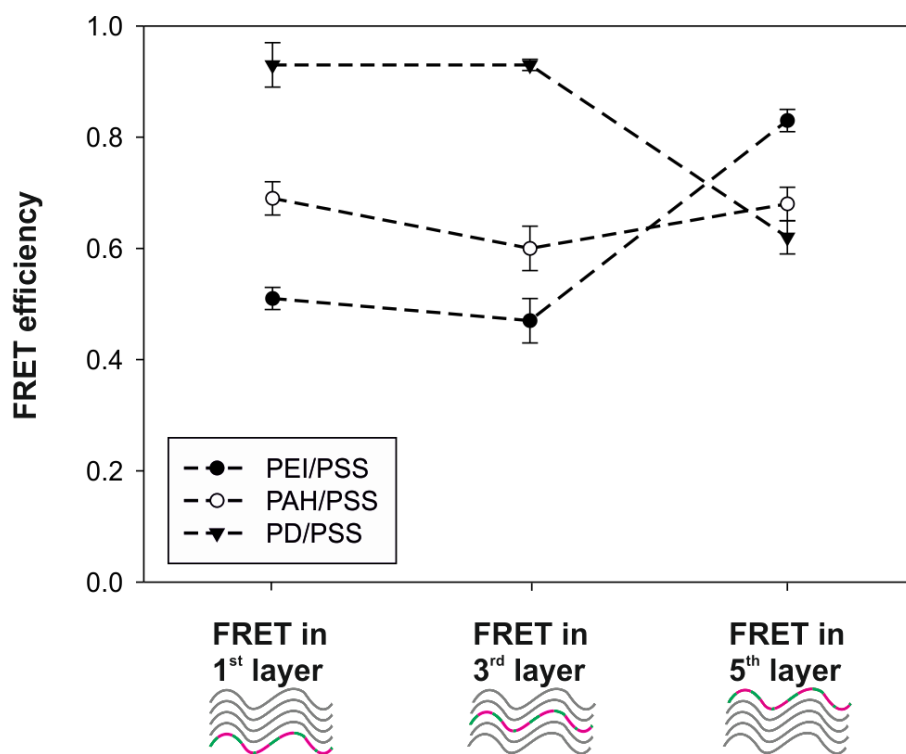


Figure 2 FRET efficiencies after incorporating the FRET pair within the same polymer layer of a multilayer film. For the PEI series, an increase of the efficiency was observed if the FRET pair was deposited in the 5th layer. In contrast, the efficiency was constant in all multilayer constructions for the PAH series. In the PD series, the FRET efficiency decreased when the FRET pair was present in the 5th layer. Dashed lines are shown only to guide the eye.

The opposite was observed for PD/PSS films; there, the efficiency of the FRET pair in the 1st or 3rd layer was close to 1, implying that the polymer chains did not diffuse nor rearrange inside the multilayer upon deposition of additional layers. When the FRET pair was deposited

in the 5th layer of a PD/PSS film, we observed lower FRET efficiency. This may be due to a minor change of the polyelectrolyte conformation upon coating, which aligned the dyes such that they could not properly interfere.³² For the PAH/PSS films, a certain degree of rearrangement was observed, although to a lesser extent than that found for PEI/PSS. The FRET efficiency in this case was about 0.6 to 0.7, independent of the deposition layer within the film.

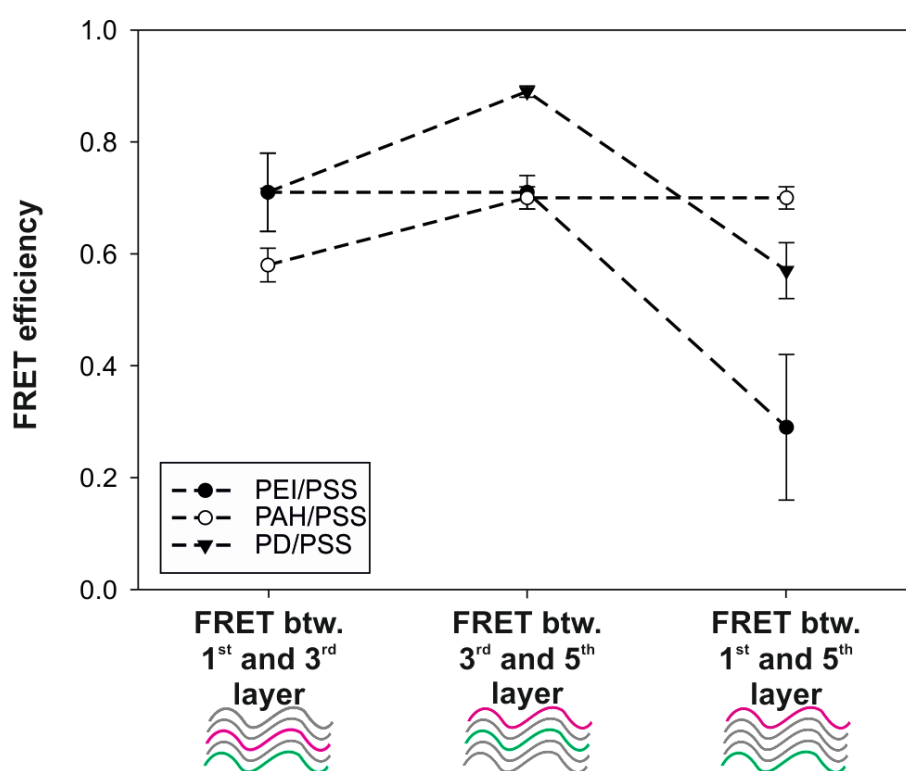


Figure 3 The FRET pair was separated by either one or three non-fluorescent spacer layers resulting in two short-distant FRET pairs (donor in 1st layer and acceptor in 3rd layer or donor in 3rd layer and acceptor in 5th layer) and a long distant FRET pair (donor in 1st layer and acceptor in 5th layer). In case of PD/PSS and PEI/PSS, a decreasing FRET efficiency was observed with an increasing distance between the donor and acceptor. For the PAH/PSS pair, the FRET efficiency remained nearly constant. The dashed lines are shown only to guide the eye.

In the next step, the FRET pairs were separated by non-fluorescent spacer layers (**Scheme 3B**). In this setup, two short-distant FRET pairs and a long-distant FRET pair were utilized. For all PAH/PSS films, the FRET efficiency and the calculated fluorophore distances were similar, even if the donor and acceptor were separated by three non-fluorescent spacer layers (**Figure 3**). These results are in good agreement with the literature, as PAH/PSS is known to be a highly interpenetrating polyelectrolyte combination, with polymer chains spreading over 3 to 5 single layers.^{15,27} In the case of PEI/PSS, both short-distant pairs had equivalent FRET efficiencies and donor-acceptor distances of about 4.7 nm. However, when the FRET pair was separated by multiple spacer layers, the FRET efficiency significantly decreased. At the same time, the calculated donor-acceptor distance increased to about 6.4 nm. Hence, polyelectrolyte stacking likely occurred to a certain degree during formation of the PEI/PSS multilayer.

A similar trend was observed for the PD/PSS pair, which can also be understood in the context of polyelectrolyte stacking. The higher efficiency when the PD-bound FRET pair was positioned in the 3rd and 5th layer, as compared to that when positioned in the 1st and 3rd layer, is probably due to better alignment of the dyes with increasing distance from the substrate. Using this straightforward FRET-based approach it was possible to characterize the internal structure of the three multilayer series; an overview of the results is given in Table 1. For the PAH/PSS films, interpenetration dominates, whereas PEI/PSS films show a greater tendency towards rearrangement, and to a lesser degree, stacking. In the PD/PSS film, the polyelectrolytes seem to prefer a stratified conformation. However, a certain degree of interpenetration is also expected to occur, as LbL assembly on the basis of stacking alone is highly unlikely.³³ These results are in good agreement with the literature.^{15-18,24,27,34,35} It is worthwhile to mention that transitions between the three categories are smooth and that several other possibilities are also well described in the literature.³⁶⁻³⁸

To further evaluate the feasibility of the FRET-based approach, we modulated the internal structure of the multilayer by adjusting the polyelectrolytes' charge density (**Figure 4**).

Table 1 Summary of the internal structure of the three multilayer series. The relative importance of the three conformations was weighted from o (moderate influence) to ++ (high influence).

	PAH/PSS	PEI/PSS	PD/PSS
Rearrangement	+	++	o
Interpenetration	++	o	+
Stacking	o	+	++

Although the pK_a values of polyelectrolytes within multilayers differ significantly from those in solution,^{11,39} complicating the estimation of the charge density, we can still make relative statements about the direction of charge density change with changes in pH, if the chemical structure of the polyelectrolyte is known. Because PAH and PEI are both weak polyelectrolytes (PAH carries only primary amino groups and has a pK_a of about 9.5⁴⁰; PEI is functionalized by primary, secondary and tertiary amino groups and has an overall pK_a of about 8.5⁴¹), their charge density is primarily controlled by the pH of the surrounding solution.^{12,13} Hence, moderately ionized films were formed at pH 10, above the pK_a of both polyelectrolytes, and more highly ionized films were formed at pH 7, below the pK_a value of both polyelectrolytes. FRET donor-acceptor fluorophores were incorporated into the PEI/PSS and PAH/PSS films as long-distant FRET pair in the 1st and 5th layer, separated by three non-fluorescent spacer layers (**Scheme 3B**). Because PD is a strong polyelectrolyte and its charge density is independent of pH, PD/PSS films were not investigated by this setup. For the PAH/PSS films, the FRET efficacy was about 0.8 and independent of the assembly

conditions. As before, the relatively high FRET efficiency is due to layer interpenetration (Table 1).

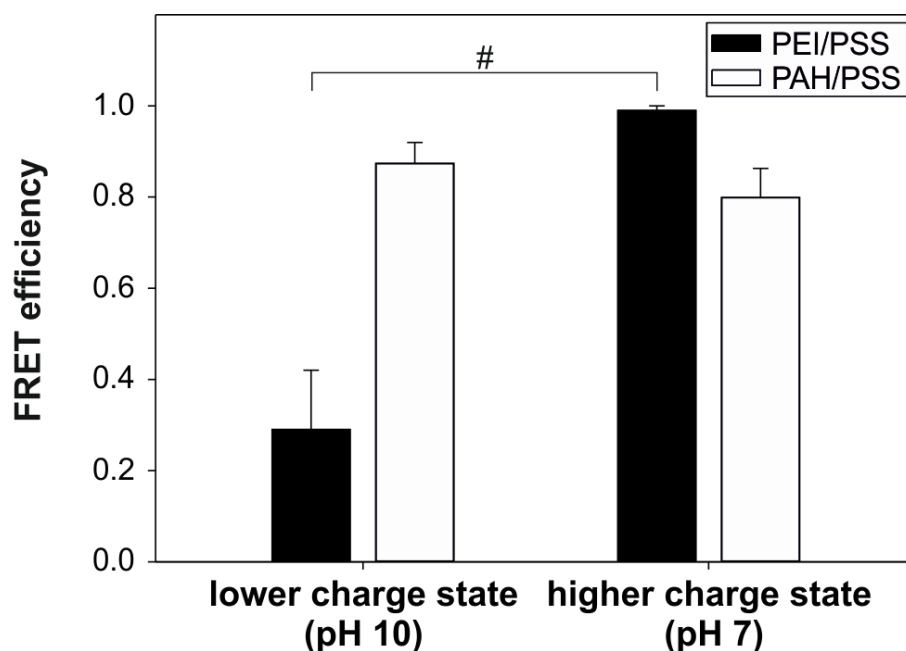
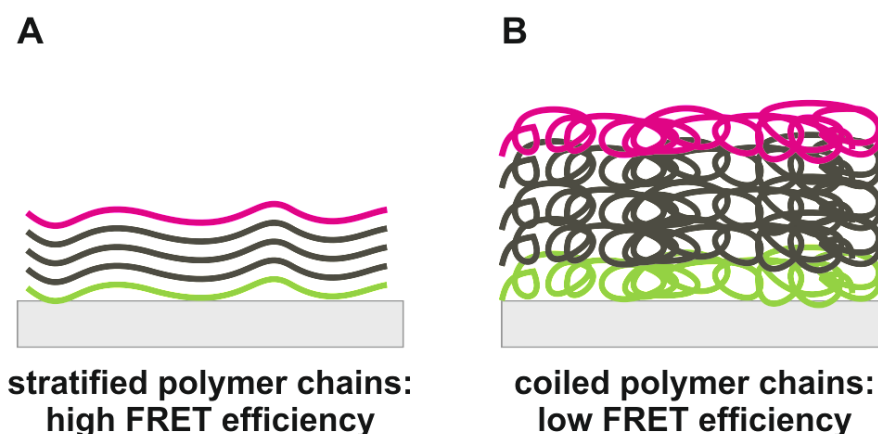


Figure 4 Multilayers were assembled at different pH values to control the degree of ionization of the weak bases PAH and PEI. Varying the charge density had no significant influence on the PAH/PSS film, but the FRET efficiency significantly increased with an increasing degree of ionization of PEI. A statistically significant difference is indicated by # with $p < 0.01$.

In contrast, assembly conditions for the PEI/PSS films significantly impacted the FRET efficacy. If PEI at higher charge density (pH 7) was applied, the donor and acceptor were forced into closer proximity, driving an increase in FRET efficiency. This suggests that the internal structure of the PEI/PSS multilayer exhibits conformational differences depending on the degree of ionization.

Above a certain degree of ionization, polyelectrolytes adopt a more stratified conformation due to electrostatic repulsion.¹³ Below a critical value, the inter-chain repulsion becomes less important, and the polyelectrolytes form loops and coils. As a consequence, multilayers prepared using polymers of high charge density commonly become thinner and vice versa.^{11,13} It can be concluded that PEI/PSS at pH 10 was present in a more looped/coiled conformation; at pH 7, the conformation is more stratified in character (**Scheme 4**). Hence, the FRET based approach is a valuable tool for highlighting charge density-induced differences in internal film structure.



Scheme 4 Polyelectrolytes adsorb to a surface in different conformations depending on their degree of ionization. **A)** If the charge density reaches a polymer-specific threshold, the polyelectrolytes adopt a more stratified conformation, the film becomes thinner and the FRET efficiency increases. **B)** In the case of weakly charged polymer chains, a looped/coiled conformation is preferred, leading to a larger average distance between FRET donors and acceptors and a correspondingly lower FRET efficiency.

Multilayer permeability to small molecules

The multilayer composition's critical importance in controlled release of drugs⁴ raised the question: does the internal structure of the film correlate with its permeability to small molecules? To this end, the polymer-bound FRET donor was deposited in the 1st layer of a film with a total of five layers (**Scheme 3C**).

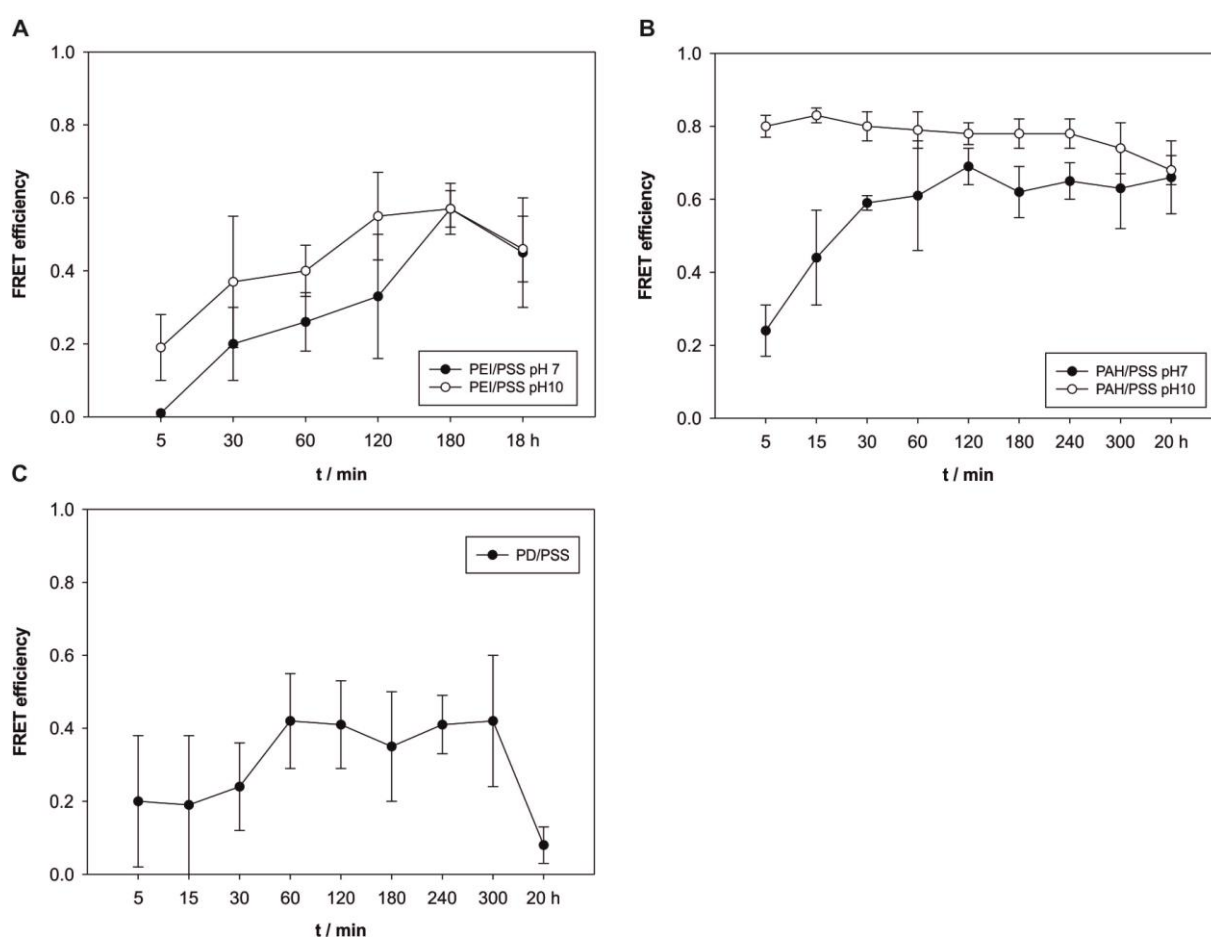


Figure 5 The permeability of the three multilayer films to rhodamine. **A)** The permeability of the PEI/PSS film was time-dependent, with slight delays seen for more highly ionized PEI. **B)** A distinct difference was found for the PAH/PSS film. Remarkable permeability was observed at a lower degree of PAH ionization. In contrast, more highly ionized PAH led to a much denser internal film structure, accompanied by lower permeability to rhodamine. **C)** The PD film showed a poor permeability to rhodamine.

Rhodamine was chosen as a FRET acceptor due to its ability to simultaneously act as a representative model of a hydrophobic small molecule drug. Rhodamine was assumed to passively diffuse through the multilayer; as soon as it neared a FITC donor molecule in the 1st layer, the FRET efficacy was expected to increase due to energy transfer (**Figure 5**).

The PEI/PSS multilayer exhibited time-dependent development of a FRET effect. With respect to PEI/PSS films with a lower degree of PEI ionization (pH 10), FRET was delayed when the PEI was more highly ionized (pH 7), but both multilayers reached the same FRET efficiency endpoint. Surprisingly, the previously detected dependence of multilayer thickness on pH had just a minor influence on the permeability of rhodamine. Since polyelectrolytes in a PEI/PSS film have a strong tendency towards rearrangement (**Table 1**), rhodamine most likely reached the FITC FRET donor after diffusing a shorter distance through the film than the distance defined by the sequence in which layers were deposited. In contrast, tremendous differences in FRET onset were found for PAH/PSS films at different pH. At a lower PAH charge density, the FRET effect reached a plateau after a few minutes, while it emerged over a longer time period for more highly ionized PAH. Again, the differences can be related to the internal structure of the multilayer.

As illustrated (**Scheme 4**), a higher charge density leads to a multilayer with more interpenetrations, acting as crosslinks between the polyelectrolytes, leading to a more densely packed multilayer and hindering rhodamine diffusion. In contrast, a lower charge density leads to a less interpenetrated structure; the multilayer is most likely loosely packed, with a porous structure that facilitates rhodamine diffusion. The permeability of the PD/PSS film to rhodamine was lower than that of the other combinations and near the detection limit of the analytical setup. As PD carries only quaternary ammonium groups, multilayer formation and structure were independent of pH. Because both PD and PSS are completely charged and

because a stratified polyelectrolyte conformation is preferred (**Table 1**), the PD/PSS film most likely represents a formidable barrier even for small molecules such as rhodamine.

The hydrophobicity of the coated surfaces is another important factor that plays a role in the permeability of a film to rhodamine.⁴ Hence, the water contact angle of the multilayers was determined (**Figure 6**).

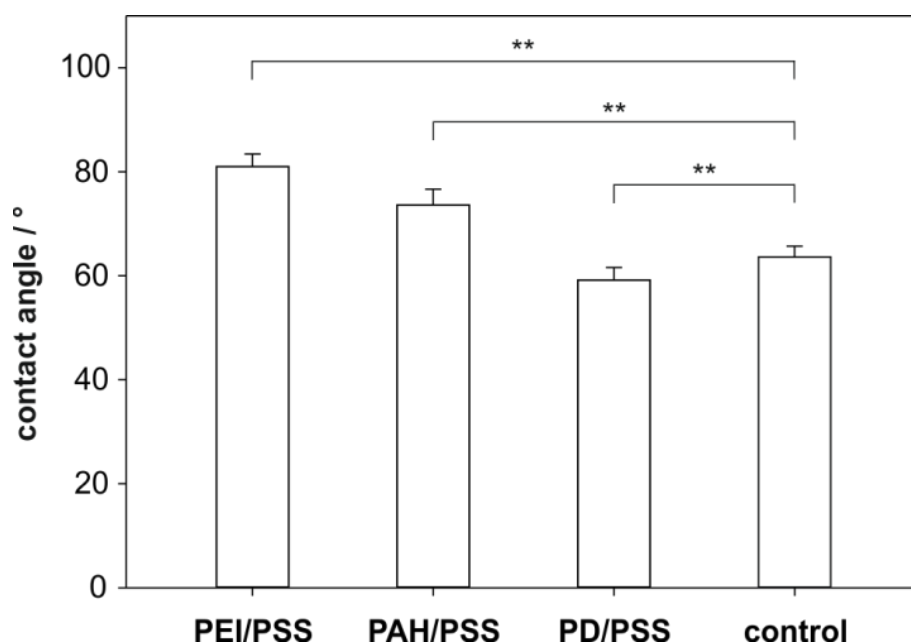


Figure 6 Contact angle measurements showed differences in the hydrophobicity of the multilayer films. The PEI/PSS system was the most hydrophobic surface with a surface contact angle of approximately 81 °, while the PD/PSS system was rather hydrophilic. Statistically significant differences are indicated by ** with $p < 0.05$.

The PEI/PSS and PAH/PSS coatings were rather hydrophobic with contact angles of 81 ° and 74 °, respectively. The PD/PSS surface was hydrophilic with a surface contact angle of 59 °. The results are in good agreement with the literature; the combination of two strong polyelectrolytes has been shown to lead to hydrophilic surfaces, while pairing a weak and a

strong polyelectrolyte produced more hydrophobic surfaces.⁴² Consequently, it is not surprising that permeation of the hydrophobic rhodamine into a hydrophilic multilayer such as PD/PSS was hindered. As a whole, this FRET-based approach is a useful tool for rapid screening of polyelectrolyte pairs for their potential to permit permeation of small molecules in different scenarios. For example, if fast drug release is desired, a multilayer of PAH/PSS prepared under basic conditions could be appropriate. On the other hand, assembled at neutral pH, the same coating might be capable of sustained release.

Multilayer swelling

Complete film disassembly is a strong requirement if the active drug substance is a polyelectrolyte and part of the multilayer construction, as would be the case with a nucleic acid therapeutic.^{2,3} In this case, multilayer disassembly can be induced by simple swelling,⁴ which resembles a vertical expansion of the film.^{43,44} We used the FRET tool to address whether or not vertical multilayer expansion due to swelling can be detected. To this end, the FRET donor and acceptor was deposited in the 1st and 3rd layer of the multilayer containing a total of five layers (**Scheme 3D**). If swelling were to occur, the FRET efficiency would be expected to decrease due to an increasing average distance between the donor- and acceptor-bearing polyelectrolytes. To mimic biological context to a certain extent, the experiments were performed in cell culture medium with or without serum. We focused on the PAH- and PEI-based films due to the ability to vary the degree of ionization by controlling the pH.

The PAH/PSS multilayers were more or less resistant to swelling (**Figure 7A** and **7B**). All samples showed a slight initial drop in FRET efficiency, but 80% of the FRET efficiency was still present after 20 h. This means that vertical expansion, due to the uptake of water

molecules, played a minor role. PEI/PSS multilayers, on the other hand, were more prone to swelling; FRET efficiency dropped appreciably over time (**Figure 7C and 7D**).

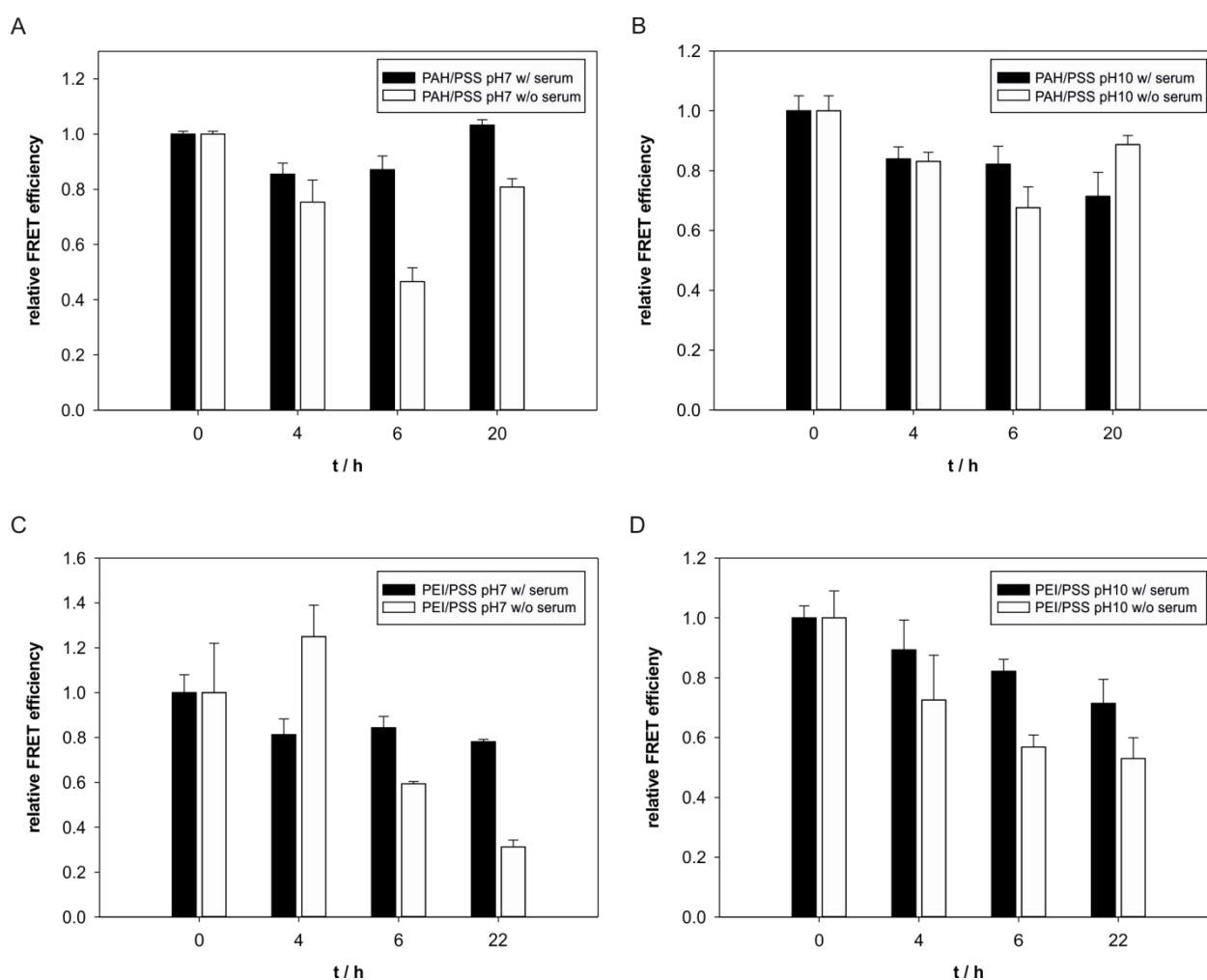


Figure 7 Swelling behavior of the three multilayer films. **A)** and **B)** Despite an initial drop, the PAH/PSS films were relatively resistant to swelling, regardless of fabrication conditions (pH 7 or 10), and hence, the degree of polyelectrolyte ionization. Likewise, the presence or absence of serum was not observed to play a substantial role. **C)** and **D)** Pronounced swelling was observed for the PEI/PSS multilayer fabricated with high-charge-density-PEI and incubated in culture medium without serum.

This decrease was less pronounced if the multilayers were incubated in culture medium containing serum. The stabilizing effect of serum proteins on multilayers has been described before.³ The swelling properties of the multilayers agreed very well with the conclusions

drawn from previous experiments regarding the films' internal structure (**Table 1**). For instance, PAH/PSS films were thought to have interpenetrating crosslinks between the polymer layers. Those strong interactions between the polymer chains led to high swelling resistance, similar to that of a highly cross-linked hydrogel.⁴⁵ In contrast, PEI/PSS film structure is believed to be driven more by stacking and rearranging than interpenetration. Hence, layer-layer cohesion is weaker, enabling water molecules to more easily expand the distance between layers. Consequently, it becomes obvious that swelling of the PEI/PSS multilayers will most likely lead to a higher release of therapeutic polyelectrolyte molecules than what would be expected from a PAH/PSS film, for instance. In this context, it is not astonishing that PEI has been successfully used as an LbL building block for the delivery of nucleic acids.^{3,46}

Conclusion

We have elucidated the internal structure of polyelectrolyte multilayers using a straightforward FRET-based approach. Highly interpenetrating polyelectrolyte multilayers were assembled by combining PAH and PSS. In contrast, PEI/PSS multilayers demonstrated a high tendency towards rearrangement due to polymer diffusion. Polymer stacking dominated the PD/PSS film structure. Here, further studies in the multilayer architecture with complementary analytical methods, such as ellipsometry, are necessary to confirm those findings. Investigation into the permeability of the multilayers and their swelling behavior revealed that the PAH/PSS multilayer could be a favorable system for the delivery of small hydrophobic drug molecules. Moreover, by adjusting film assembly conditions, the drug release mode of PAH/PSS films can be tuned from immediate to sustained release. Because the PAH/PSS system is characterized by indenting crosslinks due to its highly interpenetrating nature, it is poorly qualified for delivering drug compounds that are part of the multilayer construction, such as nucleic acids. Here, the PEI/PSS system seems to be a very promising candidate, particularly if the film assembly involved PEI with a high degree of ionization. Finally, serum was shown to have a stabilizing effect on multilayer structures, reducing their tendency towards swelling and drug release. The FRET-based approach is a powerful tool for screening polyelectrolyte pairs and their corresponding deposition conditions for suitability in a variety of drug delivery applications.

References

- (1) *Multilayer Thin Films*; Decher, G., Schlenoff, J.B., Eds.; Wiley -VCH; Weinheim, Germany, 2012.
- (2) Deng, Z. J.; Morton, S. W.; Ben-Akiva, E.; Dreaden, E. C.; Shopsowitz, K. E.; Hammond, P. T. Layer-By-Layer Nanoparticles For Systemic Codelivery Of An Anticancer Drug And siRNA For Potential Triple-Negative Breast Cancer Treatment. *ACS Nano* **2013**, *7*, 9571-9584.
- (3) Elbakry, A.; Zaky, A.; Liebl, R.; Rachel, R.; Goepferich, A.; Breunig, M. Layer-By-Layer Assembled Gold Nanoparticles For siRNA Delivery. *Nano Lett.* **2009**, *9*, 2059-2064.
- (4) Pavlukhina, S.; Sukhishvili, S. Polymer Assemblies For Controlled Delivery Of Bioactive Molecules From Surfaces. *Adv. Drug Delivery Rev.* **2011**, *63*, 822-836.
- (5) Hong, J.; Shah, N. J.; Drake, A. C.; DeMuth, P. C.; Lee, J. B.; Chen, J.; Hammond, P. T. Graphene Multilayers As Gates For Multi-Week Sequential Release Of Proteins From Surfaces. *ACS Nano* **2012**, *6*, 81-88.
- (6) Hsu, B. B.; Hagerman, S. R.; Jamieson, K.; Veselinovic, J.; O'Neill, N.; Holler, E.; Ljubimova, J. Y.; Hammond, P. T. Multilayer Films Assembled From Naturally-Derived Materials For Controlled Protein Release. *Biomacromolecules* **2014**, *15*, 2049-2057.
- (7) Hsu, B. B.; Park, M. -.; Hagerman, S. R.; Hammond, P. T. Multimonth Controlled Small Molecule Release From Biodegradable Thin Films. *Proc. Natl. Acad. Sci.* **2014**, *111*, 12175-12180.
- (8) de Koker, S.; Hoogenboom, R.; de Geest, B. G. Polymeric Multilayer Capsules For Drug Delivery. *Chem. Soc. Rev.* **2012**, *41*, 2867-2884.

- (9) Mendelsohn, J. D.; Barrett, C. J.; Chan, V. V.; Pal, A. J.; Mayes, A. M.; Mayes, A. M.; Rubner, M. F. Fabrication Of Microporous Thin Films From Polyelectrolyte Multilayers. *Langmuir* **2000**, *16*, 2017-5023.
- (10) Lynn, D. Peeling Back The Layers: Controlled Erosion And Triggered Disassembly Of Multilayered Polyelectrolyte Thin Films. *Adv. Mater.* **2007**, *19*, 4118-4130.
- (11) Choi, J.; Rubner, M. F. Influence Of The Degree Of Ionization On Weak Polyelectrolyte Multilayer Assembly. *Macromolecules* **2005**, *38*, 116-124.
- (12) Shiratori, S. S.; Rubner, M. F. Ph-Dependent Thickness Behavior Of Sequentially Adsorbed Layers Of Weak Polyelectrolytes. *Macromolecules* **2000**, *33*, 4213-4219.
- (13) von Klitzing, R. Internal Structure Of Polyelectrolyte Multilayer Assemblies. *Phys. Chem. Chem. Phys.* **2006**, *8*, 5012-5033.
- (14) Schönhoff, M. Self-Assembled Polyelectrolyte Multilayers. *Curr. Opin. Colloid Interface Sci.* **2003**, *8*, 86-95.
- (15) Lösche, M.; Schmitt, J.; Decher, G.; Bouwman, W. G.; Kjaer, K. Detailed Structure Of Molecularly Thin Polyelectrolyte Multilayer Films On Solid Substrates As Revealed By Neutron Reflectometry. *Macromolecules* **1998**, *31*, 8893-8906.
- (16) Castelnovo, M.; Joanny, J. Formation Of Polyelectrolyte Multilayers. *Langmuir* **2000**, *16*, 7524-7532.
- (17) Picart, C.; Mutterer, J.; Richert, L.; Luo, Y.; Prestwich, G. D.; Schaaf, P.; Voegel, J. -. C.; Lavalle, P. Molecular Basis For The Explanation Of The Exponential Growth Of Polyelectrolyte Multilayers. *Proc. Natl. Acad. Sci. U.S.A.* **2002**, *99*, 12531-12535.
- (18) Lavalle, P.; Vivet, V.; Jessel, N.; Decher, G.; Voegel, J.; Mesini, P. J.; Schaaf, P. Direct Evidence For Vertical Diffusion And Exchange Processes Of Polyanions And Polycations In Polyelectrolyte Multilayer Films. *Macromolecules* **2004**, *37*, 1159-1162.
- (19) Nestler, P.; Paßvogel, M.; Helm, C. A. Influence Of Polymer Molecular Weight On The Parabolic And Linear Growth Regime Of PDADMAC/PSS Multilayers. *Macromolecules* **2013**, *46*, 5622-5629.

- (20) Elzbieciak, M.; Zapotoczny, S.; Nowak, P.; Krastev, R. Influence Of pH On The Structure Of Multilayer Films Composed Of Strong And Weak Polyelectrolytes. *Langmuir* **2009**, *25*, 3255-3259.
- (21) Lungwitz, U.; Breunig, M.; Blunk, T.; Göpferich, A. Polyethylenimine-Based Non-Viral Gene Delivery Systems. *Eur. J. Pharm. Biopharm.* **2005**, *60*, 247-266.
- (22) von Klitzing, R.; Möhwald, H. A Realistic Diffusion Model For Ultrathin Polyelectrolyte Films. *Macromolecules* **1996**, *29*, 6901-6906.
- (23) Lee, L.; Johnston, A. P. R.; Caruso, F. Probing The Dynamic Nature Of DNA Multilayer Films Using Förster Resonance Energy Transfer. *Langmuir* **2012**, *28*, 12527-12535.
- (24) Lundin, M.; Blomberg, E.; Tilton, R. D. Polymer Dynamics In Layer-By-Layer Assemblies Of Chitosan And Heparin. *Langmuir* **2010**, *26*, 3242-3251.
- (25) Wu, P.; Brand, L. Resonance Energy Transfer: Methods And Applications. *Anal. Biochem.* **1994**, *218*, 1-13.
- (26) Farinha, J.; Martinho, J.; Yekta, A. Direct Nonradiative Energy Transfer In Polymer Interphases: Fluorescence Decay Functions. *Macromolecules* **1995**, *28*, 6084-6088.
- (27) Baur, J. W.; Rubner, M. F.; Reynolds, J. R.; Kim, S. Förster Energy Transfer Studies Of Polyelectrolyte Heterostructures Containing Conjugated Polymers: A Means To Estimate Layer Interpenetration. *Langmuir* **1999**, *15*, 6460-6469.
- (28) Richter, B.; Kirstein, S. Excitation Energy Transfer Between Molecular Thin Layers Of Poly(Phenylene Vinylene) And Dye Labeled Poly(Allylamine) In Layer-By-Layer Self-Assembled Films. *J. Chem. Phys.* **1999**, *111*, 5191.
- (29) Bricaud, Q.; Fabre, R. M.; Brookins, R. N.; Schanze, K. S.; Reynolds, J. R. Energy Transfer Between Conjugated Polyelectrolytes In Layer-By-Layer Assembled Films. *Langmuir* **2011**, *27*, 5021-5028.
- (30) Kato, N.; Caruso, F. Homogeneous, Competitive Fluorescence Quenching Immunoassay Based On Gold Nanoparticle/Polyelectrolyte Coated Latex Particles. *J. Phys. Chem. B* **2005**, *109*, 19604-19612.
- (31) Zacharia, N. S.; Modestino, M.; Hammond, P. T. Factors Influencing The Interdiffusion Of Weak Polycations In Multilayers. *Macromolecules* **2007**, *40*, 9523-9528.

- (32) Rasnik, I.; McKinney, S. A.; Ha, T. Surfaces And Orientations: Much To FRET About? *Acc. Chem. Res.* **2005**, *38*, 542-548.
- (33) Decher, G. Fuzzy Nanoassemblies: Toward Layered Polymeric Multicomposites. *Science* **1997**, *277*, 1232-1237.
- (34) Lavalle, P.; Picart, C.; Mutterer, J.; Gergely, C.; Reiss, H.; Voegel, J.; Senger, B.; Schaaf, P. Modeling The Buildup Of Polyelectrolyte Multilayer Films Having Exponential Growth *J. Phys. Chem. B.* **2004**, *108*, 635-648.
- (35) Wood, K. C.; Chuang, H. F.; Batten, R. D.; Lynn, D. M.; Hammond, P. T. Controlling Interlayer Diffusion To Achieve Sustained, Multiagent Delivery From Layer-By-Layer Thin Films. *Proc. Natl. Acad. Sci.* **2006**, *103*, 10207-10212.
- (36) Buron, C. C.; Filiâtre, C. Overshoots Of Adsorption Kinetics During Layer-By-Layer Polyelectrolyte Film Growth: Role Of Counterions. *J. Colloid Interface Sci.* **2014**, *413*, 147-153.
- (37) Laschewsky, A.; Wischerhoff, E.; Kauranen, M.; Persoons, A. Polyelectrolyte Multilayer Assemblies Containing Nonlinear Optical Dyes. *Macromolecules* **1997**, *30*, 8304-8309.
- (38) Fery, A.; Schöler, B.; Cassagneau, T.; Caruso, F. Nanoporous Thin Films Formed By Salt-Induced Structural Changes In Multilayers Of Poly(Acrylic Acid) And Poly(Allylamine). *Langmuir* **2001**, *17*, 3779-3783.
- (39) Burke, S. E.; Barrett, C. J. Acid-Base Equilibria Of Weak Polyelectrolytes In Multilayer Thin Films. *Langmuir* **2003**, *19*, 3297-3303.
- (40) Silva, C. P.; Carapuça, H. M. Glassy Carbon Electrodes Coated With Poly(Allylamine Hydrochloride), PAH: Characterization Studies And Application To Ion-Exchange Voltammetry Of Trace Lead(II) At Combined PAH/Mercury Film Electrodes. *Electrochim. Acta* **2006**, *52*, 1182-1190.
- (41) Neu, M.; Fischer, D.; Kissel, T. Recent Advances In Rational Gene Transfer Vector Design Based On Poly(Ethylene Imine) And Its Derivatives. *J. Gene Med.* **2005**, *7*, 992-1009.
- (42) Almodóvar, J.; Place, L. W.; Gogolski, J.; Erickson, K.; Kipper, M. J. Layer-By-Layer Assembly Of Polysaccharide-Based Polyelectrolyte Multilayers: A Spectroscopic Study Of Hydrophilicity, Composition, And Ion Pairing. *Biomacromolecules* **2011**, *12*, 2755-2765.

- (43) Itano, K.; Choi, J.; Rubner, M. F. Mechanism Of The Ph-Induced Discontinuous Swelling/Deswelling Transitions Of Poly(Allylamine Hydrochloride)-Containing Polyelectrolyte Multilayer Films. *Macromolecules* **2005**, *38*, 3450-3460.
- (44) Dubas, S. T.; Schlenoff, J. B. Polyelectrolyte Multilayers Containing A Weak Polyacid: Construction And Deconstruction. *Macromolecules* **2001**, *34*, 3736-3740.
- (45) Tieke, B.; van Ackern, F.; Krasemann, L. Ultrathin Self-Assembled Polyelectrolyte Multilayer Membranes. *Eur. Phys. J. E* **2001**, *5*, 29-39.
- (46) Elbakry, A.; Wurster, E.; Zaky, A.; Liebl, R.; Schindler, E.; Bauer-Kreisel, P.; Blunk, T.; Rachel, R.; Goepferich, A.; Breunig, M. Layer-By-Layer Coated Gold Nanoparticles: Size-Dependent Delivery Of DNA Into Cells. *Small* **2012**, *8*, 3847-3856.

Chapter 6:

Mobility of polyelectrolytes and coated nanoparticles in a collagen I matrix investigated by fluorescence recovery after photobleaching (FRAP)

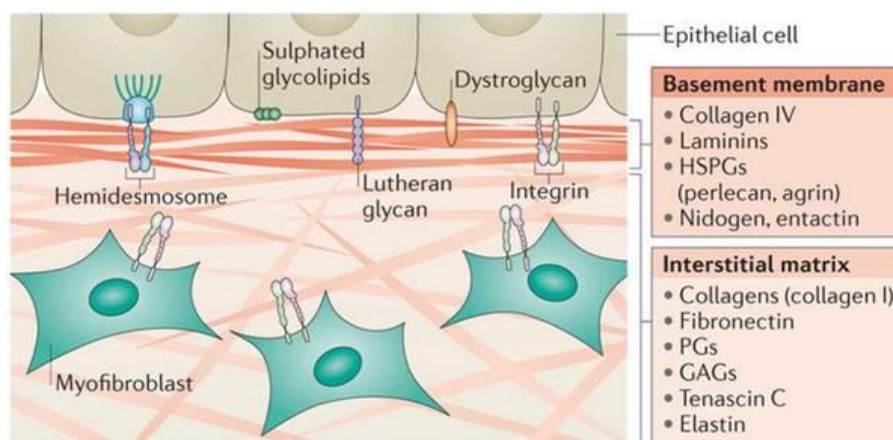
Abstract

The extracellular matrix (ECM) is known to be an effective filtering barrier in various human tissues. It consists of a highly charged hydrogel network of proteins, proteoglycans and glycosaminoglycans. Consequently, electrostatic trapping mechanisms are known to exist, which highly affect the therapeutic efficiency of drug delivery systems and have to be considered in the design of novel drug carriers.

In this chapter it is shown that, not only the basement membrane, but also the interstitial matrix, represents an electrostatic barrier for highly charged Layer-by-Layer coated nanoparticles and polyelectrolytes. Therefore, a collagen I hydrogel, which is the main component of the interstitium, was used as a model system. The mobility of coated nanoparticles and polyelectrolytes was determined with fluorescence recovery after photobleaching (FRAP). It was further shown that the constitution of the collagen I matrix is altered significantly by the incorporation of cationic polyelectrolytes. Hence, permeability studies with this model system have to be performed hand-in-hand with control experiments, such as turbidity assays to ensure comparable conditions.

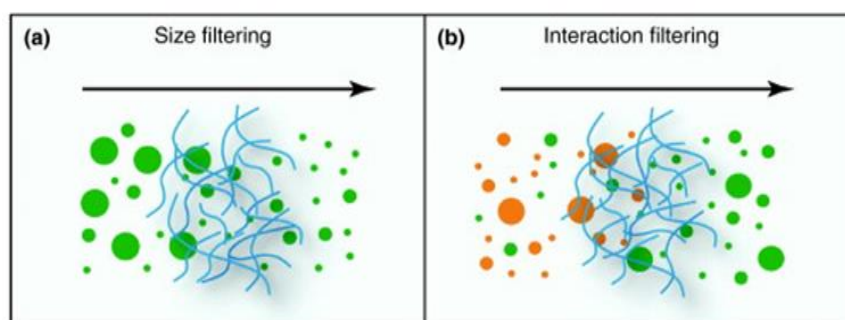
Introduction

After an intravenous injection, nanoparticle based drug delivery systems have to overcome several barriers from the injection site to their intracellular target. After escaping the bloodstream through the endothelium, the nanoparticles get in contact with the so called extracellular matrix (ECM), the filling material between cells inside an organism.



Scheme 1 The Extracellular Matrix (ECM) is divided into the basement membrane and the interstitial matrix. Both parts are under constant remodeling and contain around 300 different proteins, proteoglycans and glycosaminoglycans. The ECM is responsible for the physical constitution of tissues and organs, contains ligands to interact with cell receptors, releases growth factors and is known to be a diffusing barrier for nanoparticles and colloids due to physicochemical interactions (Reproduced (adapted) from Bonnans et al.¹. Copyright 2014 Nature Publishing Group).

The ECM can be characterized as a hydrogel of a dynamic composition containing over 300 different proteins, proteoglycans and glycosaminoglycans and can be divided into the basement membrane and the interstitial connective tissue (**Scheme 1**).¹⁻³ But, despite of only providing form and stiffness to tissues and organs, the ECM is also responsible for tissue homeostasis and signal transduction processes.¹ It was also found that the ECM and also other biological hydrogels, such as the mucus or the nuclear pores, show a highly selective filtering mechanism for cellular molecules.⁴ As the biopolymer components of those hydrogel matrices are highly charged, this filtering mechanism is based on electrostatic effects, instead of size-exclusion (**Scheme 2**).^{4,5}



Scheme 2 Two filtering mechanisms for biological hydrogels are known. **A)** The size-exclusion filtering, where only particles smaller than a distinct threshold are able to diffuse through the matrix. **B)** Particles are selected by a distinct surface property (e.g. the surface charge). Particles highly interacting with the hydrogel matrix (orange) are entrapped in the matrix. In contrast if particles interact only weak with the matrix (green), they are able to permeate through the hydrogel (Reproduced (adapted) from Lieleg and Ribbeck⁴ with permission. Copyright (2011) Elsevier.)

It was shown that particles, smaller than the mesh size of the basal membrane are effectively trapped inside the hydrogel and can be mobilized by the addition of ions, shielding the intrinsic charges of the gel matrix.⁵ It is important to remind that nanoparticles administered

for drug delivery purposes usually have to cross both parts of the ECM, the basal membrane and the interstitial connective tissue to reach their target cells. Hence, hindered diffusion or entrapment of nanoparticulate drug carriers inside one of those two compartments would have a crucial impact on the therapeutic effect. Lieleg et al, already studied the surface-charge dependent mobility of nanoparticles and liposomes inside the basal membrane.⁶ They showed that an effective electrostatic bandpass controls the permeability of this part of the ECM.⁶ Liposomes of a negative surface charge up to -30 mV were able to diffuse, whereas all cationic particles were effectively trapped inside the hydrogel matrix.⁶ A comparable effect can also be assumed for the interstitial connective tissue, containing a large amount of collagen I, which carries negative charges on its fibrils.

In this chapter, collagen I based hydrogels were used as a model system for the investigation of the mobility of Layer-by-Layer (LbL) assembled nanoparticles inside the second compartment of the ECM, the interstitium. LbL coated nanoparticles were a good tool to elucidate the charge-dependent interactions with the hydrogel matrix, because their surface charge can easily be adjusted by applying a variable amount of polymer layers. Here, commercially available silica nanoparticles⁷ (SiNP) were used as LbL templates instead of gold nanoparticles, to avoid the high quenching capacity of gold.^{8,9} As those amorphous SiNP were seldom used as substrates for LbL applications, their coating capability had to be addressed first. Later, the mobility of coated SiNP was investigated in a collagen I based matrix and further evaluated with additional experiments concerning the molecular constitution of the hydrogel.

Experimental Section

Materials

If not otherwise stated all chemicals used were purchased from Sigma-Aldrich Chemical Company (Taufkirchen, Germany). The polyelectrolytes for LbL coating of nanoparticles and all other experiments had the following molecular weights: branched poly(ethylenimine) 25000 g/mol, poly(styrene sulfonate sodium salt) 15000 g/mol (Polymer Standard Service, Mainz, Germany). Colloidal silica LUDOX[®] TM40 was a generous gift from Grace Chemicals (Worms, Germany). Ultrapure water was obtained using a Milli-Q-System (Merck Chemicals, Schwalbach, Germany).

Fluorescent labelling of PEI

PEI was fluorescently labeled by fluoresceine isothiocyanate and rhodamine isothiocyanate accordingly to a previously published protocol.¹⁰ Briefly, 0.42 ml of a 10 mg/ml solution of the dye in DMSO was added to 10 ml of a 10 mg/ml aqueous solution of the polymer at pH 9. The reaction mixture was stirred overnight in the dark. The labeled polymer was subsequently purified by dialysis using Slide-a-Lyzer Dialysis Cassettes (Thermo Scientific, Waltham, MA,

USA), MWCO 3500, against water for one week. The absence of unbound fluorescent dye was confirmed by agarose gel electrophoresis.

Preparation of LbL coated silica nanoparticles

The silica nanoparticles were supplied in a 40% (w/v) suspension and were diluted in water to a 0.1% (w/v) suspension. As the used silica colloid carried a negative surface charge, the LbL coating was started with the positively charged PEI. The coating protocol was adjusted from the previously described coating of gold nanoparticles (see Chapter 3).¹¹ The colloidal suspension was added to a stirring solution of the polyelectrolyte to give a final polymer concentration of 10 mg/ml (w/v). For the fluorescently labeled polyelectrolytes 25% of the polyelectrolyte solution needed, were surrogated by the fluorescently labeled derivative. The nanoparticles were stirred for at least 30 min and subsequently purified by ultrafiltration using either Corning Spin-X UF 6, MWCO 100 kDa (Corning, Amsterdam, The Netherlands) or Roti-Spin Mini, MWCO 100 kDa (Carl Roth, Karlsruhe, Germany), depending on the sample volume. The purified samples were either coated with the following polyelectrolyte layer or immediately used for the characterization

Characterization by particle size and zeta potential

The nanoparticles were characterized by their hydrodynamic diameter and zeta potentials using a Zetasizer Nano ZS (Malvern Instruments, Herrenberg, Germany). For size measurements 173° backward scattering in general purpose mode was applied and the maximum peak of the intensity distribution is always stated. The zeta potential measurements were processed in the monomodal mode. Additionally the non-modified silica nanoparticles

were air-dried on a carbon-coated copper grid and imaged by transmission electron microscopy (CM 12, Philips, Eindhoven, The Netherlands). Here, the particle diameter was determined by image analysis using ImageJ 1.45s software (Rasband, W.S., ImageJ, U. S. National Institutes of Health, Bethesda, Maryland, USA, <http://imagej.nih.gov/ij/>, 1997-2014).

Fluorescence spectrometry

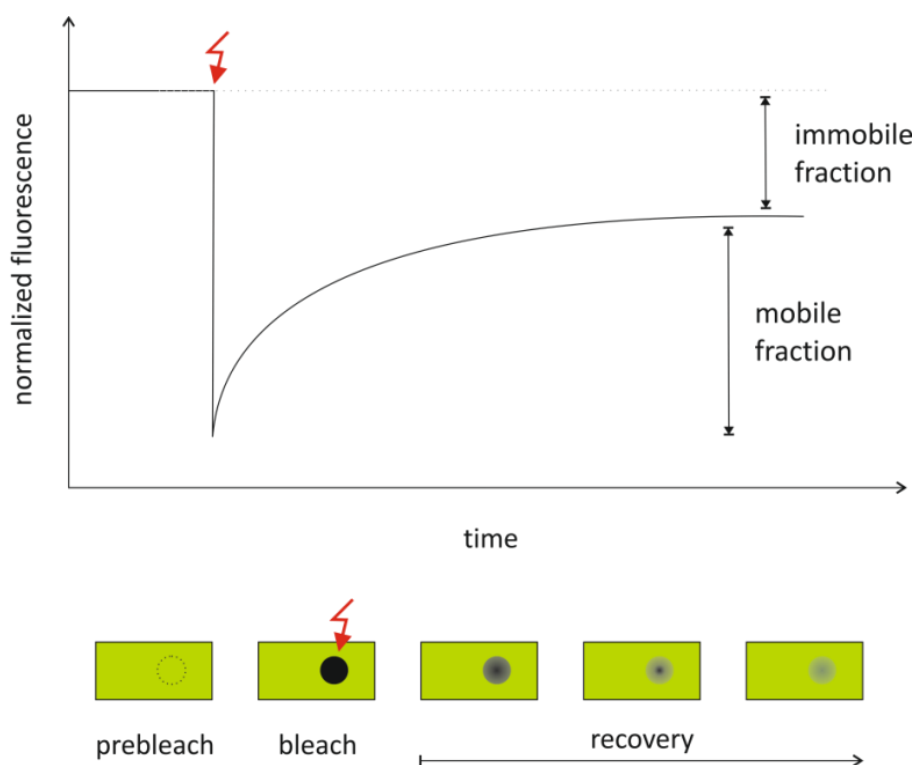
Fluorescence spectra were recorded using a Perkin Elmer LS55 fluorescence spectrometer (Perkin Elmer, Waltham, MA, USA). The excitation wavelengths were 480 nm and 550 nm for FITC and TRITC respectively and the detector voltage was set to 650 V.

Preparation of hydrogel matrices for FRAP

All hydrogel matrices were prepared in 8-well chambered coverglasses (Nunc Lab Tek, NalgeNunc, Penfield, NY, USA). Collagen I matrices were prepared as follows. The commercial collagen I solution (# C4243, Sigma-Aldrich, Taufkirchen, Germany) was lyophilized and reconstituted in 0.01 M HCl to achieve a concentrated stock solution. Prior to the experiment, the collagen solution was neutralized by 0.1 N NaOH. The desired FRAP analyte was added, which were either polymer solutions or coated SiNP. The volume was filled with Millipore water to achieve a final sample volume of 150 μ l and final collagen concentrations of 5 mg/ml or 2.5 mg/ml, respectively. The pH of the sample was checked once again for neutrality (pH 7) and finally the hydrogel was incubated for at least 3 h at 37 °C.

Fluorescence Recovery after photobleaching (FRAP)

To analyze the mobility of LbL nanoparticles the technique called fluorescence recovery after photobleaching (FRAP) was chosen.^{12,13} FRAP is a versatile method, which is often applied in cellular studies, where the mobility of biomacromolecules is concerned.^{14,15} In all cases, a fluorescence marker is needed, which is bleached at a distinct region of interest (ROI) by a high energetic laser beam. Due to the diffusion of mobile molecules back into the ROI, the fluorescence is recovering over time and at the end the diffusion coefficient can be calculated (Scheme 3).^{16,17}



Scheme 3 Example of a raw fluorescence profile as it is obtained in a FRAP experiment. The experiment is divided into three stages: The prebleach plateau, the bleaching event and the slow recovery of the fluorescence, due to diffusion.

FRAP experiments were performed with a Zeiss Axiovert 200 microscope combined with a LSM 510 laser-scanning device and a 10x/0.3 Plan Neofluar objective (Zeiss, Oberkochen, Germany). Two regions of interest (ROI) were defined per measurement with a diameter of 30 μm . The sample region was bleached with 30 iterations and fluorescence recovery was recorded with 100 images and a delay of 7.8 s. The collagen matrices were measured at 37 $^{\circ}\text{C}$. The fluorescence recovery $f(t)$ was calculated with a double-normalization, presented in equation (1), where $I(\text{Ref})_0$ and $I(\text{Ref})_t$ were the intensities of the non-bleached ROI prior to the bleaching and at the time point t .¹⁸ $I(\text{FRAP})_0$ and $I(\text{FRAP})_t$ were the fluorescence intensities of the bleached ROI prior (0) to the bleaching and at the time point t .

$$f(t) = \frac{I(\text{Ref})_0}{I(\text{Ref})_t} * \frac{I(\text{FRAP})_t}{I(\text{FRAP})_0} \quad (1)$$

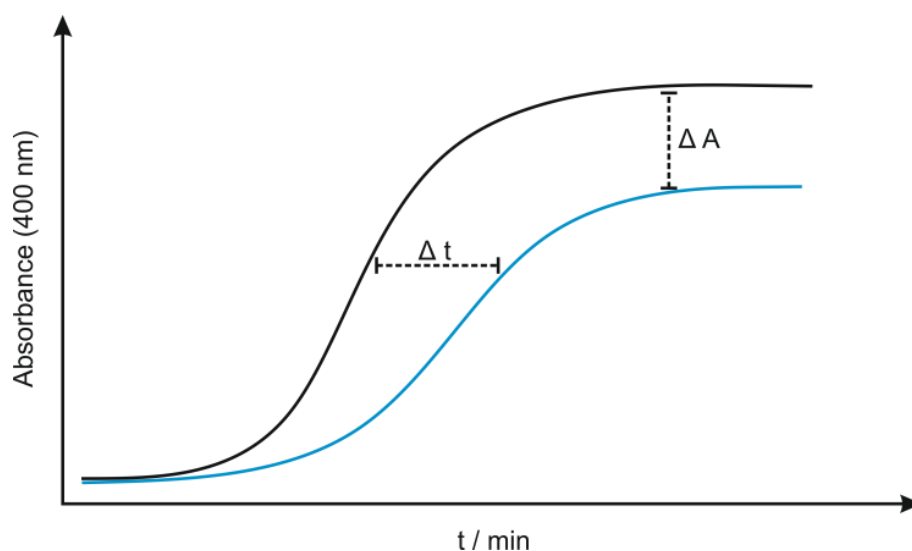
This recovery profile was further normalized to the first prebleach point ($f(\text{min})$) to achieve a better comparability between several experiments (2). Here $f(0)$ is the mean fluorescence recovery during the prebleach process.

$$F(t) = \frac{f(t) - f(\text{min})}{f(0) - f(\text{min})} \quad (2)$$

To calculate the diffusion coefficient, the recovery curves were fitted using an Soumpasis-equation fit.¹⁶ For the curve fitting IgorPro software Version 6.2.3.2 (WaveMetrics, Lake Oswego, USA) in combination with the free FRAPcalc extension (http://cmci.embl.de/downloads/frap_analysis, Oktober 2014) was used.

Turbidity assays of collagen I

Turbidity assays of collagen matrices were performed accordingly to a previously published protocol.¹⁹ The collagen matrices were prepared in standard 96-well plates and incubated on ice for 15 min to allow any air bubbles to escape. Afterwards, the turbidity, due to the polymerization of collagen fibrils, was monitored in a microplate reader (FLUOStar Omega, BMG Labtech, Ortenberg, Germany) at 400 nm, 37 °C for 90 min.



Scheme 4 In comparison to the control (black) a modified collagen I hydrogel (blue) can be characterized by two parameters. Δt corresponds to a retardation of the fibril formation (lag time), whereas the level of the equilibrium of polymerization, ΔA , describes the density of the collagen network.

A standard turbidity curve has a sigmoidal shape with a lower and an upper plateau which are attributed to the lag time and the equilibrium of the polymerization reaction.²⁰ Hence, one could define two important parameters in comparison to a reference sample (**Scheme 4**). A prolonged lag time, Δt , corresponds to a retardation of the fibrillation. If the equilibrium

plateau of the curve reaches lower absorbance values, ΔA , one could conclude a disturbed fibrillation and a looser hydrogel network.^{19,21}

Statistics

All FRAP experiments are presented as the mean of two measurements of the same sample. Standard deviations are not shown to achieve a better visualization of the curves, but were between 5% and 10% for samples containing unbound PEI and between 20% and 30% for samples containing coated SiNP.

Results and Discussion

Characterization and LbL coating of silica nanoparticles

Ludox silica nanoparticles have been seldom used as templates for LbL coatings. Hence, prior to the first experiments the SiNP had to be well characterized by transmission electron microscopy and dynamic light scattering.

In TEM the SiNP were visible as nearly monodisperse particles, which were not completely round, but rather hexagonal (**Figure 1A**). The determined averaged diameter was 26.17 ± 5.08 nm (**Figure 1B**). The dynamic light scattering analysis gave a larger hydrodynamic diameter with a broader size distribution of the particles of 39.02 ± 13.52 nm (intensity distribution) (**Figure 1C**). The difference between the two particle characterization methods was caused by the hydration shell around the nanoparticles, which was also determined in dynamic light scattering. In contrast, TEM images were performed in the dried state and, hence hydration was not taken into account, here.

The SiNP were modified by an LbL-like approach for two reasons: First, to label them with a fluorescent dye and second to investigate the charge dependent mobility inside the charged ECM matrix.

The coating of SiNP was monitored by size and zeta potential measurements. Here, an ideal LbL coating usually is characterized by a minor size increase and the change of the algebraic sign of the zeta potential for each polyelectrolyte layer.^{22,23} Hence, coating of an odd or even

number of polymer layers leads to either positively or negatively charged particles. Therefore LbL coated nanoparticles are a suitable tool for the investigation of charge-dependent interactions, for example inside hydrogel matrices.

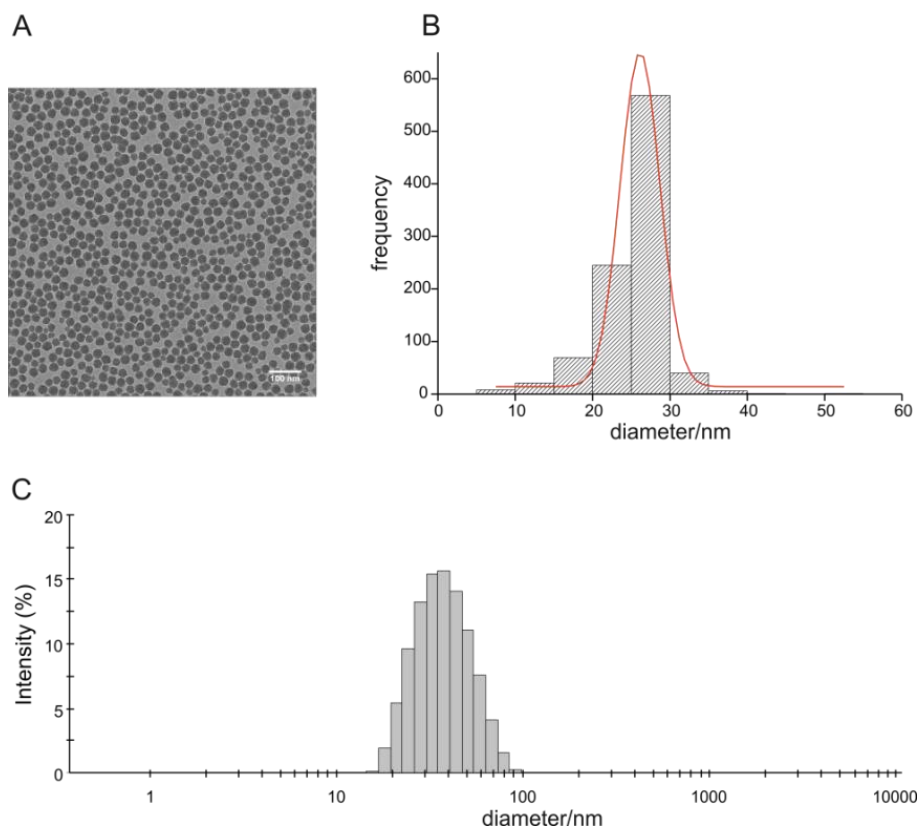


Figure 1 A) TEM image of unmodified negatively charged SiNP B) Size distribution determined of the TEM image analysis C) Intensity distribution of the hydrodynamic diameter of SiNP.

The assumed size increase was observed for the deposition of the first cationic PEI layer (**Figure 2A**) and at the same time the shift from a negative to a positive zeta potential was found (**Figure 2B**). Against a regular LbL deposition behavior, the particle size decreased upon the addition of the second and third polymer layers. Nevertheless, the algebraic sign of the zeta potential changed again for the PSS layer. But, the determination of the surface

charge of the third layer was troublesome due to the instability of the particles during the measurement of the electrophoretic mobility.

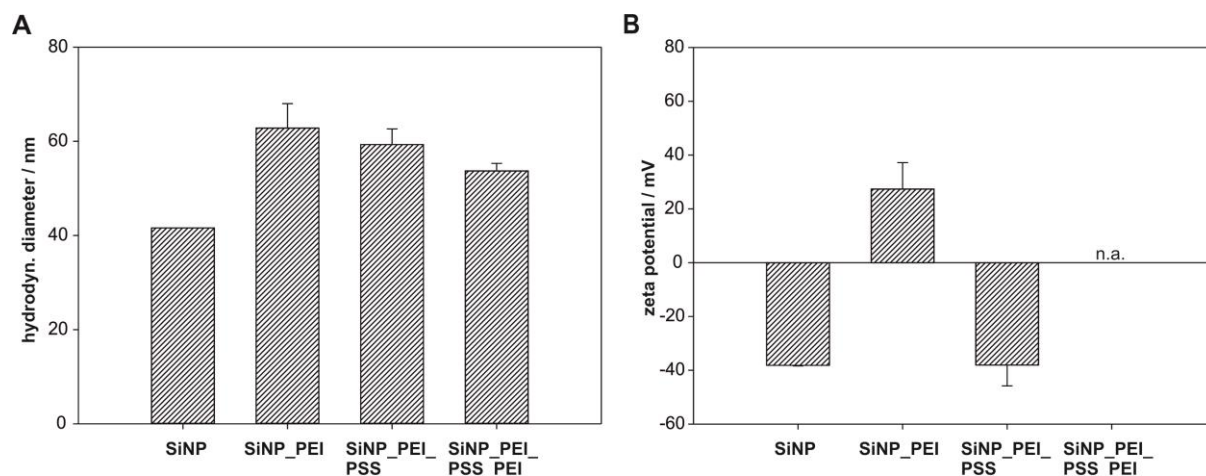


Figure 2 Characterization of the coating process of SiNP. **A)** The hydrodynamic diameter of the SiNP with coated polymer layers. **B)** The zeta potential is changing during the coating procedure. The value for SiNP_PEI_PSS_PEI was not available (n.a.) due to the instability of the particles. (Values are presented as mean \pm std of at least three independently coated batches)

Consequently, the successful coating of SiNP could not be evaluated properly. Hence, an additional approach was necessary to verify the effective LbL coating on SiNP. Therefore, to substantiate the LbL coating a Foerster resonance energy transfer (FRET) was applied.

Here, the SiNP were coated with three polymer layers, containing a FRET- pair, consisting of PEI-FITC and PEI-TRITC, or only the FRET donor, PEI-FITC, as a control sample. In case of a successful deposition of polymer layers an energy transfer from the first to the third polymer layer was expected upon excitation of the donor dye. The control sample showed the emission of the FTIC-dye at 528 nm only. For the FRET-sample this FITC emission was

clearly reduced and the emission of the rhodamine derivative at 580 nm was observed (Figure 3).

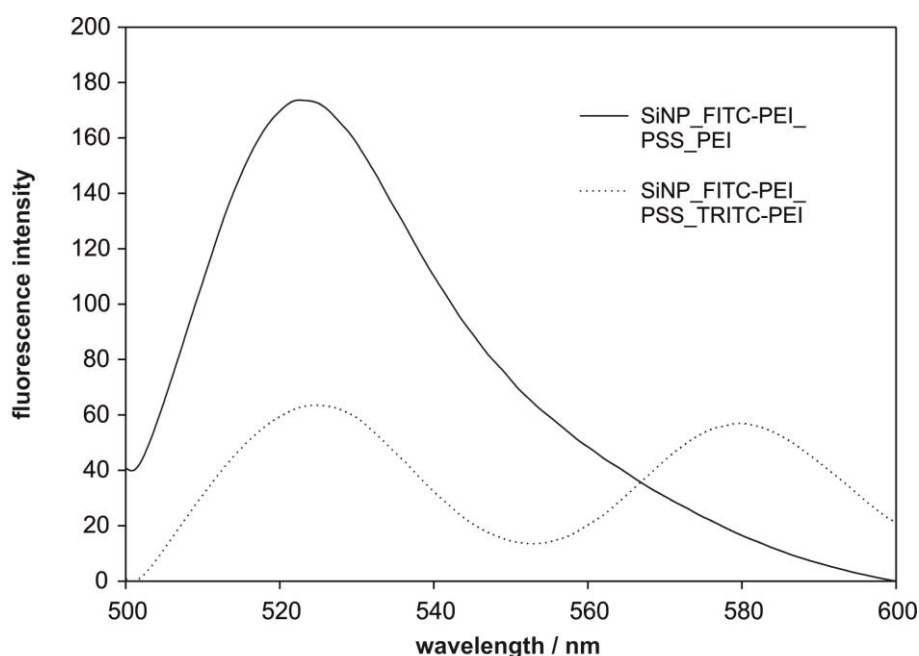


Figure 3 Fluorescence spectra of LbL SiNP. In case of particles coated only with the FRET donor (solid line), only the emission spectrum of FITC was visible. For particles containing both, the FRET donor and the acceptor (dotted line) a reduction of the FITC intensity and at the same time the appearance of the TRITC emission was observed. (Spectra are shown for a representative sample)

Another control containing the two dye-labeled polymers in solution also did not show any FRET effects (data not shown). Therefore, aggregation of the polyelectrolytes in solution was also excluded. Hence, one could follow that the LbL coating on SiNP was successful. The deviating decrease of the hydrodynamic diameter might have been originating from a compression of the polymer layers upon further addition of polyelectrolytes. As for future experiments two LbL layers were sufficient to create a positively and a negatively charged species, the stability deficit of the trilayered particles was also not a concern. Furthermore, it

was shown that Ludox SiNP were appropriate templates for the labelling with fluorescent dyes, because no quenching effects were observed. Hence, SiNP might be an interesting alternative to AuNP or other heavy metal colloids, which cannot be applied in fluorescence studies, due to their high quenching capacity.

Mobility of nanoparticles and polymers in collagen I

The mesh size of collagen I based hydrogels is known to be in the micrometer range, whereas the size of coated SiNP was several orders of magnitude smaller.^{24,25} In terms of a diffusion experiment one would expect an unhindered diffusion without any size exclusion effects of those particles through a collagen I network. But as it is shown in **Figure 4** the PEI-coated SiNP_PEI-FITC were immobile in the collagen I matrix.

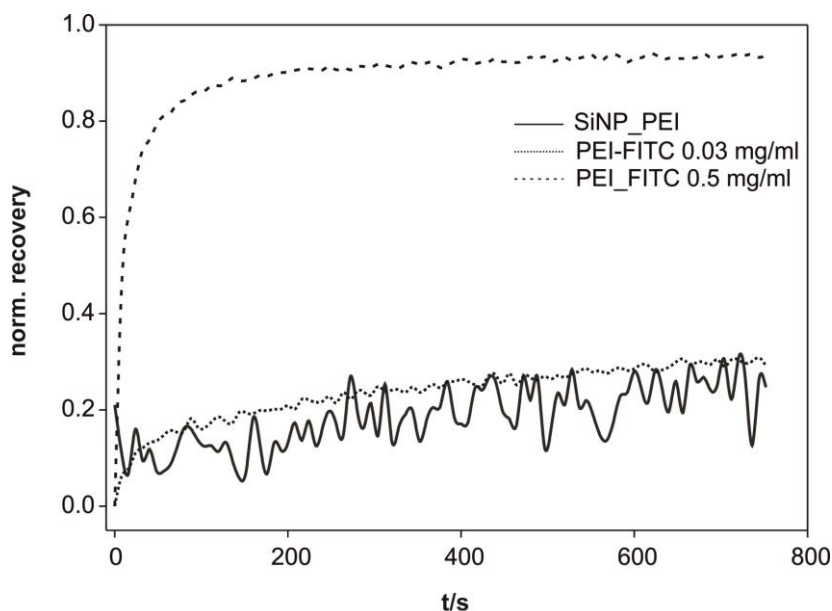


Figure 4 SiNP_PEI-FITC and unbound PEI-FITC of a concentration of 0.03 mg/ml were trapped in the collagen I matrix. But, PEI-FITC diffused when applied in a higher concentration of 0.5 mg/ml.

For comparison the fluorescence recovery of even smaller PEI-FITC molecules, which were not bound to nanoparticles, was also recorded. Also unbound PEI-FITC was immobile, when introduced in a low concentration (0.03 mg/ml). But, a complete recovery of the fluorescence was found when PEI-FITC was applied in a concentration of 0.5 mg/ml.

To further elucidate this dependency a concentration series of PEI-FITC was applied (**Figure 5 A + B**).

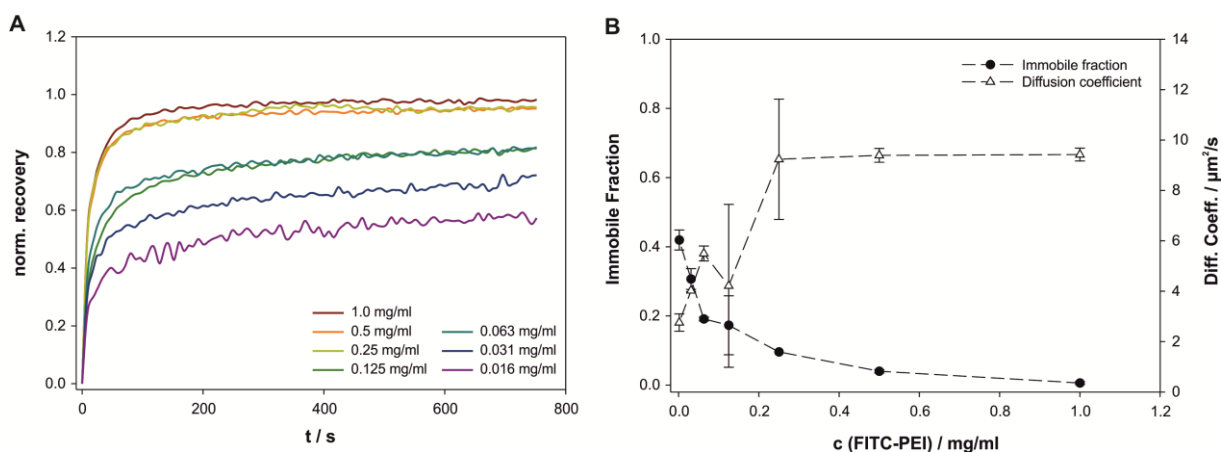


Figure 5 A) The mobility of PEI molecules depended on their concentration. **B)** The diffusion coefficient was increasing with increasing concentration and at the same time the immobile fraction of PEI molecules decreased. (Dashed lines are only to guide the eye)

Here, the mobility of the polymer chains increased stepwise and an unhindered diffusion was observed for the three highest concentrations with a recovery of 90% and higher and diffusion coefficients of approximately $10 \mu\text{m}^2/\text{s}$. The lower concentrations showed a limited mobility and also lower diffusion coefficients; down to only $2 \mu\text{m}^2/\text{s}$. These results indicated to a specific interaction between the polycationic compound PEI and the hydrogel network. Due to the ability to avoid the interaction just by the addition of a sufficient amount of PEI mechanisms consisting of a distinct amount of binding sites between the two components was

assumed. A potential option for such a saturable mechanism might be an electrostatic interaction, as it was already reported for several biological hydrogel matrices⁴. Such an electrostatic interaction is also feasible when comparing the isoelectric point (IP) of collagen I and the pK_a value of PEI. Collagen I has an IP of 7.7²⁶ and the hydrogel was also adjusted to a neutral pH prior to its gelation. Hence, the net charge of collagen I should be neutral. But, as it contains positively and negatively charged amino acids, areas of negative, as well as positive, charges are likely to be present. On the other hand PEI with its pK_a of 8.5²⁷ is highly ionized with a lot of positive charges. Hence, electrostatic interaction partners were present in this setup and therefore also an electrostatic entrapment is probable.

In a different context, Schweizer et al. investigated the sustained release of a charged antibody out of an oppositely charged alginate matrix.²⁸ Here, the electrostatic interactions were adjusted by a variation of the charge density to control the release of the antibody.²⁸ In another study Lieleg and coworkers observed an ionic interaction between charged nanoparticles and a collagen IV network.⁶ They adjusted the charge state of the matrix by the addition of ions to screen the intrinsic charge and could enhance the mobility of their nanoparticles with this approach.⁶ Hence, an electrostatic binding between the polyelectrolyte PEI-FITC either free or bound to a nanoparticle surface was highly likely. But, in case of collagen I it was not possible to adjust the interactions by a pH variation or the addition of high amounts of salt, because this would have affected the colloidal properties of SiNP.

It was tried to saturate the intrinsic charges of the collagen matrix by a large amount of the polymer PEI itself to mobilize the equally charged SiNP_PEI-FITC. This saturation step was performed with non-fluorescent PEI, prior to the incorporation of the labeled species. In fact, 0.5 mg/ml PEI were sufficient to increase the mobility of the originally immobile samples. In case of the fluorescent polymer, a preincubation with 0.5 mg/ml non-fluorescent PEI was able to completely mobilize 0.03 mg/ml labeled PEI-FITC (**Figure 6A**).

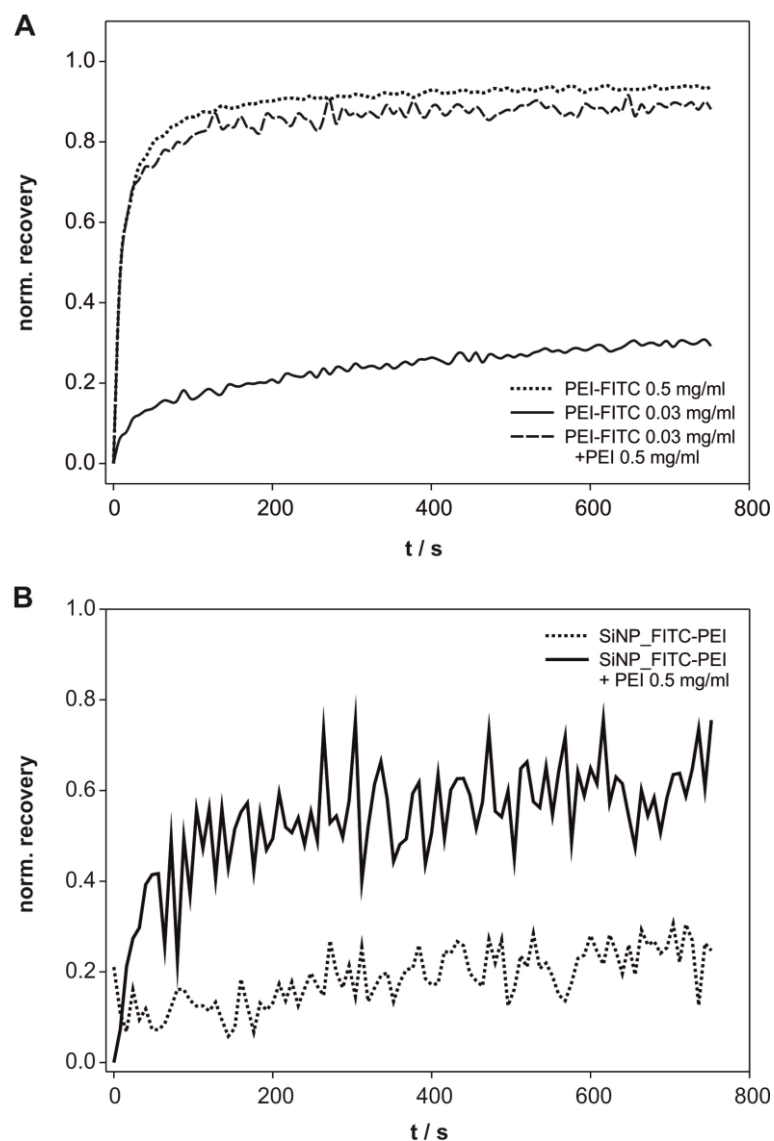


Figure 6 A) Preincubation with non-fluorescent PEI led to a mobilization of PEI-FITC **B)** The same effect was observed for positively charged SiNP_PEI

The mobility of the charged SiNP_PEI-FITC was enhanced to a mobile fraction of 50% in comparison to the control (**Figure 6 B**).

Surprisingly, also negatively charged SiNP_PEI-FITC_PSS could be mobilized with positively charged PEI (**Figure 7**).

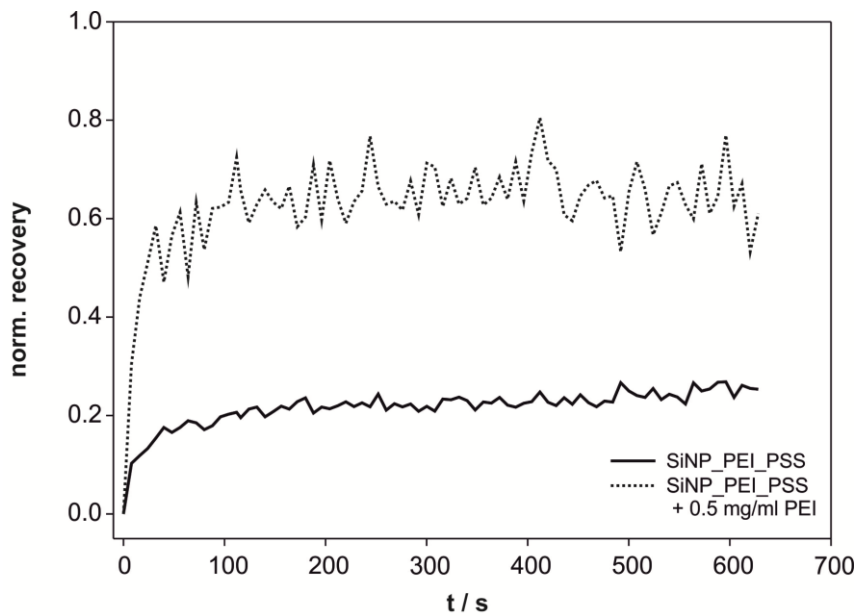


Figure 7 Negatively charged particles SiNP_PEI_PSS were also mobilized with a preincubation with cationic PEI

This indicated that solely an electrostatic interaction between charged particles and a collagen I network might be not sufficient to explain the altered mobility.

Hence, one also has to consider that the constitution of the collagen I hydrogel might have been modified by the comparably high concentration of the charged macromolecule PEI. To elucidate this question an assay to compare the fibrillation of the collagen I matrices was addressed.

Constitution of collagen I matrices in the presence of polyelectrolytes and nanoparticles

Collagen I hydrogels form linear fibrils upon gelation and as a consequence, the resulting matrices were not clear, but opaque. This turbidity was used to observe the fibrillation of the collagen I matrices with and without nanoparticles or polymer chains added.

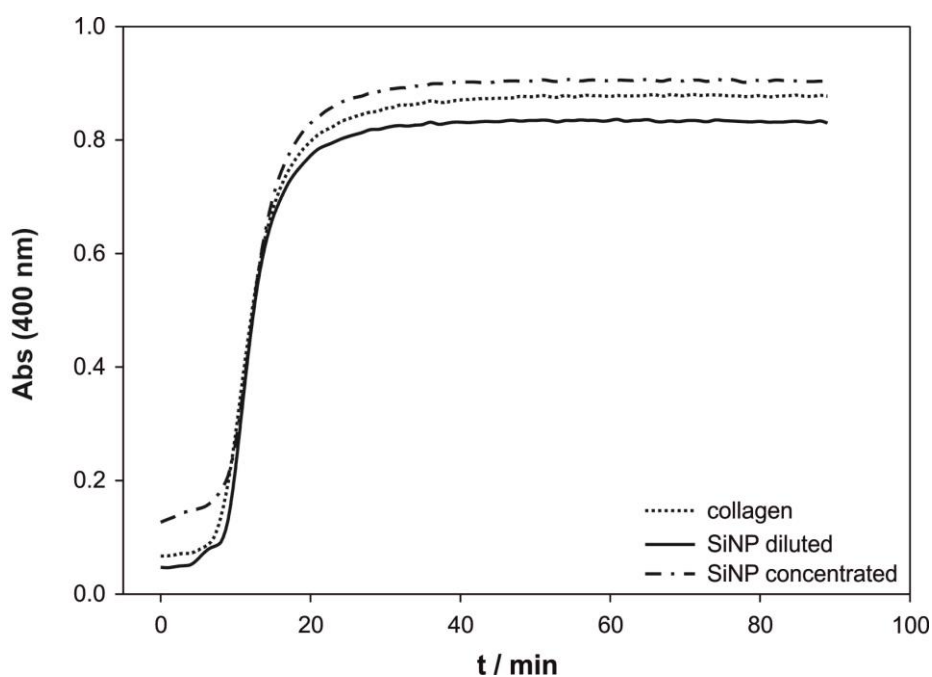


Figure 8 Turbidity of collagen matrices containing bare SiNP: The sample curves were almost superimposable to the reference sample. Hence it was concluded, that the negatively charged nanoparticles only had a minor influence on the collagen fibrillation. (The mean values of three measurements are shown)

First, bare SiNP without a polymer coating were incorporated into collagen I networks (**Figure 8**). It was observed that those negatively charged particles had a negligible influence

on the formation of collagen I fibrils, because the two sample curves were almost superimposable to the reference sample.

In case of a concentration series of PEI incorporated into collagen I matrices a major shift of the turbidity curves was observed (**Figure 9**).

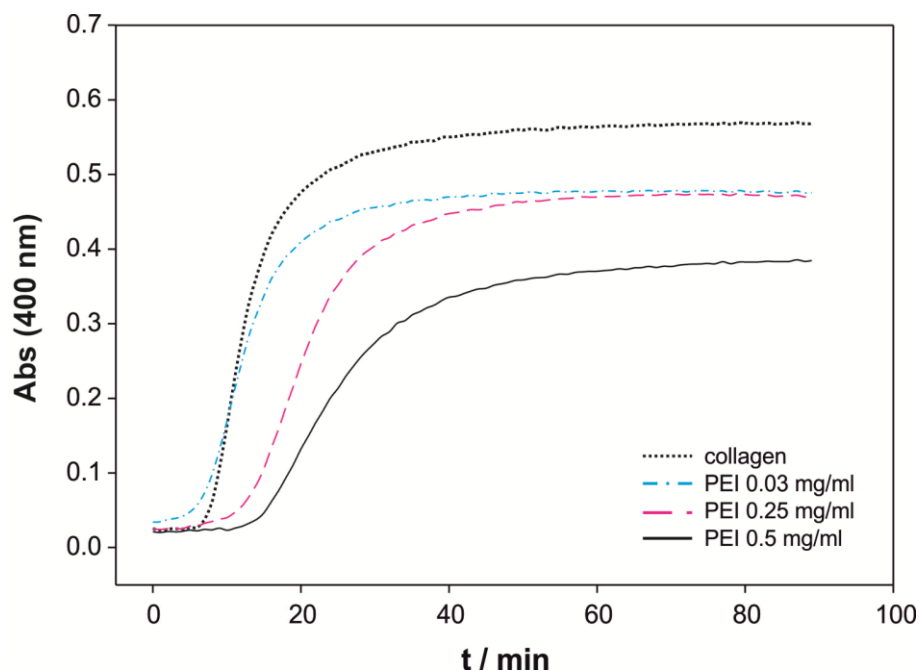


Figure 9 The incorporation of the polycation PEI had a major influence on the polymerization of collagen I. Here, the fibrillation process was retarded and the equilibrium plateau was reduced compared to the reference sample. This observation corresponded to an alteration of the collagen I matrix and probably can be attributed to a looser packed hydrogel. (The mean values of three measurements are shown)

First, the lag time, Δt , shifted to higher values with increasing PEI concentration, indicating a retarded formation of the collagen I fibrils. Second, the absorption difference, ΔA , was also reduced, corresponding to a looser collagen I network. Altogether, it was concluded that PEI macromolecules had a major impact on the formation of collagen I matrices and that the structure of the network was perturbed compared to a pure collagen I network. Here, one also

has to keep in mind that concentrations of 0.5 mg/ml PEI are much higher than the usual concentration used for a transfection experiment and are highly toxic to cells.²⁹ For the coated SiNP_PEI also a concentration dependent behavior was found (**Figure 10**).

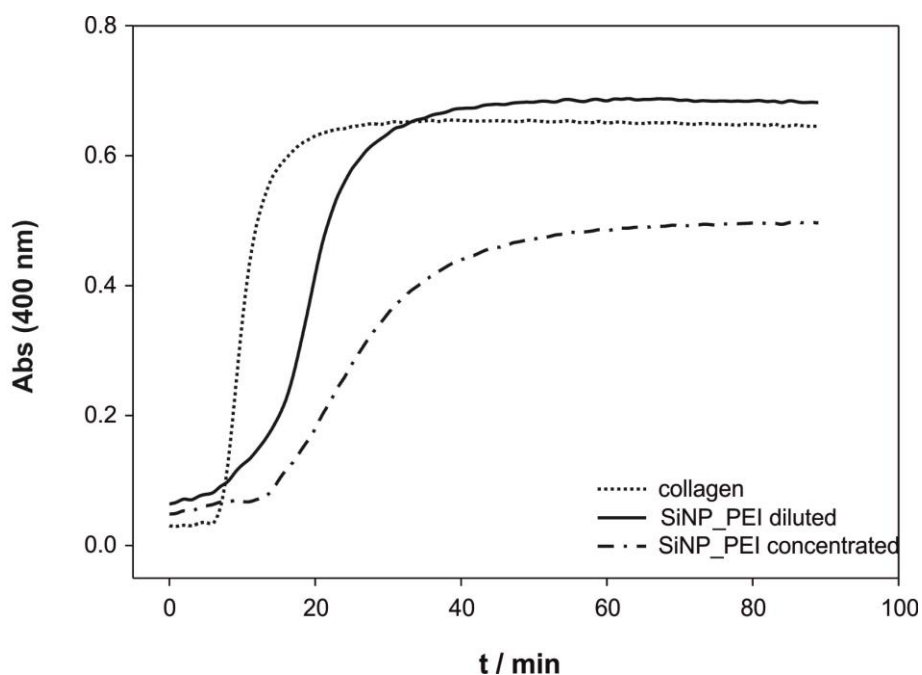


Figure 10 Turbidity of collagen I with incorporated SiNP_PEI. The diluted particles retarded the fibrillation of collagen I but the turbidity ended at a comparable level. Hence, the internal architecture of the matrix is not disturbed to a large impact. But, when the cationic SiNP_PEI were incorporated at a higher concentration, alterations of the matrix were observed which were comparable to the effect of the unbound polycation. (The mean values of three measurements are shown)

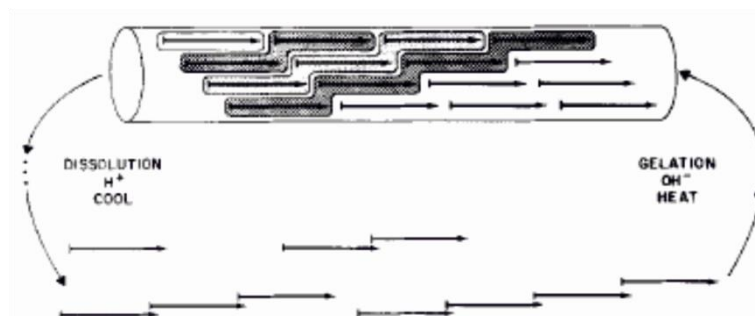
As highly concentrated SiNP_PEI influenced the collagen I fibrillation to large degree, the diluted SiNP_PEI, which were also investigated in the mobility studies, only had a minor influence on the formation of the collagen matrix.

The incorporation of the components used for the mobility studies showed that especially the influence of PEI molecules in a high concentration has a major impact on the formation of

collagen I fibrils. In contrast, the bare SiNP and the SiNP_PEI had a minor influence on the collagen I fibrillation. As a consequence, one has to assume a facilitated mobility of SiNP_PEI, when the preincubation step with non-fluorescent PEI was performed. The modification of the gel constitution by PEI might lead to a looser gel network, facilitating the diffusion of SiNP_PEI.

Especially in collagen I networks which are prepared out of an acidic solution, the intrinsic charge density is closely linked to the network architecture:

The fibrillation of collagen I from acidic solutions is still under discussion and is not understood in full detail.³⁰ In brief, the polymerization to collagen fibrils is described as the self-assembly of negatively charged collagen I aggregates of a size of only a few nanometers (Scheme 5).³¹⁻³³



Scheme 5 Schematic illustration of the collagen I dissolution and fibrillation processes. Collagen I fibrils isolated from rodent tissues can be dissolved into small aggregates under acidic conditions and reassemble again under neutral pH and elevated temperatures. (Reproduced with permission from Silver and Trelstad³². Copyright 1980 American Society for Biochemistry and Molecular Biology)

This process is usually initiated by raising the pH of the acidic solution to neutrality. The presence of those aggregates was previously detected by AFM and X-ray scattering studies and they seem to be sensitive to changes of their charge density.^{34,35} And also interactions of

those negatively charged complexes with cationic substances, such as PEI, have been reported previously.³⁶ Interestingly, Taravel and Domard described two competing processes occurring, when the polycationic biopolymer chitosan was introduced into a collagen solution.^{37,38} The first process is the complexation of chitosan and collagen precursor molecules, which can also lead to a visible precipitate. The second process is the polymerization of collagen to form a hydrogel. Taravel et al. showed that only a minimum of negative charges has to be present to trigger the gelation.³⁷ But the amount of available negative charges or initiator molecules has a major impact on the density of the polymerized product.

Therefore, it can be concluded that the same effect was observed in the FRAP and turbidity experiments, as well: The introduction of highly concentrated PEI molecules prior to the gelation, shielded the negative charges of the collagen I initiators. Therefore, the collagen molecules did polymerize to a certain degree, but the lag time of the turbidity curves was prolonged and at the same time the equilibrium of polymerization was reduced. Additionally this shielding of negative charges increased the mobility of cationic SiNP_PEI-FITC or PEI-FITC. But, it was also observed that negatively charged SiNP_PEI_PSS were immobile in the collagen network and were also mobilized by a polycationic compound as well. There are two possible hypotheses for this effect: The first is that all charges inside the matrix were in equilibrium. Hence, due to charge neutrality SiNP_PEI-FITC_PSS were not hindered in their mobility. The second hypothesis is based on previously found results for LbL gold nanoparticles (see **Chapter 4**). Due to surface roughness effects it might be possible that the SiNP_PEI_PSS carried a mixture of positive and negative surface areas. Hence, it is likely that SiNP_PEI_PSS did not behave exclusively as negative particles but could also interact electrostatically with the anionic hydrogel matrix.

Conclusion

In this chapter it was shown that not only components of the basal membrane can act as an effective molecular filter inside the ECM. Electrostatic barriers can also be assumed inside the interstitial connective tissue, where collagen I is highly abundant. Therefore, the permeability of colloidal drug carriers should also be investigated in this part of the ECM and collagen I hydrogels are a suitable model system. But, particular attention is necessary when charged agents such as polyelectrolytes or ions are incorporated into a collagen I matrix during its fibrillation and gelation process. The fibrillation of collagen I hydrogels is based on the self-assembly of negatively charged collagen complexes and is very sensitive to charge shielding effects. In this case alterations of the internal architecture of the collagen I matrix have to be considered in future experiments to achieve results which really represent *in vivo* conditions. Therefore, it is recommended to conduct the appropriate control experiments, such as fibrillation assays, side-by-side to mobility studies to early get aware of modifications of the collagen I constitution.

References

- (1) Bonnans, C.; Chou, J.; Werb, Z. Remodelling The Extracellular Matrix In Development And Disease. *Nat. Rev. Mol. Cell Biol.* **2014**, *15*, 786-801.
- (2) Hynes, R. O.; Naba, A. Overview Of The Matrisome--An Inventory Of Extracellular Matrix Constituents And Functions. *Cold Spring Harbor Perspect. Biol.* **2012**, *4*, a004903.
- (3) Hynes, R. O. The Extracellular Matrix: Not Just Pretty Fibrils. *Science* **2009**, *326*, 1216-1219.
- (4) Lieleg, O.; Ribbeck, K. Biological Hydrogels As Selective Diffusion Barriers. *Trends Cell Biol.* **2011**, *21*, 543-551.
- (5) Arends, F.; Baumgärtel, R.; Lieleg, O. Ion-Specific Effects Modulate The Diffusive Mobility Of Colloids In An Extracellular Matrix Gel. *Langmuir* **2013**, *29*, 15965-15973.
- (6) Lieleg, O.; Baumgärtel, R. M.; Bausch, A. R. Selective Filtering Of Particles By The Extracellular Matrix: An Electrostatic Bandpass. *Biophys. J.* **2009**, *97*, 1569-1577.
- (7) Grace Technologies,. Ludox Silica Nanoparticles Product Information.
- (8) Dulkeith, E.; Morteani, A.; Niedereichholz, T.; Klar, T.; Feldmann, J.; Levi, S.; van Veggel, F.; Reinhoudt, D.; Möller, M.; Gittins, D. Fluorescence Quenching Of Dye Molecules Near Gold Nanoparticles: Radiative And Nonradiative Effects. *Phys. Rev. Lett.* **2002**, *89*, 203002.
- (9) Schneider, G.; Decher, G.; Nerambourg, N.; Praho, R.; Werts, M. H.; Blanchard-Desce, M. Distance-Dependent Fluorescence Quenching On Gold Nanoparticles Ensheathed With Layer-By-Layer Assembled Polyelectrolytes. *Nano Lett.* **2006**, *6*, 530-536.

- (10) Kato, N.; Caruso, F. Homogeneous, Competitive Fluorescence Quenching Immunoassay Based On Gold Nanoparticle/Polyelectrolyte Coated Latex Particles. *J. Phys. Chem. B* **2005**, *109*, 19604-19612.
- (11) Wurster, E.; Elbakry, A. Layer-By-Layer Assembled Gold Nanoparticles For The Delivery Of Nucleic Acids. In *Nanotechnology for Nucleic Acid Delivery: Methods and Protocols*; Ogris, M.; Oupicky, D., Eds.; Methods in Molecular Biology, 2013; Vol. 948, pp. 171-182.
- (12) Axelrod, D.; Koppel, D. E.; Schlessinger, J.; Elson, E.; Webb, W. W. Mobility Measurement By Analysis Of Fluorescence Photobleaching Recovery Kinetics. *Biophys. J.* **1976**, *16*, 1055-1069.
- (13) Meyvis, T. K. L.; Smedt, S. C.; van Oostveldt, P.; Demeester, J. Fluorescence Recovery After Photobleaching: A Versatile Tool For Mobility And Interaction Measurements In Pharmaceutical Research. *Pharm. Res.* **1999**, *16*, 1153-1162.
- (14) Matsuda, T.; Nagai, T. Quantitative Measurement Of Intracellular Protein Dynamics Using Photobleaching Or Photoactivation Of Fluorescent Proteins. *Microscopy* **2014**, *63*, 403-408.
- (15) Rayan, G.; Guet, J.; Taulier, N.; Pincet, F.; Urbach, W. Recent Applications Of Fluorescence Recovery After Photobleaching (FRAP) To Membrane Bio-Macromolecules. *Sensors* **2010**, *10*, 5927-5948.
- (16) Soumpasis, D. M. Theoretical Analysis Of Fluorescence Photobleaching Recovery Experiments. *Biophys. J.* **1983**, *41*, 95-97.
- (17) Phair, R. D.; Misteli, T. Kinetic Modelling Approaches To In Vivo Imaging. *Nat. Rev. Mol. Cell Biol.* **2001**, *2*, 898-907.
- (18) Phair, R.; Gorski, S.; Misteli, T. Measurement Of Dynamic Protein Binding To Chromatin In Vivo, Using Photobleaching Microscopy. *Methods Enzymol.* **2003**, *375*, 393-414.
- (19) Wilson, C. G.; Sisco, P. N.; Gadala-Maria, F. A.; Murphy, C. J.; Goldsmith, E. C. Polyelectrolyte-Coated Gold Nanorods And Their Interactions With Type I Collagen. *Biomaterials* **2009**, *30*, 5639-5648.

- (20) Sisco, P. N.; Wilson, C. G.; Mironova, E.; Baxter, S. C.; Murphy, C. J.; Goldsmith, E. C. The Effect Of Gold Nanorods On Cell-Mediated Collagen Remodeling. *Nano Lett.* **2008**, *8*, 3409-3412.
- (21) Wood, G.; Keech, M. The Formation Of Fibrils From Collagen Solutions 1. The Effect Of Experimental Conditions: Kinetic And Electron-Microscope Studies. *Biochem. J.* **1960**, *75*, 588-598.
- (22) Deng, Z. J.; Morton, S. W.; Ben-Akiva, E.; Dreaden, E. C.; Shopsowitz, K. E.; Hammond, P. T. Layer-By-Layer Nanoparticles For Systemic Codelivery Of An Anticancer Drug And siRNA For Potential Triple-Negative Breast Cancer Treatment. *ACS Nano* **2013**, *7*, 9571-9584.
- (23) Schneider, G.; Decher, G. Functional Core/Shell Nanoparticles Via Layer-By-Layer Assembly. Investigation Of The Experimental Parameters For Controlling Particle Aggregation And For Enhancing Dispersion Stability. *Langmuir* **2008**, *24*, 1778-1789.
- (24) Kuntz, R. M.; Saltzman, W. M. Neutrophil Motility In Extracellular Matrix Gels: Mesh Size And Adhesion Affect Speed Of Migration. *Biophys. J.* **1997**, *72*, 1472-1480.
- (25) Arevalo, R.; Urbach, J.; Blair, D. Size-Dependent Rheology Of Type-I Collagen Networks. *Biophys. J.* **2010**, *99*, L65-L67.
- (26) Highberger, J. H. The Isoelectric Point Of Collagen. *J. Am. Chem. Soc.* **1939**, *61*, 2302-2303.
- (27) Neu, M.; Fischer, D.; Kissel, T. Recent Advances In Rational Gene Transfer Vector Design Based On Poly(Ethylene Imine) And Its Derivatives. *J. Gene Med.* **2005**, *7*, 992-1009.
- (28) Schweizer, D.; Schönhammer, K.; Jahn, M.; Göpferich, A. Protein–Polyanion Interactions For The Controlled Release Of Monoclonal Antibodies. *Biomacromolecules* **2013**, *14*, 75-83.
- (29) Breunig, M.; Lungwitz, U.; Liebl, R.; Goepferich, A. Breaking Up The Correlation Between Efficacy And Toxicity For Nonviral Gene Delivery. *Proc. Natl. Acad. Sci.* **2007**, *104*, 14454-14459.

- (30) Christiansen, D.; Huang, E.; Silver, F. Assembly Of Type I Collagen: Fusion Of Fibril Subunits And The Influence Of Fibril Diameter On Mechanical Properties. *Matrix Biol.* **2000**, *19*, 409-420.
- (31) Kadler, K.; Holmes, D.; Trotter, J.; Chapman, J. Collagen Fibril Formation. *Biochem. J.* **1996**, *316*, 1-11.
- (32) Silver, F.; Trelstad, R. Type I Collagen In Solution. Structure And Properties Of Fibril Fragments. *J. Biol. Chem.* **1980**, *10*, 9427-9433.
- (33) Trelstad, R.; Hayashi, K.; Gross, J. Collagen Fibrillogenesis: Intermediate Aggregates And Suprafibrillar Order. *Proc. Natl. Acad. Sci.* **1976**, *73*, 4027-4031.
- (34) Gobeaux, F.; Mosser, G.; Anglo, A.; Panine, P.; Davidson, P.; Giraud-Guille, M.; Belamie, E. Fibrillogenesis In Dense Collagen Solutions: A Physicochemical Study. *J. Mol. Biol.* **2008**, *376*, 1509-1522.
- (35) Cisneros, D. A.; Hung, C.; Franz, C. M.; Muller, D. J. Observing Growth Steps Of Collagen Self-Assembly By Time-Lapse High-Resolution Atomic Force Microscopy. *J. Struct. Biol.* **2006**, *154*, 232-245.
- (36) Schurer, J. W.; Kalicharan, D.; Hoedemaeker, P. J.; Molenaar, I. The Use Of Polyethyleneimine For Demonstration Of Anionic Sites In Basement Membranes And Collagen Fibrils. *J. Histochem. Cytochem.* **1978**, *26*, 688-689.
- (37) Tavel, M.; Domard, A. Relation Between The Physicochemical Characteristics Of Collagen And Its Interactions With Chitosan: I. *Biomaterials* **1993**, *14*, 930-938.
- (38) Tavel, M.; Domard, A. Collagen And Its Interaction With Chitosan: II. Influence Of The Physicochemical Characteristics Of Collagen. *Biomaterials* **1995**, *16*, 865-871.

Chapter 7

Summary and Outlook

Summary

This thesis was focused on the interactions of Layer-by-Layer (LbL) thin films with biological counterparts during a drug delivery scenario. Several physiological barriers of an organism, the adsorption of serum proteins, the cellular association or the barrier function of biological hydrogels, limit the transport efficacy and hence the therapeutic effect of a drug delivery system. All those processes are mainly influenced by the physicochemical properties, such as the size and surface charge, of the drug delivery system. Here, thin film technologies, like the LbL strategy are an ideal tool to fine-tune these properties on the nanoscale and hence can lead to a profound knowledge of the ideal parameters for the design of future drug delivery systems.

At the starting point of this work a suitable nanoparticle material, which can easily be modified by an LbL strategy had to be found and characterized in detail. Gold nanoparticles were found to be an interesting colloidal material, due to their distinct optical properties. Gold nanoparticles of different sizes were synthesized according to the Frens method and their size-dependent extinction coefficients were calculated ([Chapter 2](#)). This connection was the fundamental basis for all further quantitative experiments, for example the cell association and protein adsorption studies. Those gold nanoparticles were used as templates for Layer-by-Layer (LbL) thin film surface modifications. As the coating procedure, especially the purification, of nanoparticles is troublesome, due to their high tendency against aggregation, a

general protocol for the LbL coating of gold nanoparticles was established ([Chapter 3](#)). This protocol was later transferred to various other polyelectrolyte pairs and other core materials such as silica nanoparticles.

These tools were the basis for a comparative study on the cell association and protein adsorption behavior of different LbL coated gold nanoparticles ([Chapter 4](#)). Here, the multilayer formation of three different polycations poly(ethylene imine) (PEI), poly(allylamine hydrochloride) (PAH) and poly(diallyl dimethyl ammonium chloride) (PD) in combination with the polyanion poly(styrene sulfonate) (PSS) was investigated with surface plasmon resonance spectroscopy. Those polycations were chosen because of their comparable chemical composition and, in case of PEI, because of its known transfection capacity. But, an unusual deviation of the LbL deposition, a so called overshoot-effect, was found for the PEI/PSS polyelectrolyte pair. Atomic force microscopy revealed that this overshoot phenomenon increased the surface roughness by 12-fold upon adsorption of the third polymer layer and at the same time sharp surface features appeared. It was further assumed that the overshoot effect happened also upon the coating of gold nanoparticles, due to a decrease of the particle size at the same coating step. Hence, it was also concluded that a comparable surface structure was present on the trilayered PEI/PSS coated particles. This surface structure had a major influence on two known physiological barriers; on the adsorption of serum proteins and consequently on the association to cells. The protein adsorption increased significantly for the trilayered PEI/PSS particles, compared to the corresponding bilayered particle species. And this elevated protein shell hindered the association to HeLa cell *in vitro*. As all other physicochemical properties of the particles, the particle size and the surface charge, were comparable for all particle types, it was concluded that the surface topography had a major influence on the interactions with the biological counterparts. As a consequence,

this property should be considered for the design of future nanoparticle based drug delivery systems.

Further specialties of LbL systems were highlighted in [Chapter 5](#). LbL multilayers are known to be dynamic constructs with an internal conformation of the polymer chains that highly depends on the applied fabrication conditions. The internal conformation of the above mentioned polyelectrolyte pairs were investigated with an approach based on Foerster resonance energy transfer. It was found that the combination of PAH/PSS led to a highly interpenetrated polymer network. Those interpenetrations acted as crosslinks between the polymer chains and increased the stability of this polymer films against swelling in a biological milieu. Hence, it was found that PAH/PSS multilayers are disadvantageous for drug delivery systems, where a charged macromolecular drug is incorporated into the multilayer itself. In contrast, PAH/PSS films might be suitable as coating for drug reservoirs, because they showed a good permeability for small molecular drugs. Additionally the mode of release of drugs could be fine-tuned by the degree of ionization of PAH.

The extracellular matrix as another important physiological barrier for colloidal drug carriers was addressed in [Chapter 6](#). So far, the interstitial connective tissue, which contains large amounts of collagen I, was less regarded as an effective molecular filter. But with fluorescence recovery after photobleaching studies in collagen I hydrogels it was found that cationic LbL coated particles and unbound polycations were effectively trapped inside those model matrices. It was further shown, that the addition of a high concentrated PEI-solution of 0.5 mg/ml increased the mobility of the trapped species. But at the same time, these high concentrated polycations altered the constitution of the collagen I fibrils, as it was found with turbidity assays. Hence, it was concluded, that an effective electrostatic filter can also be assumed for the interstitial connective tissue and collagen I hydrogels are a suitable model systems, if the appropriate control experiments are performed side-by-side.

Outlook

Layer-by-Layer based thin films will be of ongoing interest for the development of potent drug carrier systems in the future. This is due to the endless versatility of the technique, where almost any material of synthetic or natural origin can be applied. But just because of this myriad of available materials and fabrication conditions, a lot of open question remain, which need to be resolved.

For an effective drug delivery on the basis of LbL multilayers the counterplay between materials science and biology has to be understood in more detail. In case of the LbL technique the internal structure and the outer appearance of a thin film highly affect the barrier systems of living organisms, which at the end will limit the therapeutic effect. Complex biological processes, such as the adsorption of serum proteins are known to highly depend on particle size or surface charge of the applied material. But, in the future further physicochemical properties, for example the surface topography or the hydrophobicity of the surface, have to be investigated in the same way to get the full scope of the complexity of nano-bio interactions.

Another important challenge for LbL modifications will be to increase the release of drugs which were incorporated into or separated by multilayers. Especially electrostatic LbL thin films seem to be very stable in a biological environment, and this fact reduces their applicability to a large extent. Hence, studies on multilayers which disassemble in an

intracellular regime have to be pronounced. Some promising examples which are already under investigation are the incorporation of intracellular cleavable synthetic polyelectrolytes or the use of hydrogen-bonded multilayers. Finally, one has to consider, that the *in vitro* situation of a cell culture experiment never resembles the complex situation *in vivo*. Therefore, promising material combinations have to be transferred to the *in vivo* level sooner or later.

Appendix

List of Abbreviations

μm	Micrometer
AFM	Atomic force microscopy
ANOVA	Analysis of variance
ATCC	American type culture collection
AuNP	Gold nanoparticle
DLS	Dynamic light scattering
DNA	Deoxyribonucleic acid
ECM	Extracellular matrix
EMEM	Eagle`s minimal essential medium
FITC	Fluorescein isothiocyanate
FRAP	Fluorescence recovery after photobleaching
FRET	Foerster resonance energy transfer
HAuCl_4	Tetrachloroauric(III) acid
HeLa	Human cervical carcinoma cell line
ICP-MS	Inductively coupled plasma mass spectrometry
ICP-OES	Inductively coupled plasma optical emission spectrometry
IP	Isoelectric point

kDa	Kilo Dalton
LB	Langmuir-Blodgett films
LbL	Layer-by-Layer
ml	Milliliter
mM	Millimolar
MUA	Mercapto undecanoic acid
MWCO	Molecular weight cut-off
Na ₃ Cit	Trisodium citrate
nm	Nanometer
PAH	Poly(allylamine hydrochloride)
PD	Poly(diallylamine diammonium chloride)
PEI	Poly(ethylene imine)
PEM	Polyelectrolyte multilayer
pM	Picomolar
PSS	Poly(styrene sulfonate)
rms	Root mean square
RNA	Ribonucleic acid
ROI	Region of interest

SAM	Self-assembled monolayer
SDS	Sodium dodecyl sulfate
SDS-PAGE	Sodium dodecyl sulfate polyacrylamide gel electrophoresis
SiNP	Silica nanoparticle
siRNA	Small-interfering ribonucleic acid
SNK	Student-Newman-Keuls test
SPR	Surface plasmon resonance spectroscopy
TEM	Transmission electron microscopy
TRITC	Tetramethylrhodamine isothiocyanate
X-ray	Röntgen radiation

Curriculum Vitae

Personal Information

Name	Eva-Christina Wurster
Date of birth	February 3 rd , 1985
Place of birth	Karlsruhe
Nationality	Germany

Scientific Education

Since 09/2010	PhD student Department of Pharmaceutical Technology, University of Regensburg
04/2010	Graduation “Diplom Chemikerin” Johannes-Gutenberg-University Mainz
08/2009 - 04/2010	Diploma thesis Institute of Pharmaceutical Technology and Biopharmacy, Prof. Peter Langguth, Johannes-Gutenberg-University Mainz <i>“Entwicklung und Erprobung einer Methode zur Bestimmung der Wirkstofffreisetzung aus therapeutischen Nanopartikeln”</i>
04/2008 - 09/2008	Research internship Department of Chemical Engineering, Prof. David Tirrell, California Institute of Technology, Pasadena, CA, USA
10/2004 - 04/2010	Study of Biomedical Chemistry, Johannes-Gutenberg University Mainz,

School Education

06/2004	Graduation: Abitur, Helmholtz-Gymnasium, Karlsruhe
09/1998 - 06/2004	Grammar school: Helmholtz-Gymnasium, Karlsruhe
09/1995 - 07/1998	Grammar school: Humboldt-Gymnasium, Karlsruhe
09/1991 - 07/1995	Elementary school: Viktor-von-Scheffel Schule, Karlsruhe-Knielingen

List of publications

Publications

Elbakry, A.*; **Wurster, E***; Zaky, A.; Liebl, R.; Schindler, E.; Bauer-Kreisel, P.; Blunk, T.; Rachel, R.; Goepferich, A.; Breunig, M. Layer-By-Layer Coated Gold Nanoparticles: Size-Dependent Delivery of DNA Into Cells. *Small* **2012**, 8, 3847-3856. (* equally contributing authors)

Wurster, E.; Elbakry, A.; Breunig, M.; Göpferich, A. Layer-By-Layer Assembled Gold Nanoparticles For The Delivery Of Nucleic Acids. In *Nanotechnology for Nucleic Acid Delivery: Methods and Protocols*; Ogris, M.; Oupicky, D., Eds.; Methods in Molecular Biology, **2013**; Vol. 948, pp. 171-182.

Conference Abstracts

Wurster, E.; Elbakry, A.; Liebl, R.; Breunig, M.; Göpferich A. Layer-by-Layer assembled gold nanoparticles for nucleic acid delivery: size-specific cellular uptake. *Symposium 20 years Layer-by-Layer*, Strasbourg, France, **2011**

Wurster, E.; Elbakry, A.; Liebl, R.; Breunig, M.; Göpferich A. Layer-by-Layer assembled core-shell nanoparticles for the delivery of nucleic acids, *Gemeinsame Jahrestagung der Deutschen und Österreichischen Pharmazeutischen Gesellschaften*, Innsbruck, Austria, **2011**

Wurster, E.; Elbakry, A.; Liebl, R.; Göpferich A.; Breunig, M. Size-dependent cellular uptake of core-shell assembled nanoparticles for the delivery of nucleic acids, *ACS National meeting*, Philadelphia, USA, **2012**

Wurster, E.; Liebl, R.; Göpferich A.; Breunig, M. Layer-by-Layer coatings on gold nanoparticles: Polyelectrolyte properties and cellular interactions, *ACS National meeting*, Indianapolis, USA, **2013**

Wurster, E.; Liebl, R.; Göpferich A.; Breunig, M. Layer-by-Layer coated gold nanoparticles: Cellular interaction and multilayer composition, *9th Worldmeeting on Pharmaceutics, Biopharmaceutics and Pharmaceutical Technology*, Lisbon, Portugal, **2014**

Acknowledgments

An dieser Stelle möchte ich mich bei allen bedanken, die auf vielfältige Weise zum Gelingen dieser Arbeit beigetragen haben.

Mein besonderer Dank gilt PD Dr. Miriam Breunig für die Überlassung des Themas und die wissenschaftliche Betreuung dieser Arbeit sowie die Möglichkeit an zahlreichen wissenschaftlichen Konferenzen teilnehmen zu können.

Ich danke Prof. Achim Göpferich für das Ermöglichen dieser Arbeit an seinem Lehrstuhl und die Übernahme des Zweitgutachtens.

Prof. Joachim Wegener danke ich für seine Beteiligung als Drittprüfer und die gute Zusammenarbeit mit seinem Lehrstuhl im Zuge der SPR-Kooperation.

Ich bedanke mich bei Dr. Rudolf Robelek für die konstruktive Zusammenarbeit und seine Mühe bei zahlreichen SPR-Messungen. Ebenso danke ich Dr. Stefanie Michaelis für die spontane Weiterführung dieser Experimente.

Daniel Wastl und Prof. Franz J. Giessibl danke ich für die Durchführung der AFM-Messungen und die Offenheit für die entstandene Kooperation.

Prof. Reinhard Rachel danke ich für die TEM-Aufnahmen der Goldnanopartikel.

Ich danke der Deutschen Forschungsgemeinschaft, die diese Arbeit im Rahmen des Projekts BR 3566/1-2 finanziell gefördert hat.

Ich danke allen aktuellen und ehemaligen Mitarbeitern und Doktoranden des Lehrstuhls für Pharmazeutische Technologie für das angenehme Klima auch außerhalb des Labors und die gute Zusammenarbeit.

Hierbei gilt ein besonderes Dankeschön meiner Laborkollegin und Freundin Susanne Kirchhof für die schöne gemeinsame Zeit im Labor.

Außerdem bedanke ich mich bei:

- Renate Liebl für ihre Unterstützung bei unzähligen Experimenten innerhalb und außerhalb des Zelllabors, für ihre Überstunden und ihre eigenen Ideen.
- Edith Schindler für die Hilfe bei den Proteinadsorptionsexperimenten.
- Angelika Berié und Viktoria Meßmann für ihre technische Unterstützung.
- Andrea Blaimer für die Ausstattung des Praktikums, insbesondere der Sterilstation.
- Johannes Thoma für die Unterstützung bei der Entwicklung des photometrischen Zellaufnahmeassays.
- Dr. Ferdinand Brandl für fachliche Anregungen in den Seminaren und Meetings.
- Eva Wrobel für alles Organisatorische und fürs Einfach-Mal-So-Vorbeikommen.
- Kelsey Knewton und Paul Bisso für das Korrekturlesen zweier Manuskripte.

Ein außerordentlicher Dank gilt meiner Familie, die mir diesen Weg ermöglicht hat und mich dabei jederzeit liebevoll unterstützt hat.

Erklärung

Ich versichere hiermit, dass ich die vorliegende Arbeit selbst verfasst habe und keine anderen als die angegebenen Quellen und Hilfsmittel verwendet habe.

Eva-Christina Wurster

Regensburg, den 24. Februar 2015

